Chapter 3

Results and Discussion

CONTENTS

Part I

Microemulsion Polymerization - Batch Process

The microemulsions under present study were transparent, isotropic and thermodynamically stable. The polymerized microemulsions were stable but translucent due to the increase in the size of the dispersed phase.

3.1 Phase diagram

The composition of microemulsion was selected from the partial phase diagram of sodium dodecyl sulphate/water/oil, constructed at 27°C. The oil used was methyl methacrylate, butyl acrylate and 1:1 (w/w) mixture of methyl methacrylate and butyl acrylate. The partial phase diagrams show the boundaries between respective emulsions (turbid) and o/w microemulsions (clear) in Figure 3.1.a, 3.1.b and 3.1.c. The clear and turbid boundaries were established from systematic titrations as described in section 2.4. Lines A and B were drawn arbitrarily from fixed weight ratios of water and oil at 19.0 and 7.0 directed to the apex of SDS respectively. The systems at 27°C changed progressively from turbid emulsions in region E to transparent fluid microemulsions in region M, to viscous mixtures and finally to the liquid crystalline region L as SDS concentration increased gradually along line A and line B. The dotted curve represents the ill defined phase boundary between a turbid emulsion and clear microemulsion. On comparison of the data from phase diagrams it is observed that with line A the amount of SDS at the boundaries between emulsion and microemulsion goes on increasing for MMA to MMA-BA to BA. The lower concentration of SDS required to solubilize MMA is due to its higher solubility in water which is 1.6 gm/100 gm of water while for BA, it is 0.2 gm/100 gm of water.

Similar nature for the phase diagram was observed for water / MMA/(DTAB/DDAB 3:1) by Bleger et al[1]. A partial phase diagram of DTAB/styrene/water at 25°C with

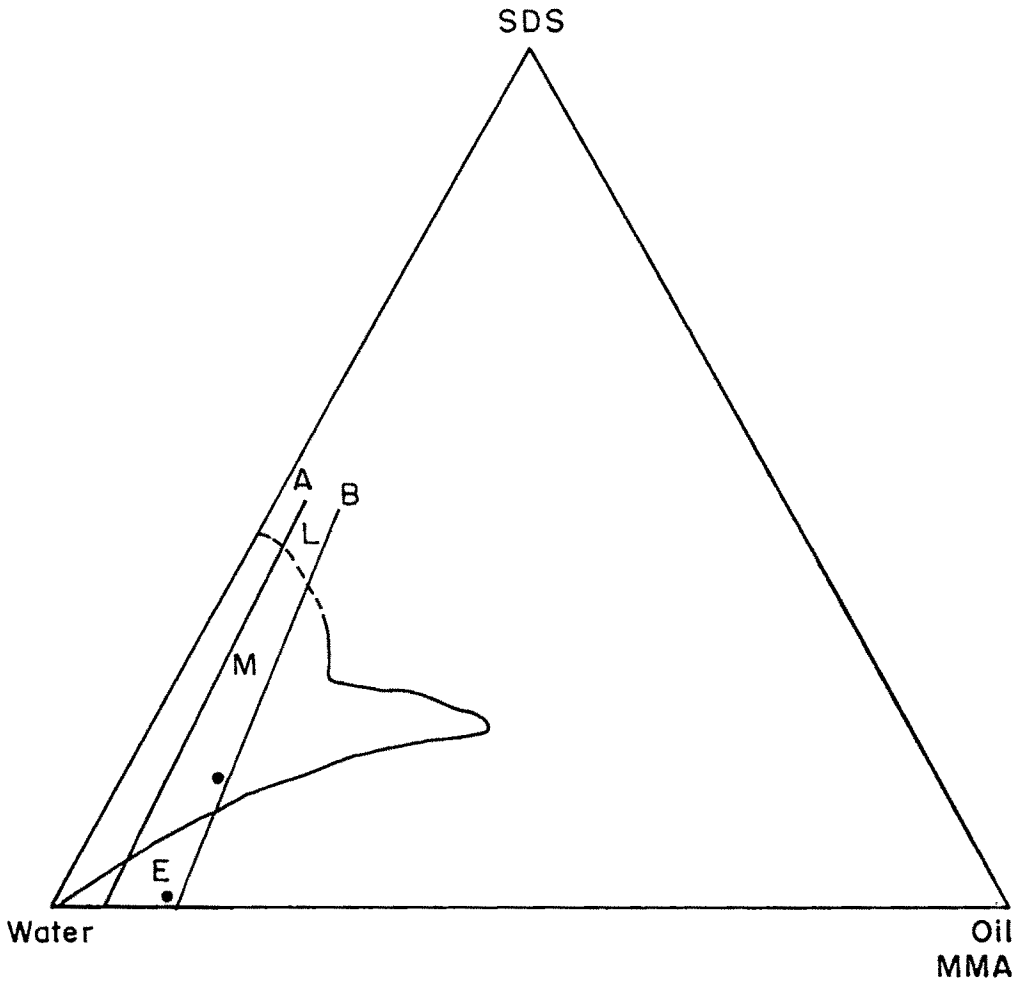

Fig. 3·1· a Phase diagram of MMA–water–SDS at 27 °C
E, emulsion region ; M, microemulsion region ; L, liquid crystalline region ;

- Emulsion and microemulsion compositions used for polymerization

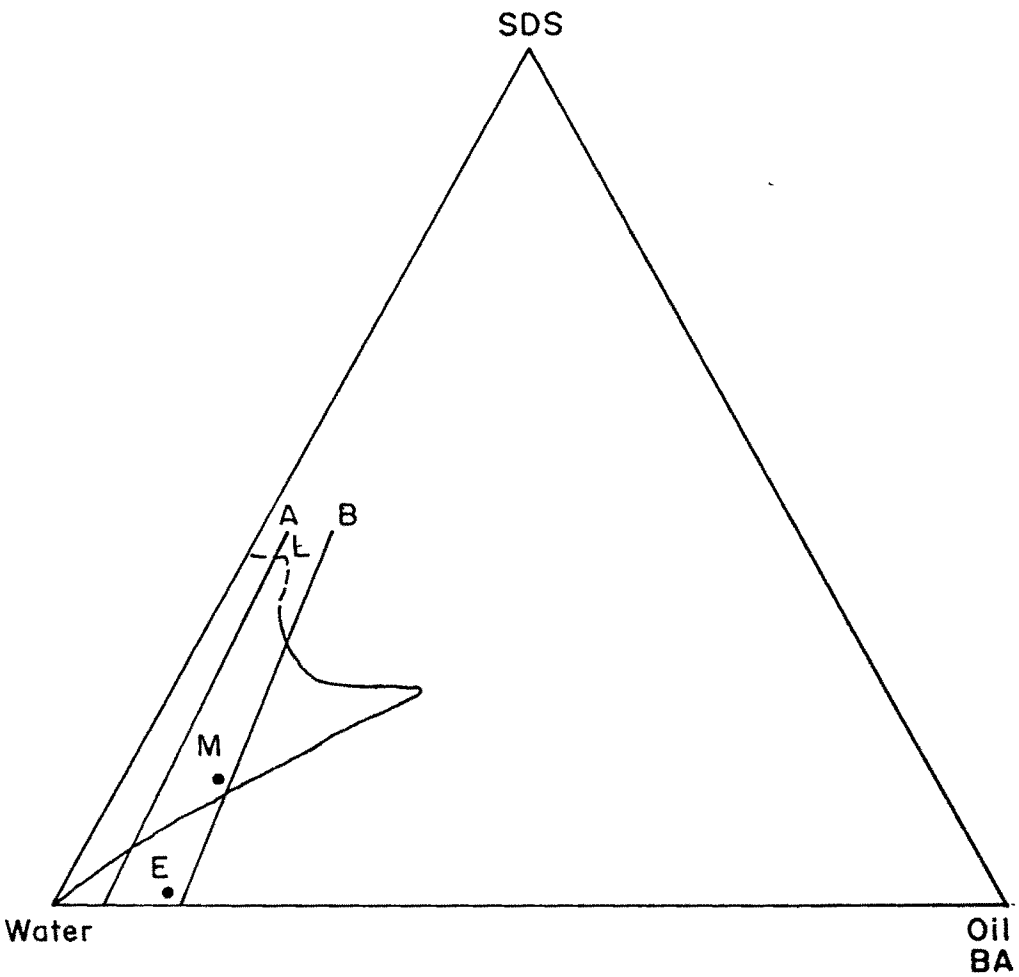

Fig. 3·1·b Phase diagram of BA-water-SDS at 27 °C
E, emulsion region ; M, microemulsion region; L, liquid crystalline region ;

- Emulsion and microemulsion compositions used for polymerization

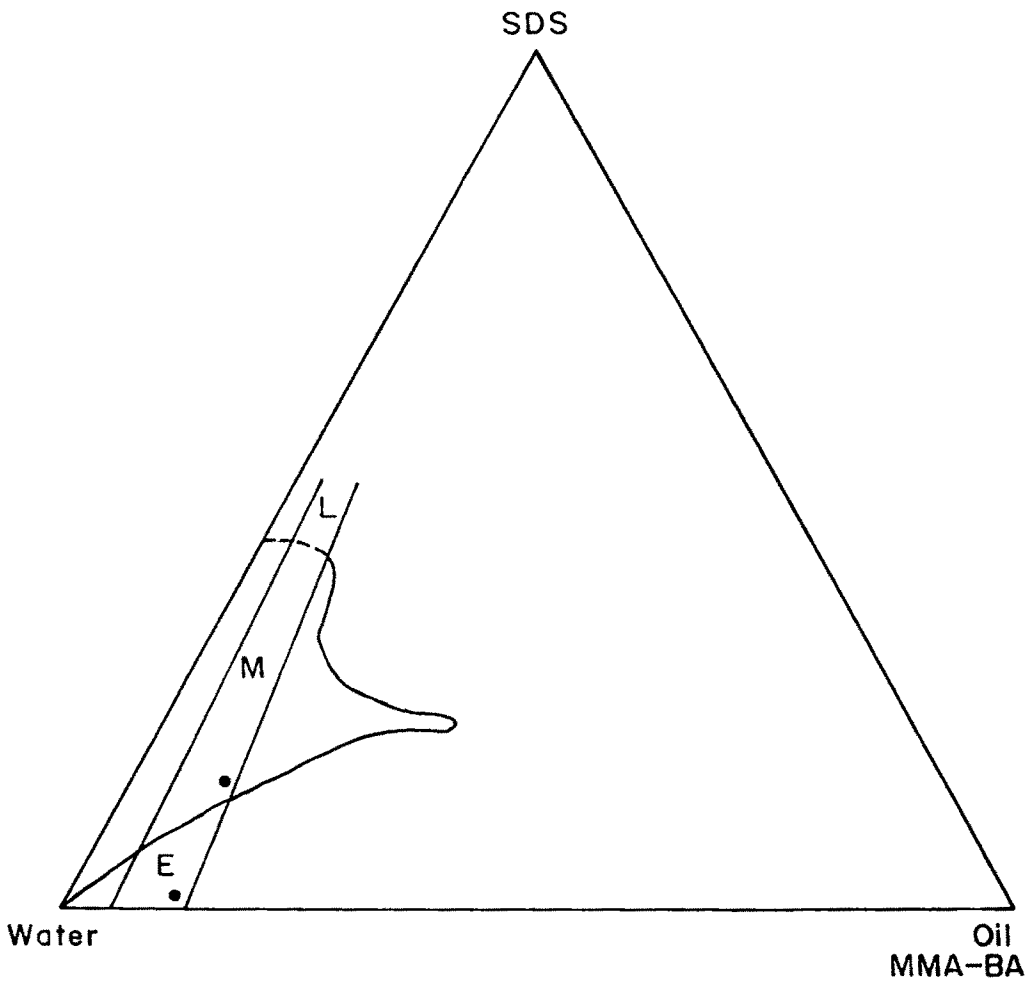

Fig. 3·1·C Phase diagram of MMA-BA (1:1 w/w)-water-SDS at 27 °C

E, emulsion region; M, microemulsion region; L, liquid crystalline region;

- Emulsion and Microemulsion compositions used for polymerization

viscous regions and ill defined boundaries due to high surfactant concentration was reported by Perez-Luna et al[2].

The microemulsion and emulsion at positions shown in Figures 3.1.a,b and c with compositions : Water 76.1%, SDS 14.0% and oil 9.9% (microemulsion) and water 87.7%, SDS 0.9% and oil 11.4% (emulsion) were extensively studied for the polymerization process and the properties of the polymers synthesized.

3.2 Copolymerization of MMA-BA in microemulsion medium

The reaction parameters such as type and concentration of initiator, temperature, cosurfactant, monomer concentration and time were optimized with respect to percentage conversion and particle size using the microemulsions containing, water 76.1%, SDS 14.0% and MMA-BA (1:1 w/w) 9.9%. The results obtained are discussed here.

3.2.1 Initiator type and concentration

Figures 3.2. a and b show the effect of variation in concentration of water soluble initiators : potassium persulphate (KPS) and ammonium persulphate (APS) and oil soluble initiators : azo bis isobutyronitrile (AIBN) and benzoyl peroxide (BPO) on percentage conversion at 80°C and reaction time 120 minutes. The percentage conversion was maximum (90 %) at 1.25 mM concentration of both potassium persulphate and ammonium persulphate. The intrinsic viscosity and average particle size for the copolymers synthesized using KPS and APS were 1.14 dl/g and 1.31 dl/g and 15.63 nm and 20.43 nm respectively. At 0.7 mM concentration of AIBN, 80 % conversion was achieved while at 1.25 mM concentration of BPO, 94 %

conversion was achieved (Fig. 3.2.b) at 80°C. The intrinsic viscosities for the copolymers synthesized using AIBN and BPO was 1.35 and 1.52 dl/g respectively. It was observed that BPO gives polymers with higher viscosity average molecular weights.

3.2.2 Temperature

Optimization of temperature for higher % conversion and lower particle size was done by selecting KPS and BPO as water soluble and oil soluble initiators and performing the polymerization of the microemulsions of compositions mentioned in section 3.2 at various temperatures for 120 minutes reaction time. The results are illustrated in Figure 3.3. It was observed that both the initiators show maximum efficiency at 80°C.

3.2.3 Cosurfactant concentration

As mentioned in section 2.6.3 until 1990 it was believed that cosurfactant is necessary for the microemulsion formation. Generally alcohols are reported to act as cosurfactants. Hence we have tried to examine the effect of cosurfactant pentanol on % conversion during polymerization. Figure 3.4 shows the variation in percentage conversion with respect to cosurfactant pentanol concentration in the microemulsion composition: Water 76.7 %, monomer 10.0 % and SDS 13.3 % at 80°C using 1.25 mM KPS and 120 minutes reaction time. Decrease in percentage conversion was observed with increase in pentanol concentration. Increased particle size and decreased intrinsic viscosity for the copolymers synthesized using 0.83 % pentanol was observed when compared with the copolymers synthesized from compositions without containing pentanol (Table 3.8). The pentanol replaces

some of the ionic surfactant molecules and hence reducing the droplet-droplet repulsive forces. This results in ease of coalescence and thus particle size increases. The particles formed, on using pentanol, were not of uniform and regular shape (Figure 3.25d). The decrease in $|\eta|$ may be due to the increased chain transfer termination.

3.2.4 Monomer concentration

Figure 3.5 shows the % conversion with respect to effective monomer concentration. Reaction duration was 120 minutes. The effective monomer concentration was considered as 100 x [monomer]/[monomer] + [surfactant] which also can be expressed as monomer : surfactant ratio in the systems. It was observed that as the monomer concentration increases the percentage conversion increases. Above 42% effective monomer concentration microemulsion composition changes to emulsion due to increased ratio of monomer : surfactant.

3.2.5 Time

The results obtained in the study of effect of reaction time on percentage conversion are illustrated in Figure 3.6. The maximum rate of polymerization was observed at 44% conversion (1.48×10^{-3} moles/l/sec). The intrinsic viscosities and average particle sizes for the copolymers synthesized using 1.25 mM KPS at 80°C and 41.4% monomer concentration are given in Table 3.11. With increase in time, % conversion increases attaining 87% conversion within 30 minutes. The particle size and intrinsic viscosity increase with reaction time and particle size levels off at around 15.6 nm when maximum percentage conversion is achieved.

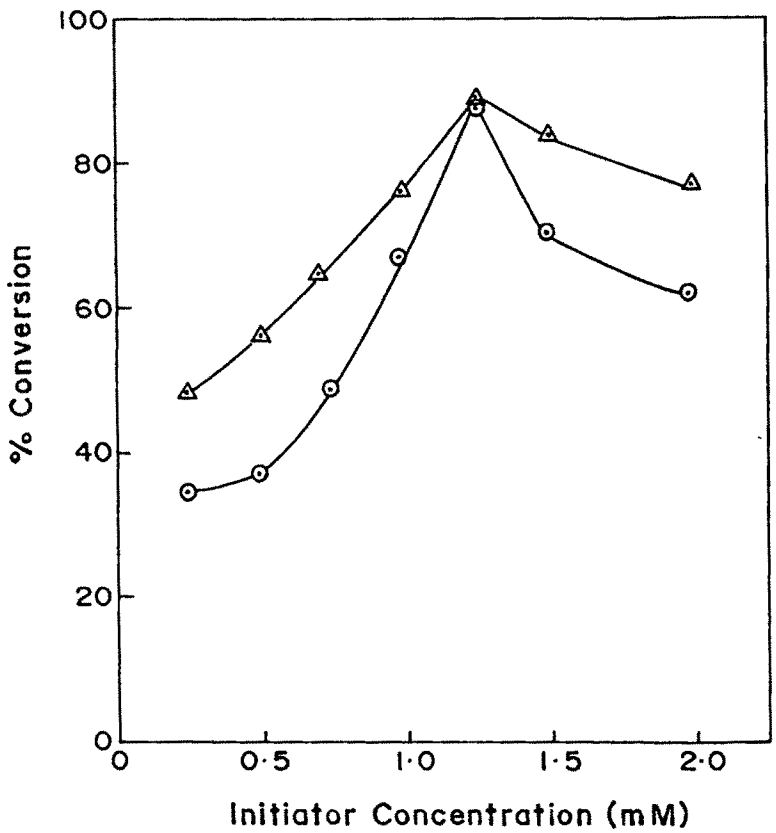

Fig. 3·2a, Effect of initiator concentration on MMA-BA copolymerization at 80 °C, time 120 minutes, ⊙ KPS and △ APS

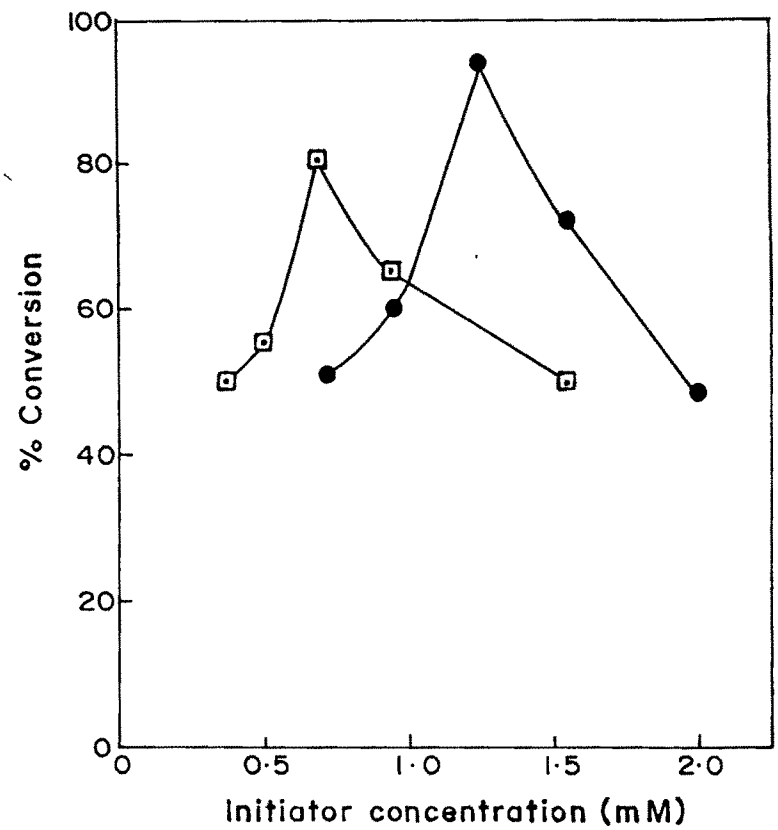

Fig.3·2b Effect of initiator concentration on MMA-BA copolymerization at 80 °C, time 120 minutes, ● BPO, ⊡ AIBN

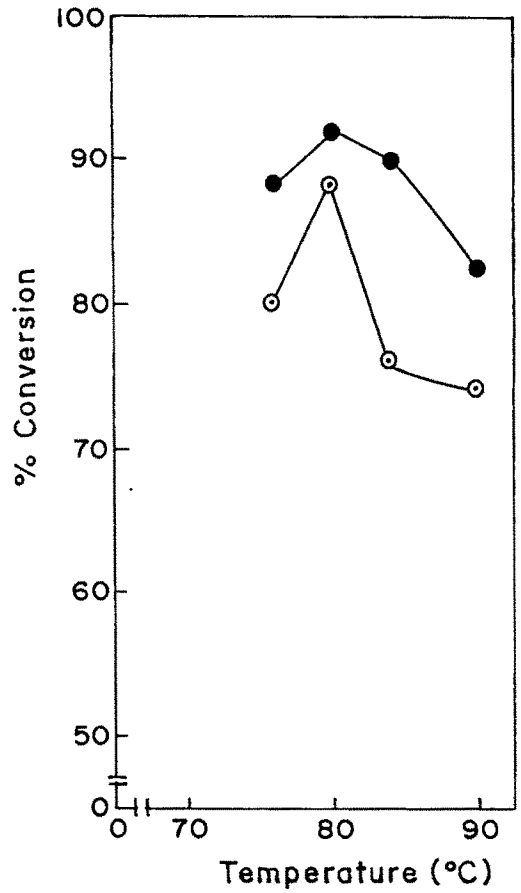

Fig. 3·3 Effect of temperature on % conversion for MMA-BA copolymerization, initiator concentration 1·25mM, time 120 minutes, ⊙ KPS and ● BPO

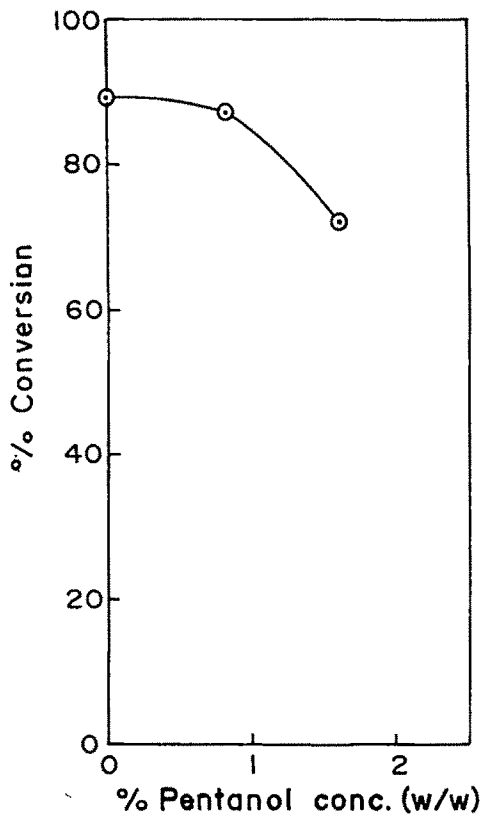

Fig. 3·4 Effect of cosurfactant concentration on % conversion at 1·25 mM KPS concentration, 80° C and 120 minutes reaction time

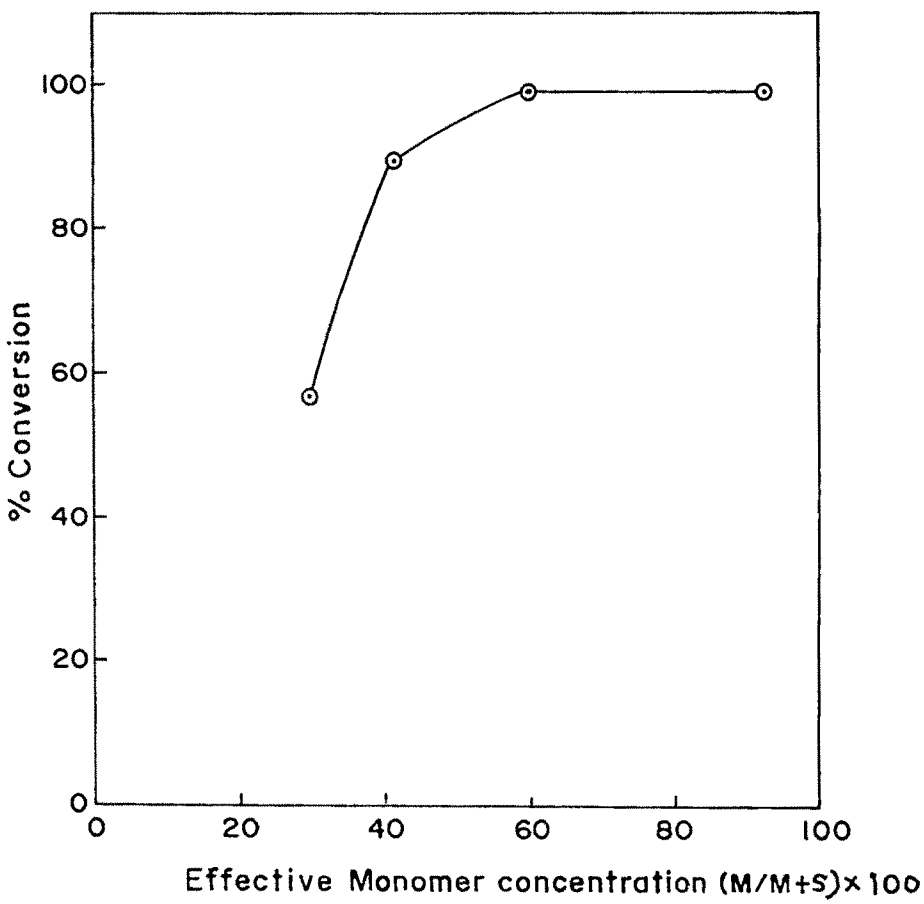

Fig. 3·5 Effect of monomer concentration on % conversion at 1·25 mM KPS concentration, 80°C and 120 minutes reaction time ⊙ microemulsion, ● emulsion

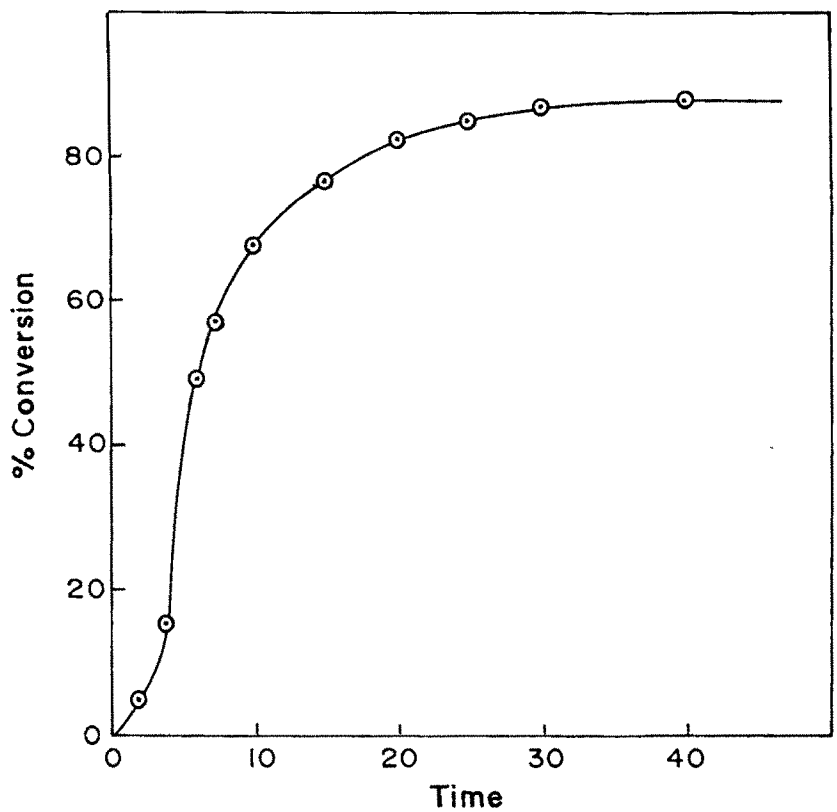

Fig. 3·6 Effect of time on % conversion of MMA-BA at 80°C, 1·25 mM KPS and monomer concentration 41·4 % (MMA-BA 1:1 w/w)

3.3 Kinetics of polymerization of MMA, MMA-BA and BA in emulsion and microemulsion medium

Kinetics of polymerization in the emulsion and microemulsion medium was studied at various temperatures, using different concentrations of potassium persulphate and effective monomer concentration of methyl methacrylate, butyl acrylate and 1:1 w/w mixture of methyl methacrylate and butyl acrylate. The results obtained are given as % conversion vs time plots and log Rp vs % conversion in Figures 3.7 to 3.16.

It was observed that rate of polymerization in microemulsion was slower than in emulsion. Similar observation was made earlier by other workers for methyl methacrylate[3] and butyl acrylate[4]. In the present study of polymerization in microemulsion medium within 20 minutes polymerization attains its maximum, around 90% conversion. The highest rate of polymerization was observed at relatively high conversions, ~40%, in microemulsion whereas in emulsion polymerization it was observed at 25% conversion. The polymerization rate vs % conversion plots show two distinct regions for microemulsion polymerization (Figures 3.7.b to 3.16.b). Interval I is considered to be the nucleation stage, which is characterized by the increase in the rate of polymerization due to increase in number of polymerization locii with time. In interval III the polymerization rate decreases due to decreased monomer concentration in the monomer swollen polymer particles. Similar two rate intervals were observed for microemulsion polymerization of Styrene and MMA by Guo et al[5] and Gan et al[6]. However, emulsion polymerization exhibits three regions. The additional region interval II observed (in log Rp vs % conversion plots) is assigned to the steady state polymerization due to nucleated polymer particles growing by diffusion of

monomer from monomer droplets acting as reservoirs. Due to relatively high solubility of MMA, considerable amount (1.6 gm/100 gm water) of it remains dissolved in the aqueous phase. Hence homogeneous nucleation should be important both in emulsion and microemulsion polymerization of MMA. Due to very small amount of surfactant, number of monomer swollen micelles are less in emulsion than the number of monomer droplets stabilized by surfactant in microemulsion. Hence, the amount of MMA in monomer swollen micelles as well as in aqueous phase of emulsion will be comparable. However, large amount of MMA will remain in monomer droplets acting as reservoirs, in emulsions. Whereas in case of microemulsions, monomer is mainly present as surfactant stabilized droplets, which act as monomer swollen micelles and not as monomer reservoirs. Hence, there will be a large difference in the concentration of MMA in surfactant stabilized monomer droplets and MMA in aqueous phase. The difference results into free radicals generated from KPS in emulsion, reacting with MMA through usual micellar nucleation as well as through homogeneous nucleation mechanism. On the other hand, in microemulsion initiation takes place mainly at the monomer droplets which act as monomer swollen micelles. Our NMR, thermal and viscometric results[7] also support the proposed mechanism of predominant nucleation in monomer droplets in o/w microemulsion and will be discussed in sections 3.6.2, 3.6.5 and 3.6.6.

As solubility of butyl acrylate in water (0.2 gm/100 gm of water) is low compared to that of MMA, homogeneous nucleation will not be significant both in emulsion and microemulsion polymerization of butyl acrylate. Thus in emulsion, micellar nucleation is expected while in microemulsion it is in the surfactant stabilized monomer droplets.

In the case of copolymerization of MMA-BA, contribution due to homogeneous nucleation will be less significant in emulsion than that in homopolymerization of methyl methacrylate as the solubility of MMA-BA (1:1 w/w) will be less than that of MMA but more than that of butyl acrylate. In the microemulsion medium it will be mainly in the surfactant stabilized monomer droplets.

3.3.1 Effect of temperature

The effect of temperature on polymerization was studied by initiating the polymerization in microemulsion and emulsion media using 0.5 mM potassium persulphate (KPS) at different temperatures (70°C, 80°C and 90°C). The % conversion vs time and log Rp vs % conversion plots are given in figures 3.7 - 3.9 for methyl methacrylate, butyl acrylate and 1:1 w/w mixture of methyl methacrylate and butyl acrylate. From Figures 3.7.b, 3.8.b and 3.9.b it is observed that in all the cases polymerization rate increases with increase in temperature. Three distinct intervals for the emulsion polymerization and two for microemulsion polymerization were also observed in these studies as discussed earlier. Table 3.1 shows maximum rate of polymerization and the % conversion at which it is achieved for microemulsion polymerization. From the results obtained using Arrhenius equation,

$$K = A e^{-E/RT}$$

where K is a rate constant at temperature T, A is a constant known as frequency factor and E is the energy of activation, activation energy for the polymerization of MMA, BA and MMA-BA (1:1 w/w) in emulsion at 25% conversion and microemulsion media at 40% conversion was calculated from the plots of log Rp vs 1/T. The activation energy is given in Table 3.2.

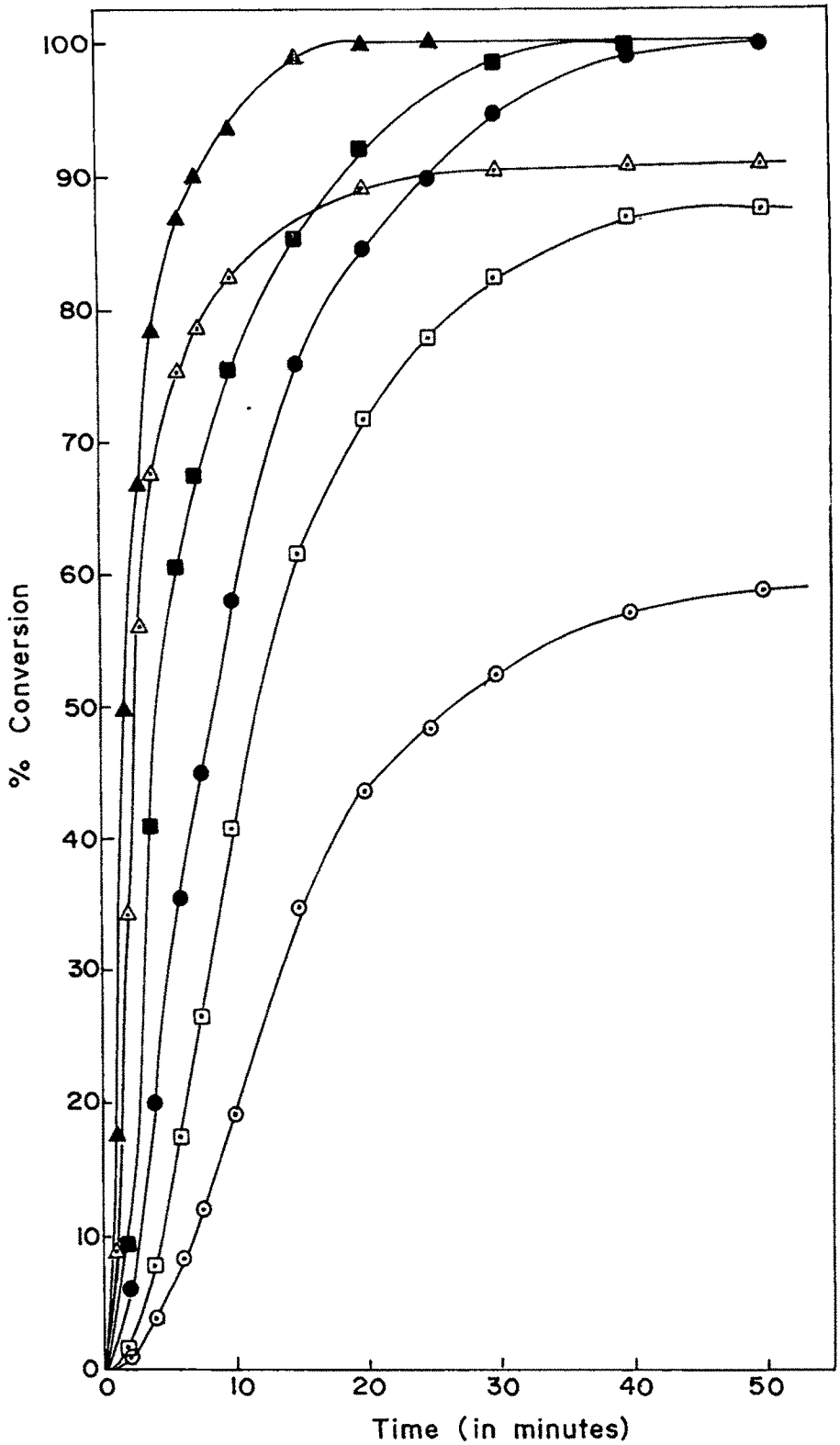

Fig. 3·7 a % Conversion vs Time plots for MMA with 0·5 mM KPS; microemulsions: ⊙, ⊡, △ and emulsions: ●, ■, ▲ at 70° C, 80° C and 90° C respectively

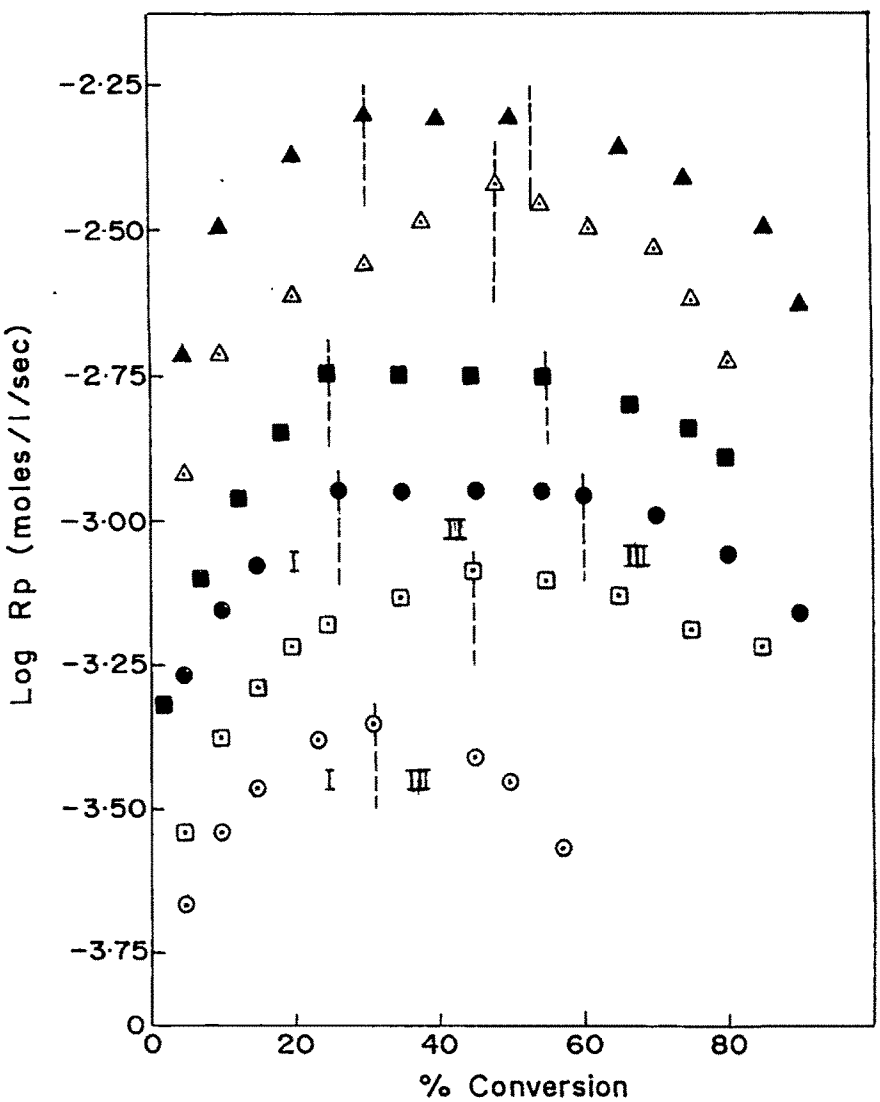

Fig.3·7 b Log Rp vs % conversion for MMA with 0·5 mM KPS; microemulsions: ⊙, ⊡, △ and emulsions: ●, ■, ▲ at 70° C, 80° C, and 90° C respectively

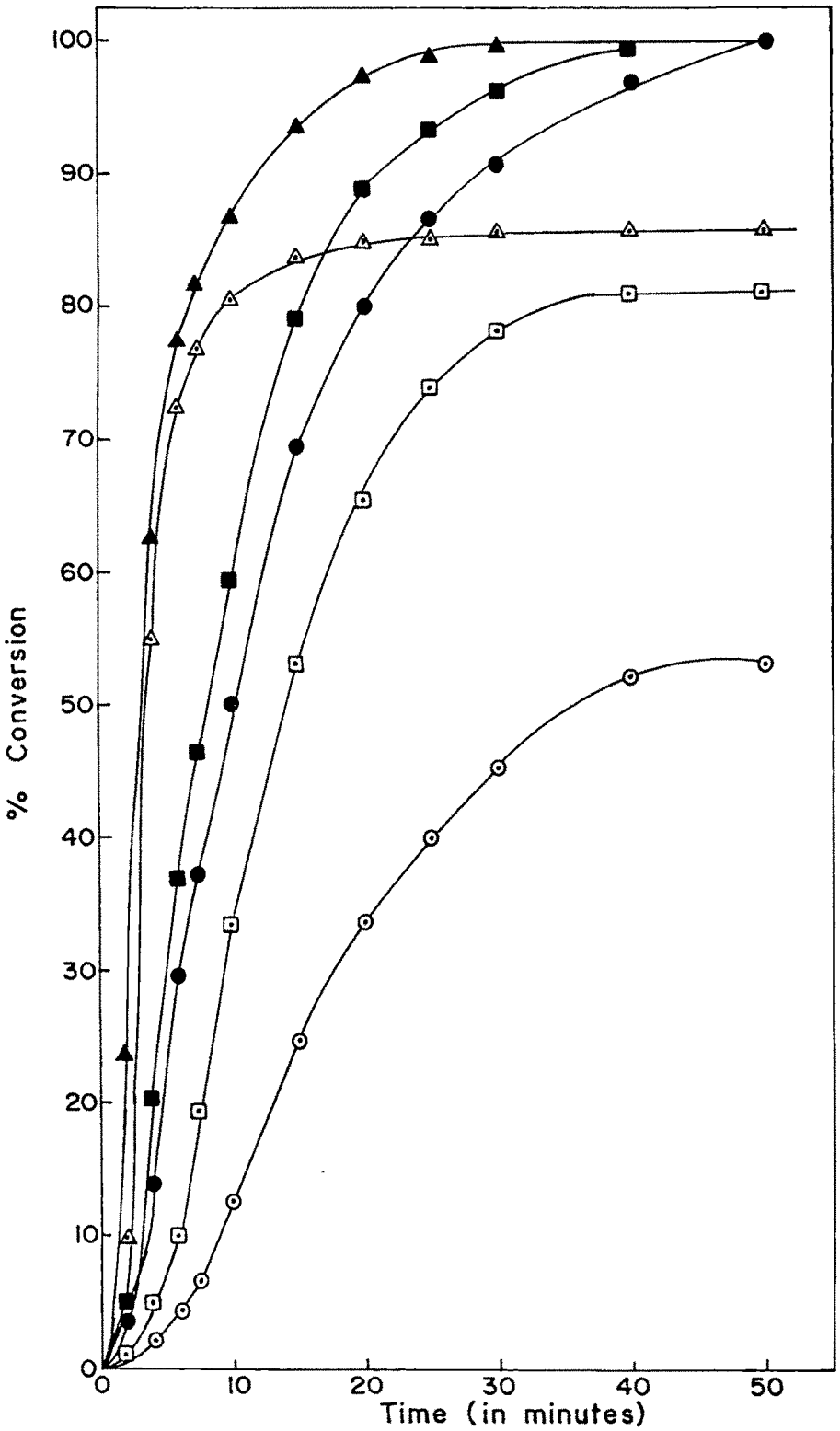

Fig. 3·8a % Conversion vs Time plots for BA with 0·5 mM KPS; microemulsions: ⊙, ⊡, △ and emulsions: ●, ■, ▲ at 70° C, 80° C, and 90° C respectively

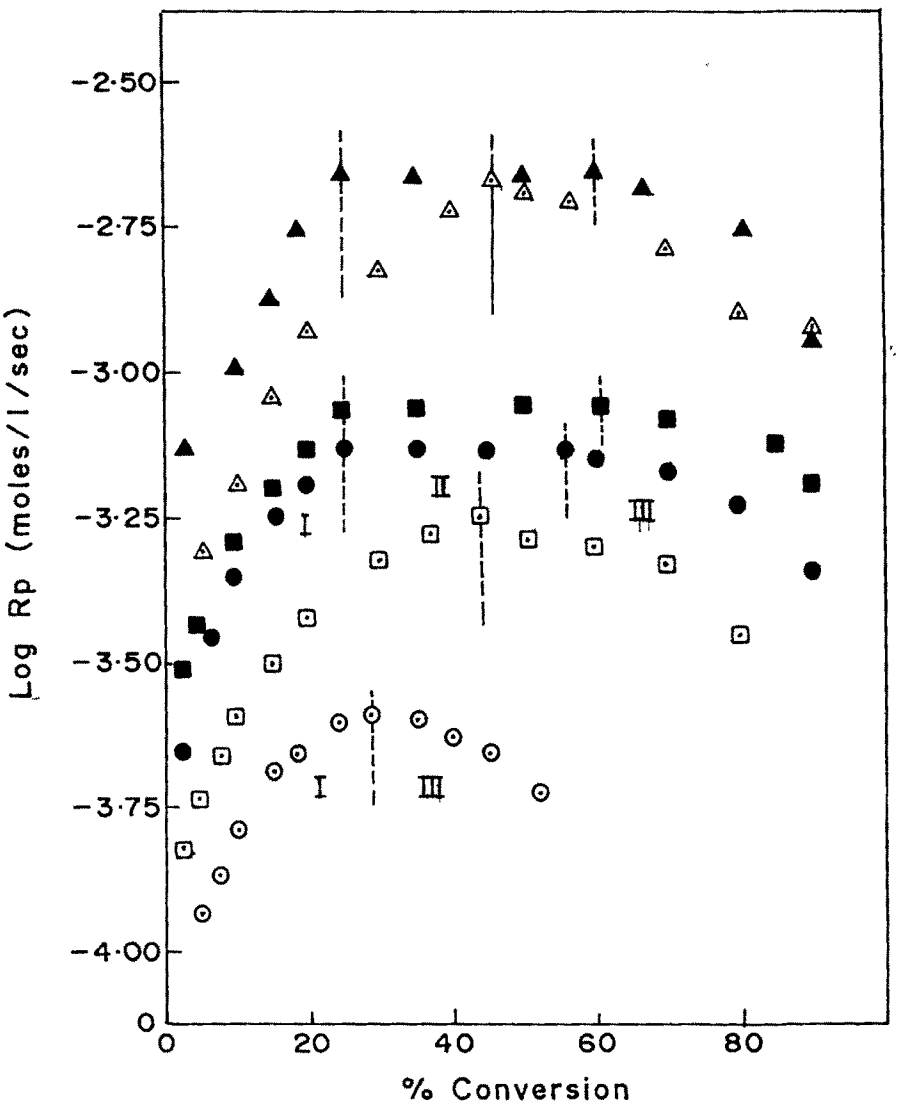

Fig.3·8b Log Rp vs % conversion plots for BA with 0·5mM KPS; microemulsions: ⊙, ⊡, △ and emulsions: ●, ■, ▲ at 70° C, 80° C and 90° C respectively

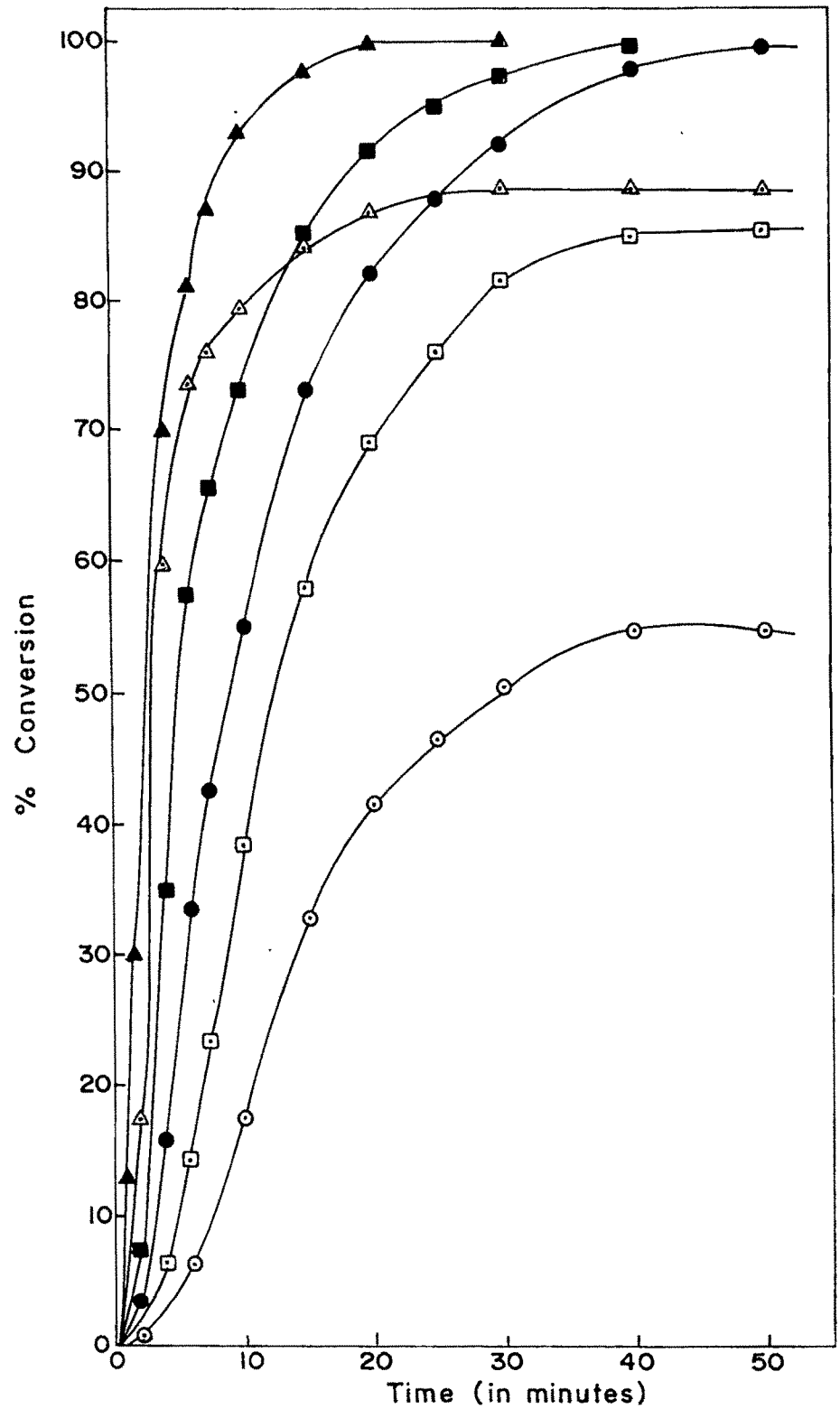

Fig.3·9a % Conversion vs Time plots for MMA-BA with 0·5 mM KPS; microemulsion : ⊙ , ⊡ , △ and emulsions: ● , ■ , ▲ at 70° C 80° C and 90° C respectively

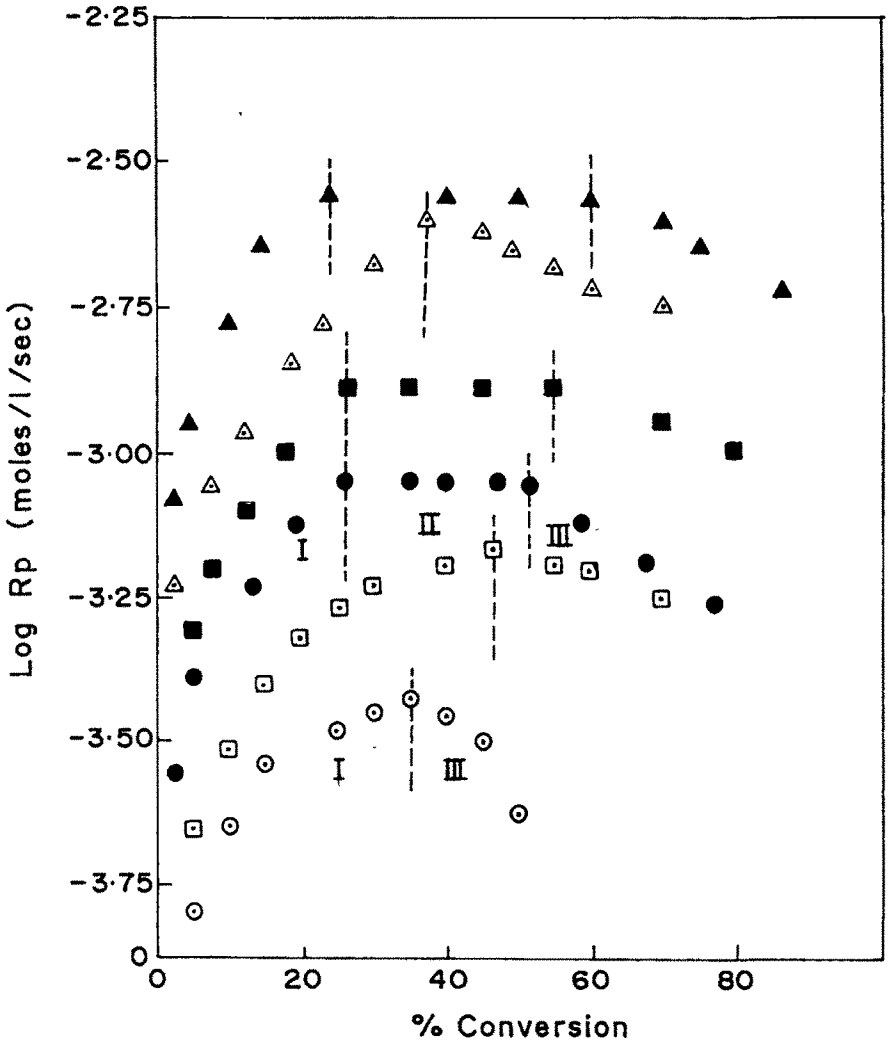

Fig.3·9 b Log Rp vs% conversion plots for MMA-BA with 0·5 mM KPS; microemulsions: ⊙, ⊡, △ and emulsions; ●, ■, ▲ at 70°C, 80°C and 90°C respectively

Table 3.1 : Effect of Temperature on Rp and % conversion at which Rp (max) is attained in microemulsion media.

Data calculated from the results in Figure 3.7 b, 3.8 b, 3.9 b.

Monomer	Temperature °C	$Rp_{(max)}$ (x 10^{-4}) (moles/l/sec)	% conversion at $Rp_{(max)}$
MMA	70	4.5	31.0
	80	8.1	46.0
	90	37.2	48.0
MMA-BA	70	3.7	35.0
(1:1 w/w)	80	6.8	46.6
	90	25.1	44.5
BA	70	2.6	29.0
	80	5.8	44.0
	90	20.0	46.0

Table 3.2 : Activation energy (KJ/mole) calculated from Arrhenius plots.

	Microemulsion	Emulsion
PMMA	116.04	84.25
PBA	105.31	71.61
P(MMA-BA)	95.73	52.65

In all the cases it was observed that overall activation energy for microemulsion polymerization is higher than emulsion polymerization. In microemulsion system, 'shell' structure has been postulated[5] by the adsorption of surfactant and cosurfactant, if present, on the monomer droplets which retards the entry of radicals. In addition high ionic concentration in microemulsion also contributes to high activation energy. Similar results for activation energy were observed by Potisk and Capek[4] for the butyl acrylate polymerization in emulsion and microemulsion system.

3.3.2 Effect of initiator concentration

The effect of initiator concentration on polymerization was examined by initiating the microemulsion and emulsion compositions with 0.1, 0.5 and 1.25 mM potassium persulphate concentration (based on water) at 80°C. The % conversion vs time plots and log Rp vs % conversion plots are illustrated in figures 3.10, 3.11 and 3.12 for methyl methacrylate, butyl acrylate and 1:1 w/w mixture of methyl methacrylate and butyl acrylate respectively. In all the cases the rate of polymerization increases with increase in initiator concentration as observed in figure 3.10.b, 3.11.b and 3.12.b. The plots also show three intervals for emulsion and two for microemulsion polymerization as discussed earlier. Table 3.3 shows maximum rate of polymerization and the % conversion at which it is achieved for microemulsion polymerization. With increasing concentration of initiator maximum rate of polymerization increases.

Fig. 3.13 shows the linear relationship between log Rp and log [KPS] concentration. The straight lines obtained for microemulsion polymerization for

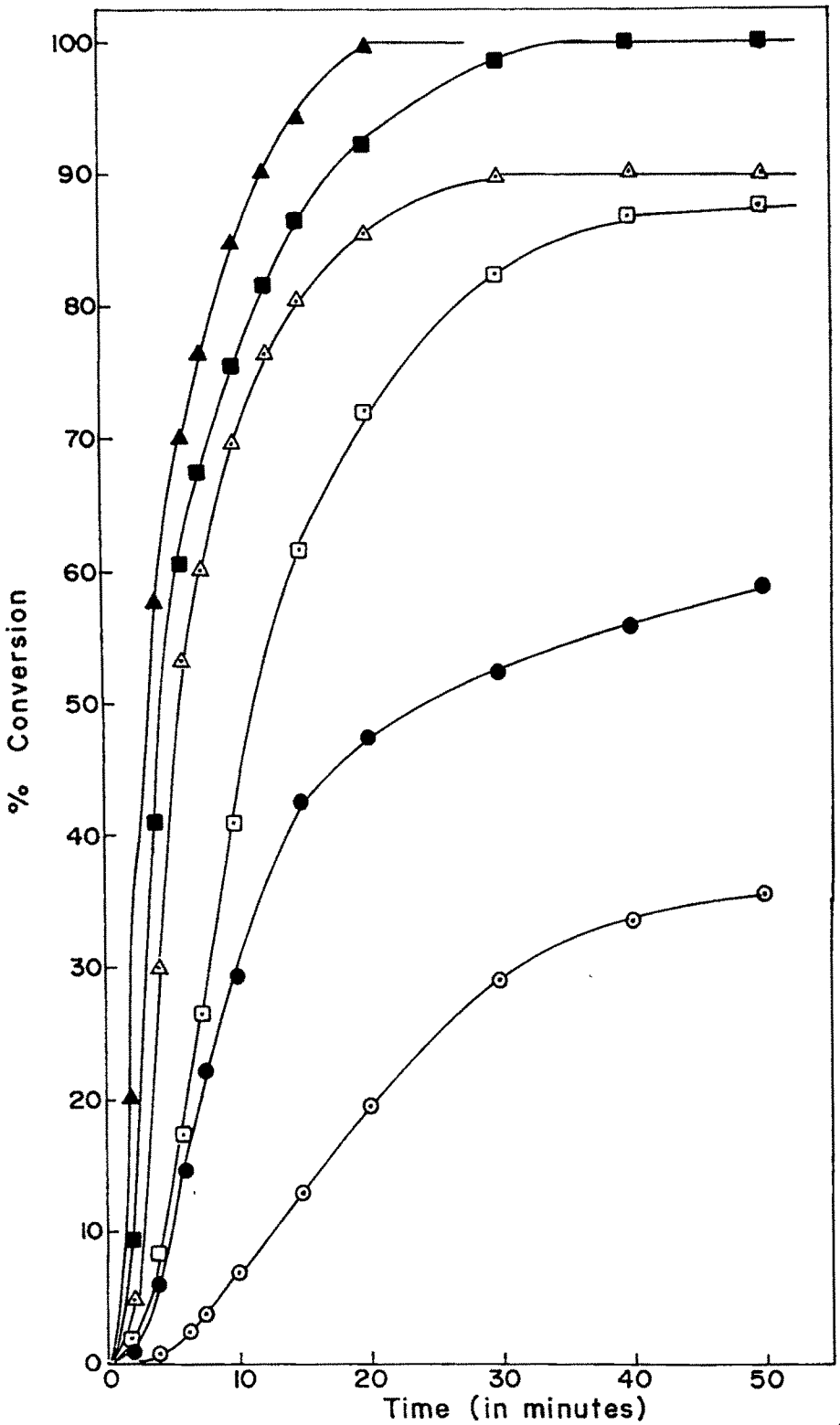

Fig.3·10a % Conversion vs Time plots for MMA at 80° C; microemulsion : ⊙,⊡,△ and emulsions : ●, ■,▲ at 0·1 mM, 0·5mM and 1·25 mM, KPS concentration respectively

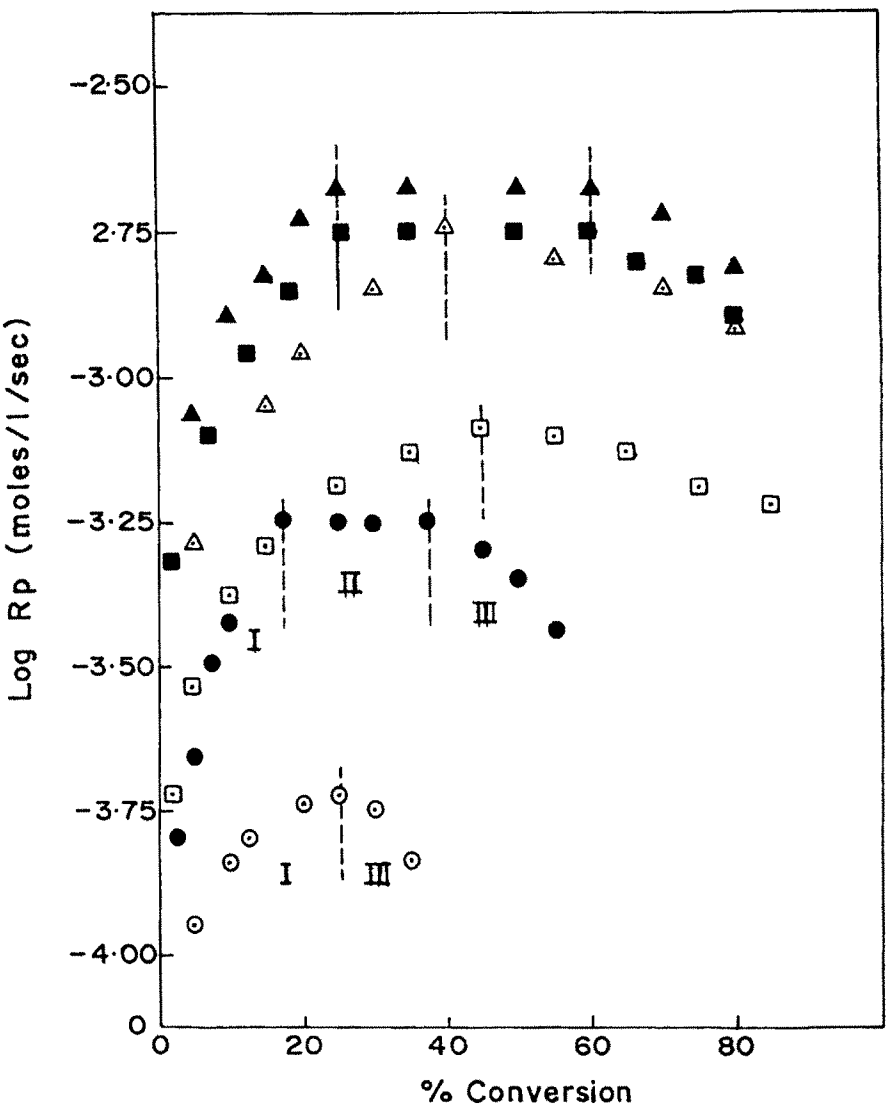

Fig. 3·10 b Log Rp vs % conversion plots for MMA at 80° C; microemulsions: ⊙, ⊡, △ and emulsions: ●, ■, ▲ at 0·1 mM, 0·5 mM and 1·25 mM KPS respectively

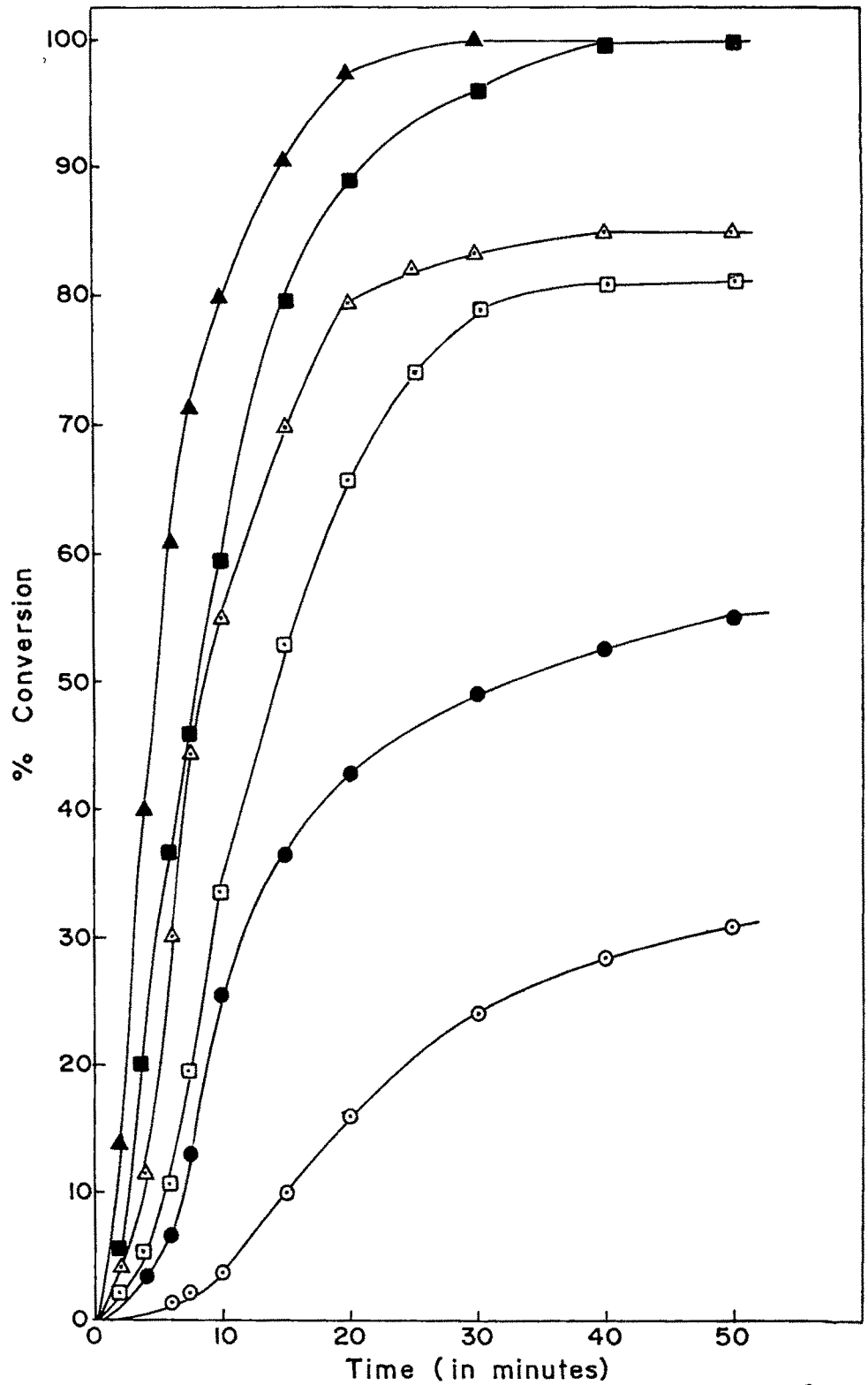

Fig.3·11a % Conversion vs Time plots for BA at 80° C; microemulsions: ⊙, ⊡, △ and emulsions: ●, ■, ▲ at 0·1 mM, 0·5 mM and 1·25 mM KPS concentration respectively

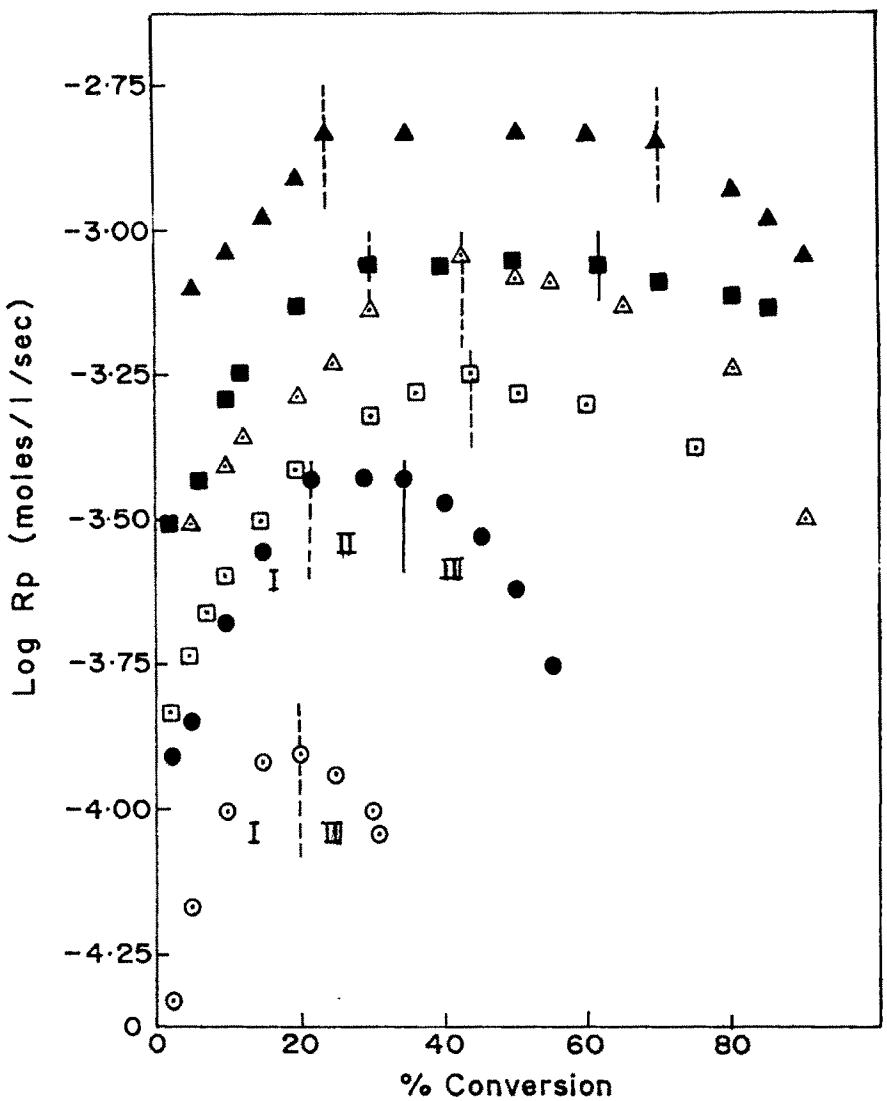

Fig.3·11b Log Rp vs % conversion plots for BA at 80° C; microemulsion :⊙,⊡,△ and emulsions :●,■,▲ at 0·1 mM, 0·5 mM and 1·25 mM KPS concentration respectively

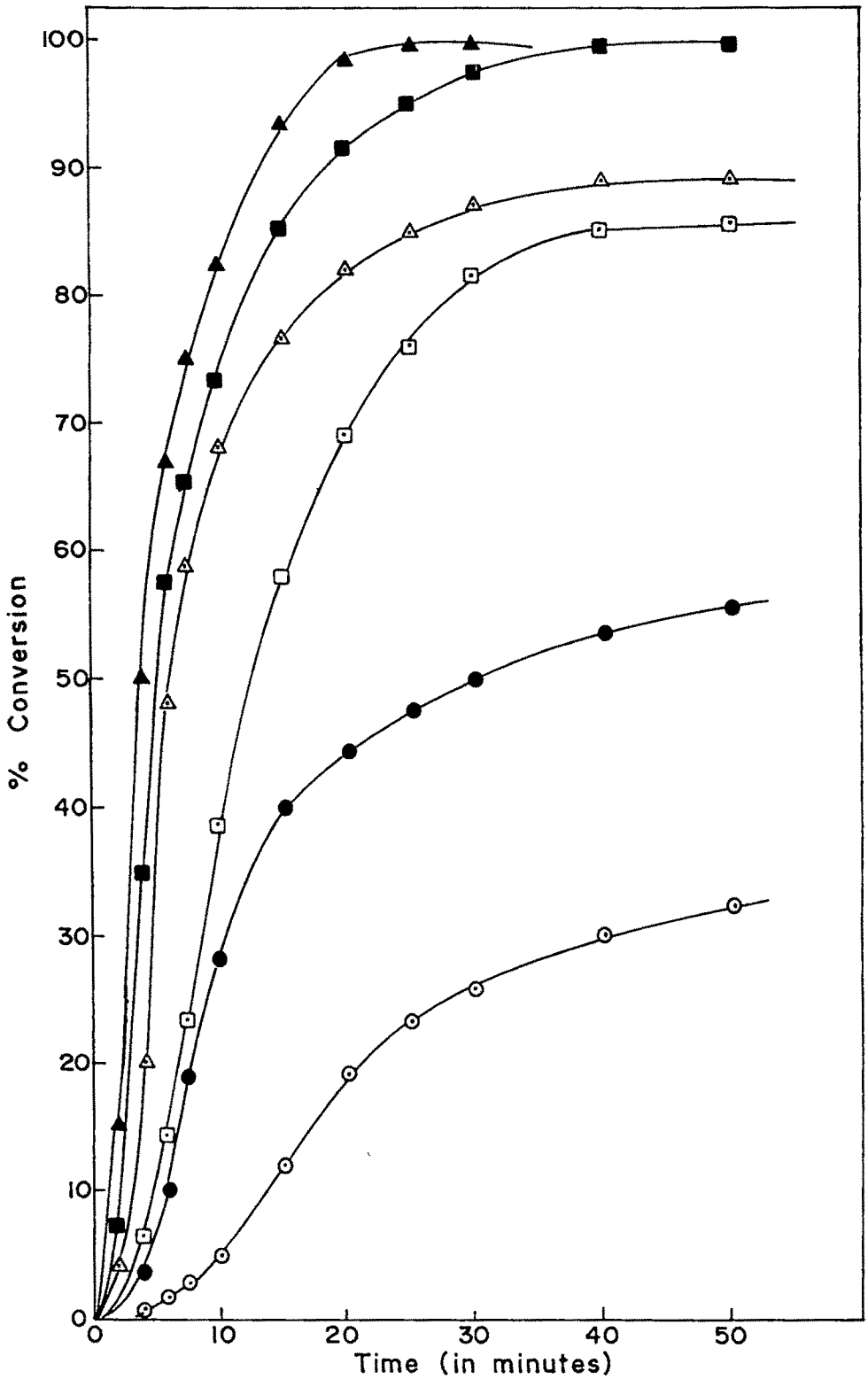

Fig.3·12 a % Conversion vs Time plots for MMA-BA at 80° C; microemulsions: ⊙, ⊡, △ and emulsions: ●, ■, ▲ at 0·1 mM, 0·5 mM and 1·25 mM KPS concentration respectively

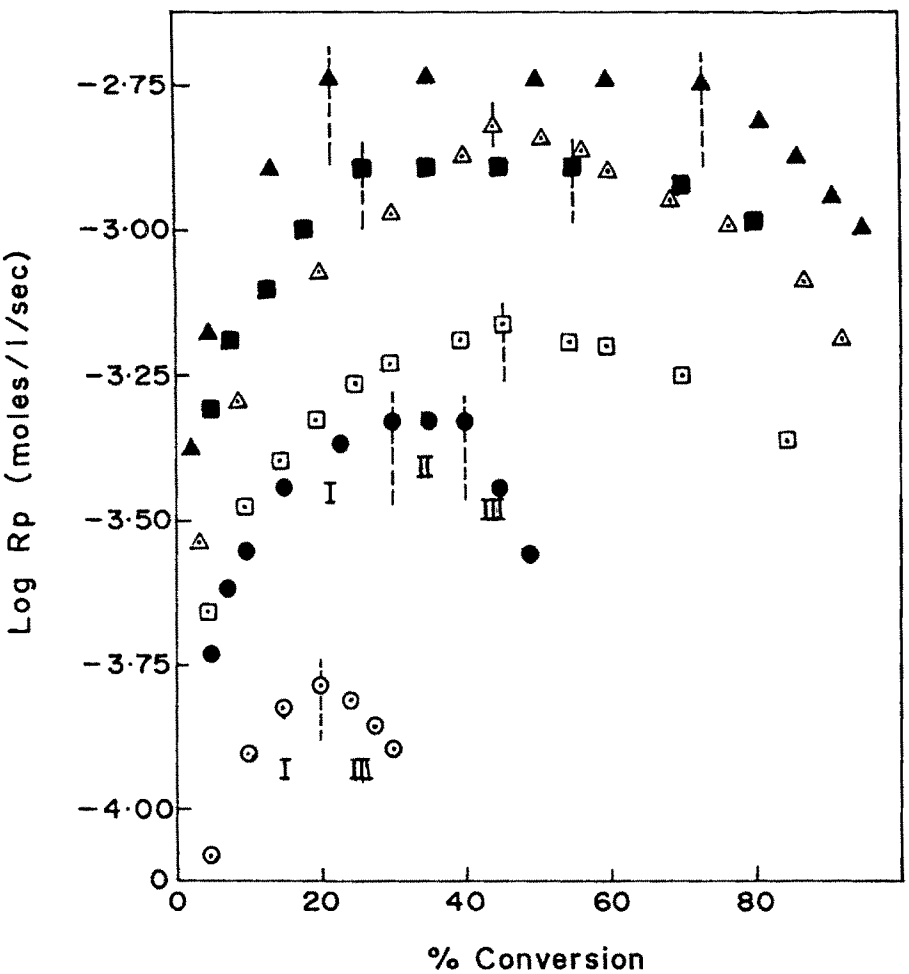

Fig.3·12 b Log Rp vs % conversion for MMA-BA at 80° C; microemulsions: ⊙, ⊡, △ and emulsions: ●, ■, ▲ at 0·1mM, 0·5mM and 1·25 mM KPS concentration respectively

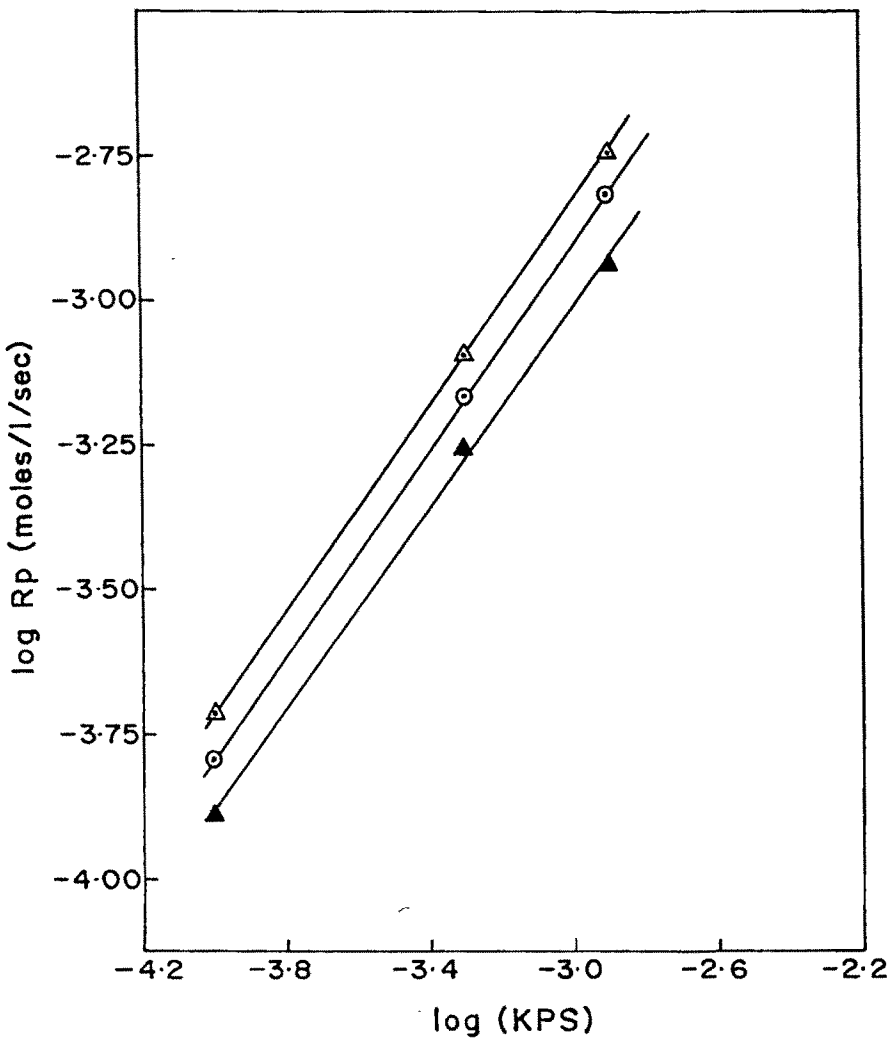

Fig. 3·13 Dependence of rate of polymerization on KPS initiator concentration ; △ MMA, ⊙ MMA-BA, ▲ BA

Table 3.3 : Effect of Initiator Concentration on $Rp_{(max)}$ and % conversion at which $Rp_{(max)}$ is attained.

Data calculated from Fig. 3.1.10 b, 3.1.11 b and 3.1.12 b.

Monomer	KPS concentration (mM)	$Rp_{(max)}$ (moles/l/sec)	% conversion at $Rp_{(max)}$
MMA	0.10	1.91×10^{-4}	25.0
	0.50	8.13×10^{-4}	46.0
	1.25	1.78×10^{-3}	40.0
MMA-BA	0.10	1.62×10^{-4}	20.0
	0.50	6.76×10^{-4}	46.0
	1.25	1.48×10^{-3}	44.0
BA	0.10	1.23×10^{-4}	20.0
	0.50	5.75×10^{-4}	44.0
	1.25	9.12 x 10-4	43.0

MMA, MMA-BA and BA show 0.99, 0.999 and 0.989 correlation coefficients. A general equation can be developed for the purpose as

$$\log Rp = \text{slope} \times \log[KPS] + \text{Intercept}$$

Hence for MMA, it is

$$\log Rp = 0.883 \log[KPS] - 0.183,$$

for MMA-BA (1:1 w/w), it is

$$\log Rp = 0.875 \log[KPS] - 0.289,$$

and for BA,

$$\log Rp = 0.810 \log[KPS] - 0.644$$

where KPS concentration is in molarity.

3.3.3 Effect of Monomer concentration

In order to elucidate the effective monomer concentration effect, the reaction temperature and initiator concentration were kept constant during polymerization process. The effective monomer concentration[8] is defined as the ratio of [monomer] x 100/[monomer]+[SDS]. The rate of reaction for 30%, 41.4% and 92.3% monomer concentration was examined with 1.25 mM KPS concentration at 80°C and results obtained for methyl methacrylate, butyl acrylate and 1:1 w/w mixture of methyl methacrylate and butyl acrylate are presented in figures 3.14, 3.15 and 3.16 respectively. In all the cases, rate of polymerization increases with increase in effective monomer concentration. At lower monomer concentration i.e. high surfactant content, the rate of polymerization was observed to be suppressed. It may be due to high ionic concentration in the system. The log Rp vs % conversion plots (Figure 3.14.b, 3.15.b and 3.16.b) show three distinct

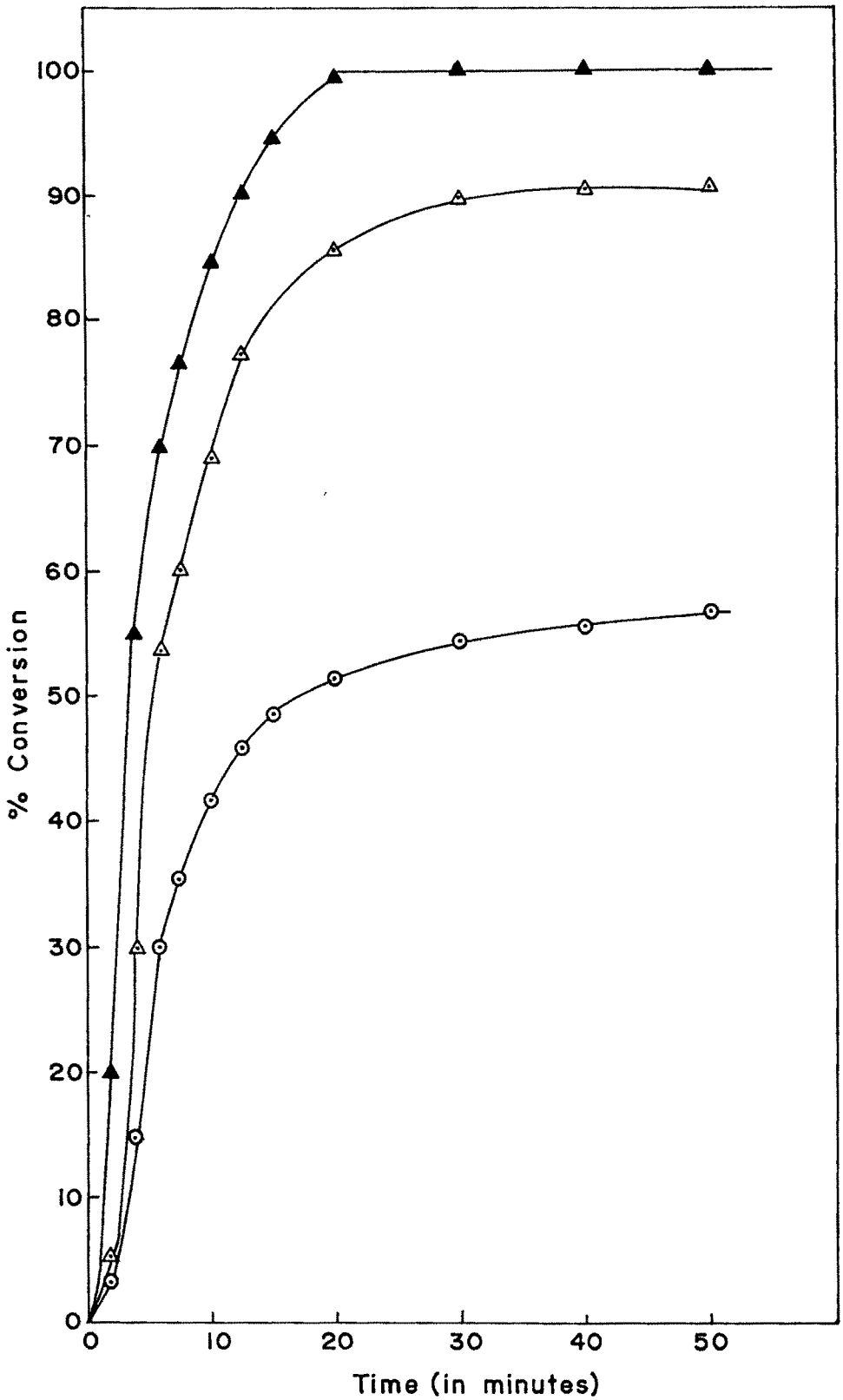

Fig. 3·14 a % Conversion vs Time plots of MMA for different Monomer concentration with 1·25 mM KPS at 80° C; ⊙ 30 %, △ 41·4 %, ▲ 90 % Monomer concentration

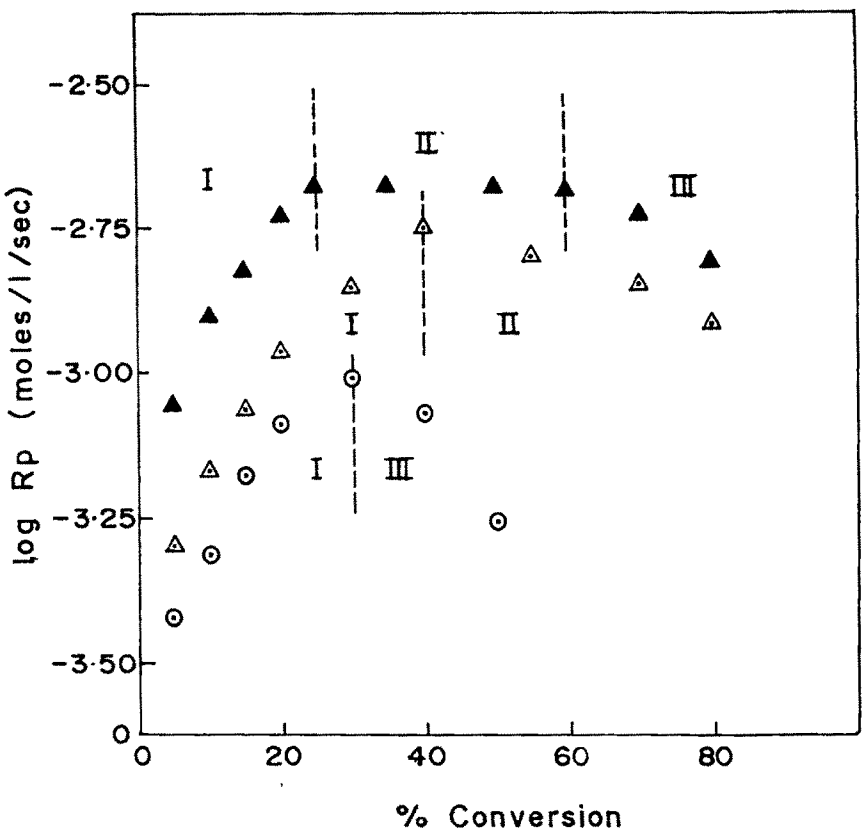

Fig.3·14 b Log Rp vs % conversion plots of MMA for different Monomer concentration at 1·25 mM KPS at 80° C; ⊙ 30 %, △ 41·4 %, ▲ 90 % Monomer concentration

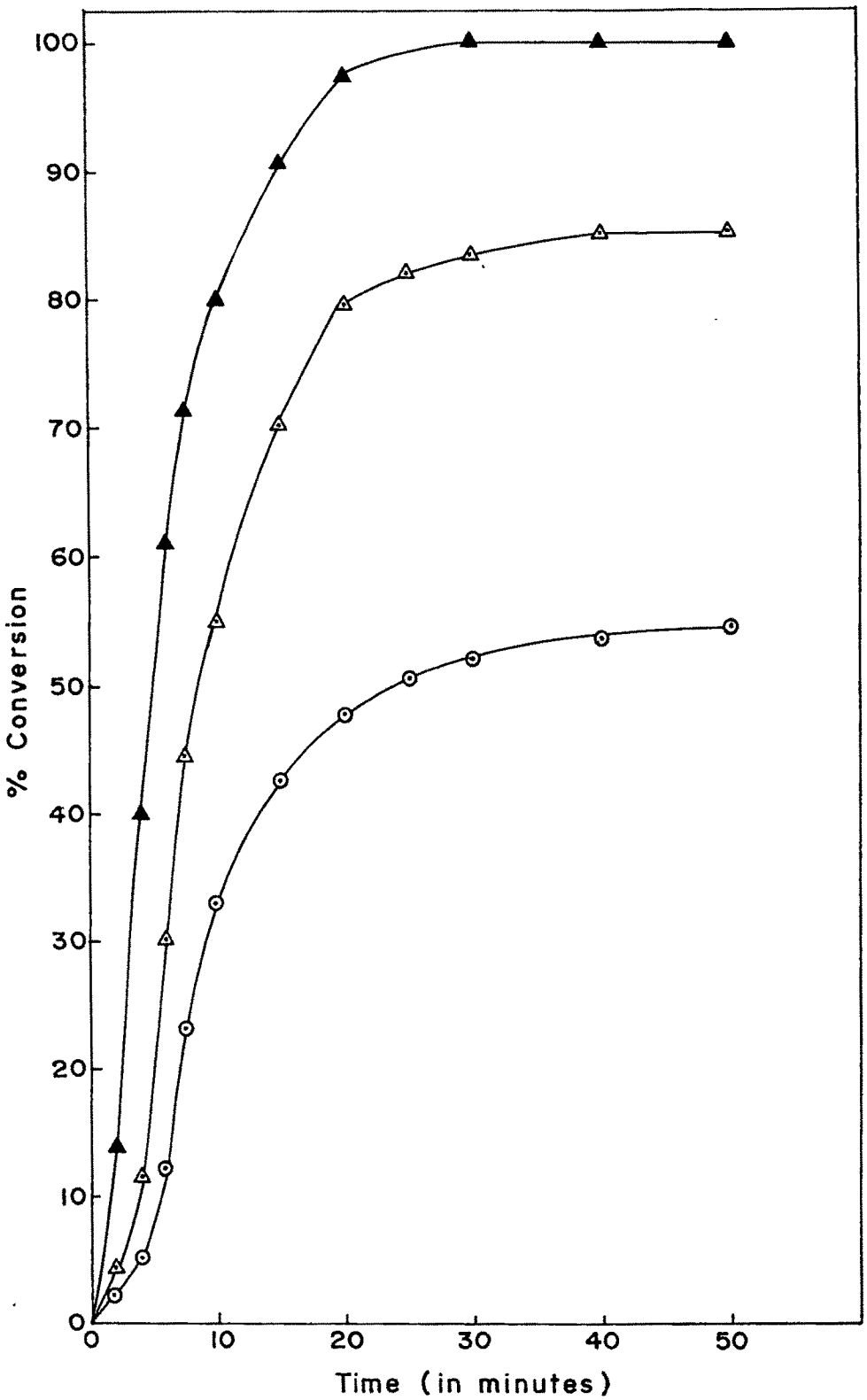

Fig.3·15 a % Conversion vs Time plots of BA for different Monomer concentration with 1·25 mM KPS at 80° C; ⊙ 30 %, △ 41·4 %, ▲ 90·0 % Monomer concentration

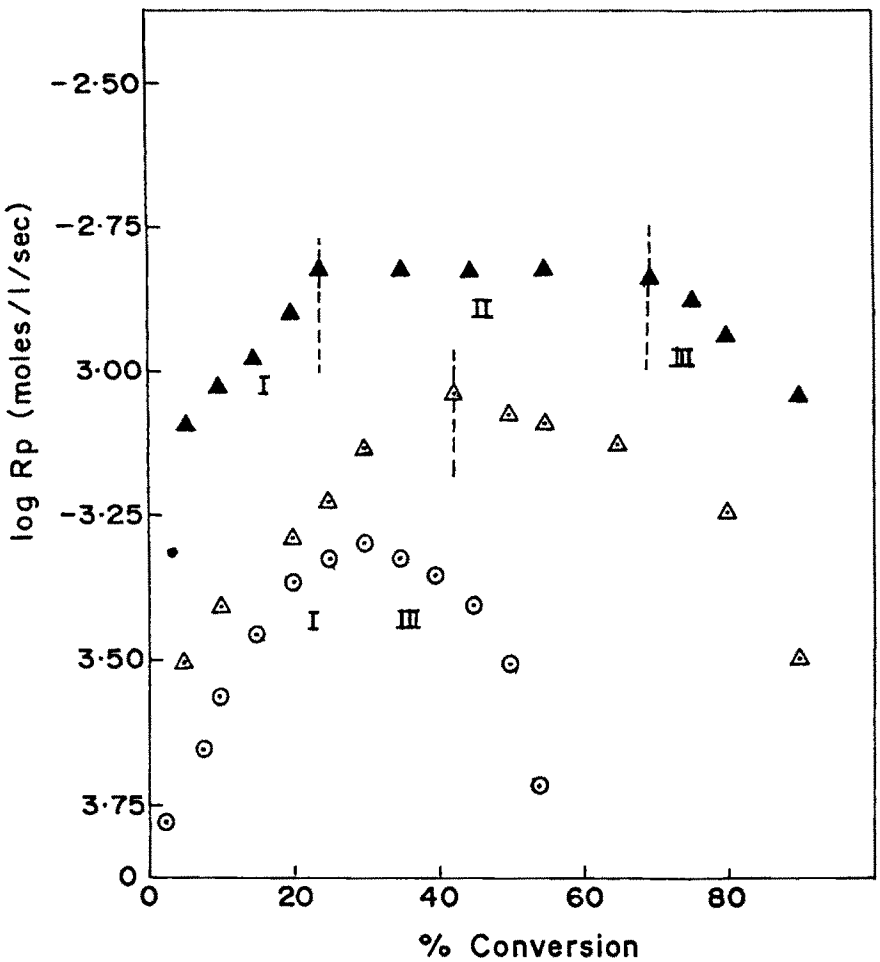

Fig.3·15b Log Rp vs % conversion plots of BA for different Monomer concentration at 1·25 mM KPS at 80° C

⊙ 30 %, △ 41·4 %, ▲ 90·0 % Monomer concentration

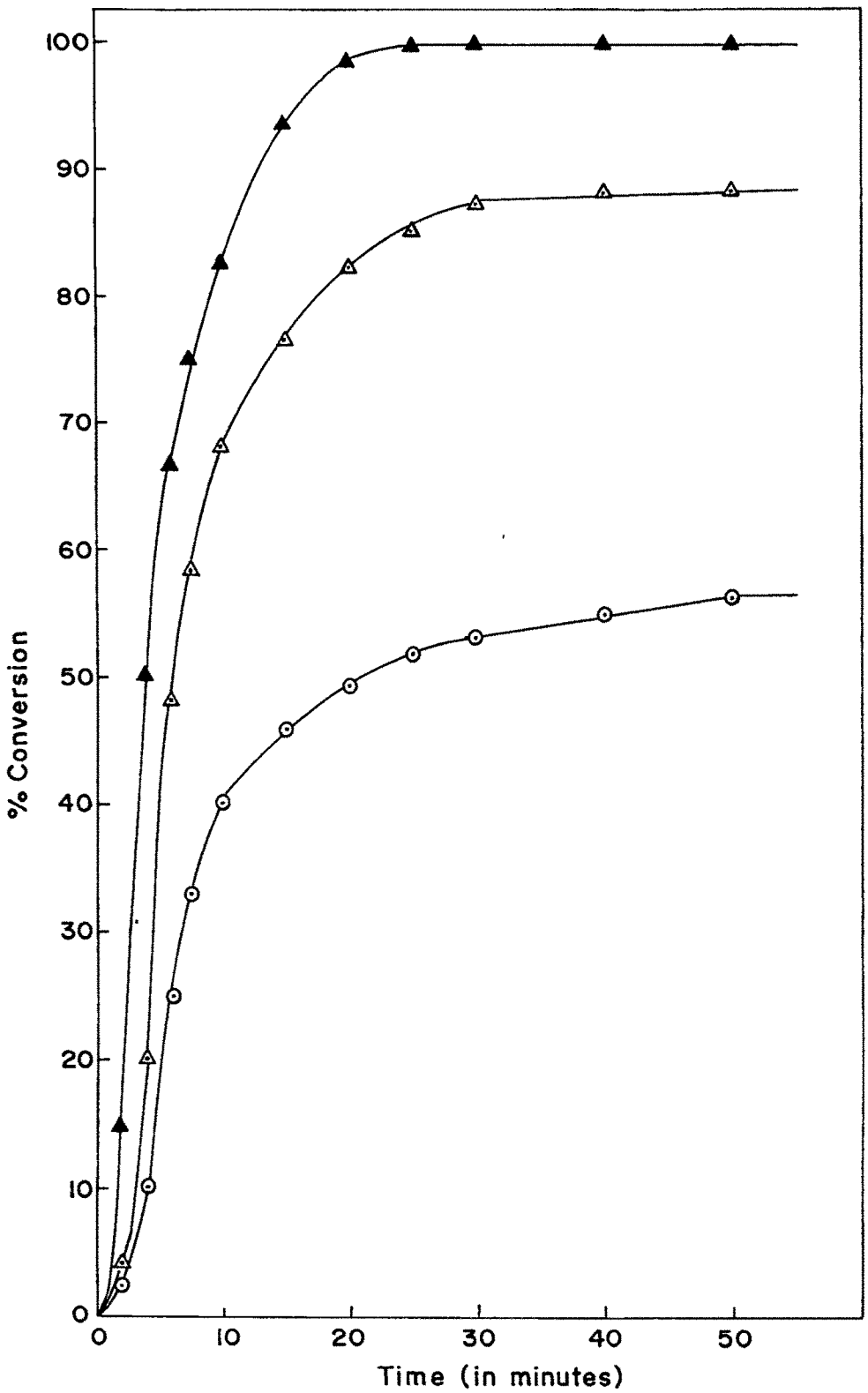

Fig. 3·16 a % Conversion vs Time plots of MMA-BA for different Monomer concentration with 1·25 mM KPS at 80°C
30%, 41·4%, 90·0% Monomer concentration

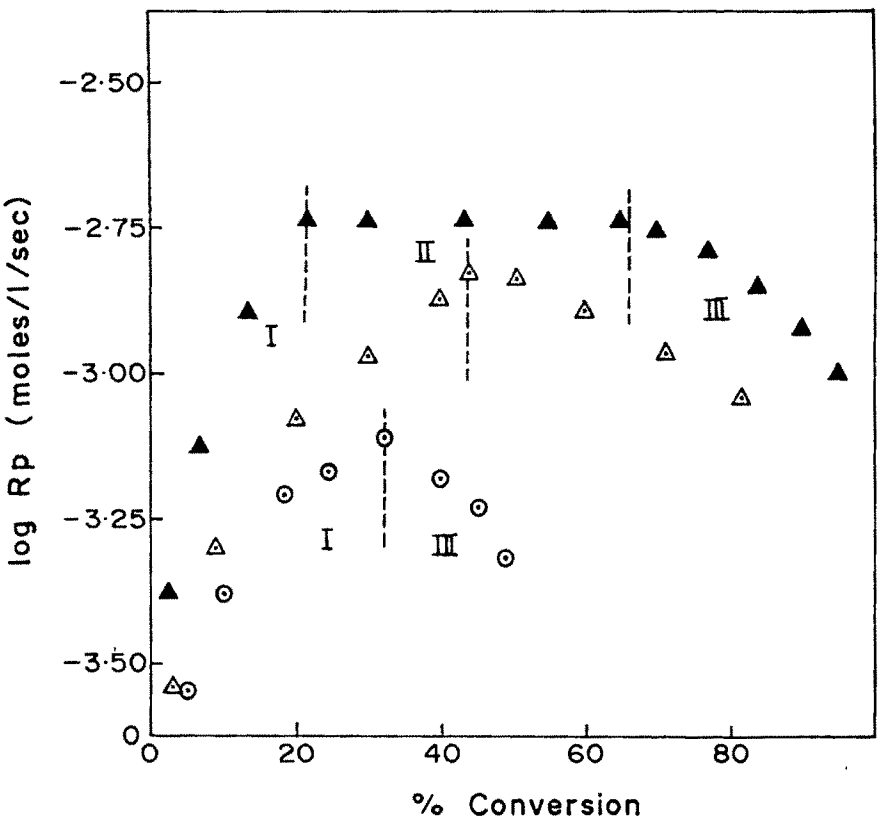

Fig. 3·16b Log Rp vs % conversion plots of MMA-BA for different Monomer concentration with 1·25 mM KPS at 80° C
⊙ 30 %, △ 41·4%, ▲ 90·0% Monomer concentration

intervals for emulsion (92.3% monomer concentration) while two for microemulsion polymerization (41.4% and 30% monomer concentration) as discussed earlier.

3.4 Reactivity Ratios

For the determination of reactivity ratios, copolymers synthesized at lower conversion (<10%) were used. The composition of the monomers in the copolymers was determined from the intensities of the NMR signals for $-OCH_3$ of methyl methacrylate (δ3.60 ppm) and $-OCH_2$ of butyl acrylate (δ4.00 ppm). The mole fraction of the monomers MMA and BA are m_1 and m_2 in the polymer and M_1 and M_2 in the feed respectively. P denotes m_1/m_2 while M denotes M_1/M_2. Several methods[9,10] are available for the determination of reactivity ratios but all depend on careful analysis of the copolymers formed from monomer mixtures using series of compositions. We have used Fineman-Ross method[11] to determine the reactivity ratios of the monomers in microemulsion medium, where the equation used is

$$M - (M/P) = -r_2 + r_1 (M^2/P)$$

From the straight line plot (Fig. 3.17) obtained from M- (M/P) vs M^2/P (Table 3.4) the ordinate intercept gives $-r_2$ and the slope gives r_1. The reactivity ratios r_1 (MMA) and r_2 (BA) were calculated by using above method, and were found to be 0.854 and 0.878 respectively.

Table 3.4 : Parameters for Fineman-Ross equation for the copolmers of MMA and BA.

M (= M_1/M_2 in feed)	P (= m_1/m_2 in polymer)	M-M/P	M^2/P
1.282	1.231	0.241	1.335
1.162	1.125	0.129	1.200
0.888	0.876	-0.125	0.900
0.640	0.634	-0.370	0.646

m_1, m_2 = mole fraction of monomer MMA and BA in polymer.

M_1, M_2 = mole fraction of monomer MMA and BA in feed.

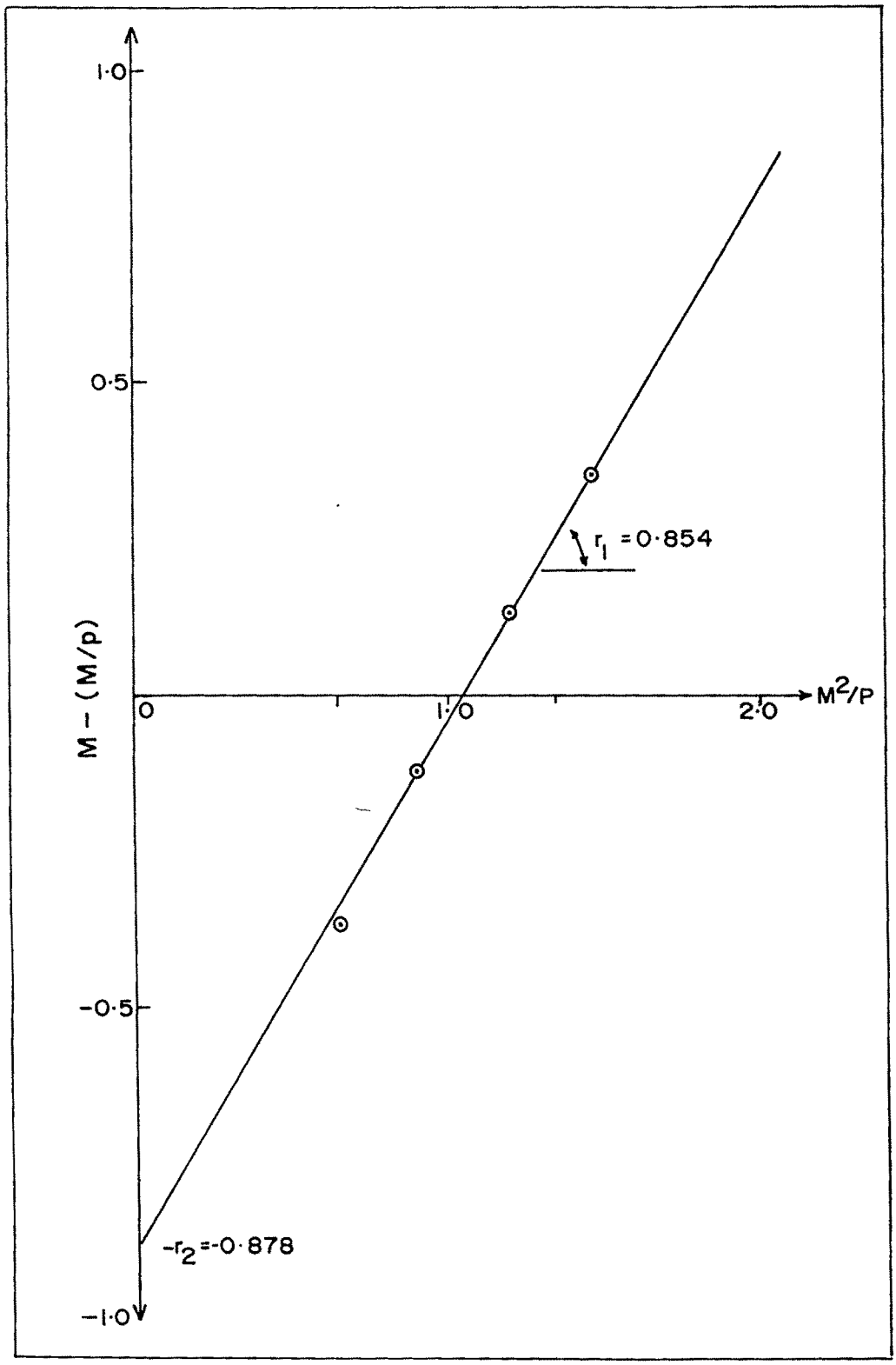

Fig.3·17 Plot for computing r_1 and r_2 according to the Fineman-Ross method

The values obtained in the present study differ greatly from the literature values reported for solution copolymerization of MMA and BA. Bevington and Harris[12] have reported 0.92 and 0.13 whereas Grassie et al[13] have reported 1.88 and 0.43 reactivity ratios for MMA and BA respectively. The observed differences in the reactivities can be attributed to the microenvironment of polymerization medium.

Recent studies of Corpart et al[14] and Kozakiewicz and Lipp[15] also show that the reactivity ratios of various pairs of water soluble monomers are affected by the microenvironment. As seen in Table 3.5 the reactivity ratios of monomer pairs depend upon whether the polymerization reaction medium is solution, emulsion or micro emulsion.

Reactivity values for some monomer pairs :

Table 3.5

Monomer pair	Aqueous solution		Emulsion		Microemulsion	
	r_A	r_B	r_A	r_B	r_A	r_B
Acrylamide(A) Sodium Acrylate (B) pH g	0.95 (ref. 16)	0.30	1.06	0.29	0.95 ±0.15 (ref. 18)	0.89 ±0.15
Acrylamide(A) MADQUAT (B)	0.43 ±0.18 (ref. 19)	2.39 ±0.38	values close to those in solution (ref. 19)		0.74 (ref. 15)	1.23

The product of the reactivity ratios (i.e. r_1 r_2) in the present system is less than one indicating random nature of the copolymers.

3.5 Number of polymer particles

The most difficult parameter to predict in an unseeded emulsion polymerization is the number of polymer particles generated in the system and the variation of this number during the polymerization process. This difficulty arises from the poor understanding of the exact mechanism[20-23]. In many mathematical simulations of emulsion polymerization, this problem was avoided by considering seeded emulsion polymerizations where the polymer particle number is kept constant.

We have calculated the number of monomer droplets initially in the microemulsions and number of polymer particles after 30 minutes of reaction time. For this the following assumptions were made :

(i) Monomer droplets and polymer particles are spherical in shape.

(ii) Initial droplet diameter in microemulsion was ~4 nm.

(iii) Density of monomer and polymer was assumed to be same.

(iv) Concentration of monomer in aqueous phase and in micelles is negligible and

(v) Surface of the microdroplets of monomers is adsorbed with emulsifier.

For MMA, MMA-BA (1:1 w/w) and BA the number of microemulsion droplets were calculated to be 4.77×10^{18}, 4.753×10^{18} and 4.735×10^{18} droplets per ml. Number of polymer particles calculated for PMMA by considering 45 nm average diameter obtained in TEM study at 90% conversion (Table 3.8) for PMMA was 2.29×10^{15} per ml. For PBA, the TEM analysis gave 15 nm average diameter and hence at 87% conversion (Table 3.8) 2.65×10^{17} particles per ml were obtained. For P

(MMA-co-BA) (1:1 w/w) TEM analysis gave 15.6 nm average diameter at 89% conversion (Table 3.8) and hence number of particles were calculated to be 2.34 x 10^{17} particles per ml.

3.6 Characterization

The synthesized polymers PMMA, PBA and P(MMA-co-BA) were characterized by spectral IR, NMR, GPC, thermal (TGA, DSC) and viscometry, whereas polymerized latexes were characterized for the particle size by TEM and Particle Size Analyzer.

Charaterization of Polymers

3.6.1 IR Studies

The IR spectra of PMMA, PBA and copolymer of MMA and BA are given in Figures 3.18 a, b and c. The spectrum of PMMA (Figure 3.18.a) shows sharp distinct bands at 1728 cm^{-1} for C=O stretch and 1274 cm^{-1} for C—O stretch of ester, at 1386 cm^{-1} for C-CH_3 of α-methyl and at 1456 cm^{-1} for -CH_2- bending of β-CH_2 of MMA.

The spectrum of PBA (Figure 3.18.b) shows distinct bands at 1730 cm^{-1} for C=O stretch and at 1278 cm^{-1} for C—O stretch of ester, at 2874 cm^{-1} for C—H stretch of α-C-H and at 1454 cm^{-1} due to -CH_2- bending of β-CH_2 of butyl acrylate.

In Figure 3.18.c for the copolymers of MMA and BA the presence of vibrational stretching bands at 2868 cm^{-1} due to -C-H of butyl acrylate and 1366 cm^{-1} due to C-CH_3 of methyl methacrylate are observed. A sharp band at 1726 cm^{-1} due to C=O, at 1268 cm^{-1} due to C—O of ester and at 1456 cm^{-1} due to -CH_2 are also observed. This indicates the formation of copolymer of MMA and BA.

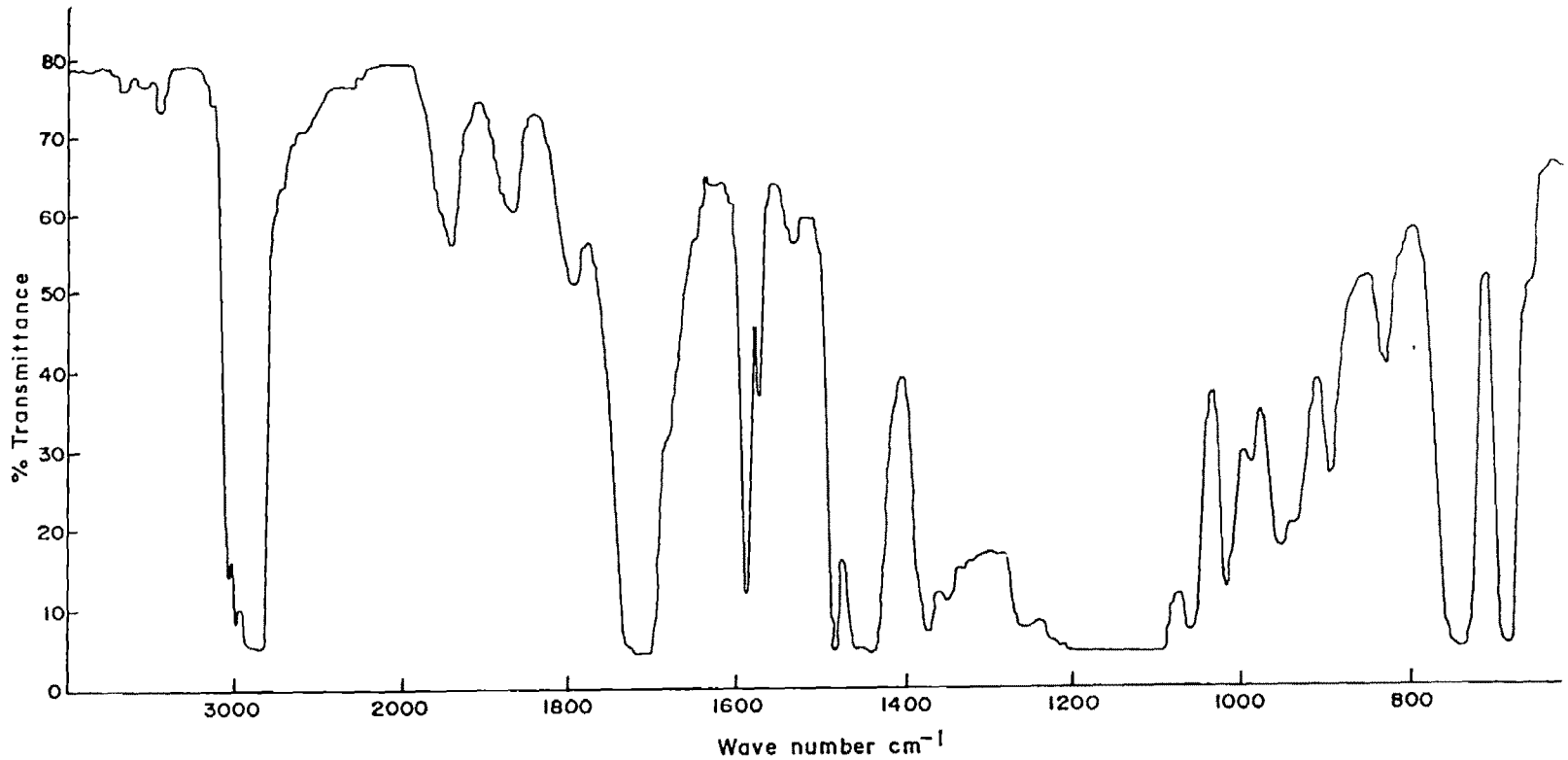

Fig. 3·18 a IR spectra of PMMA synthesized from microemulsion medium

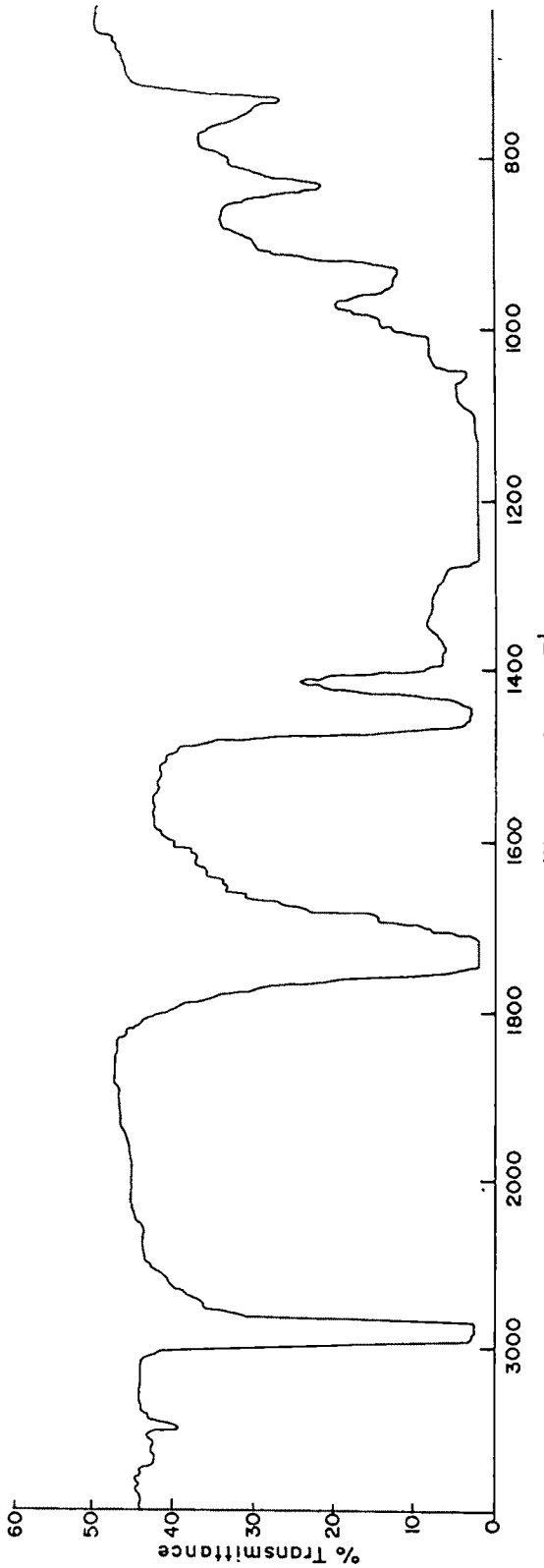

Fig. 3·18b IR spectra of PBA synthesized from microemulsion medium

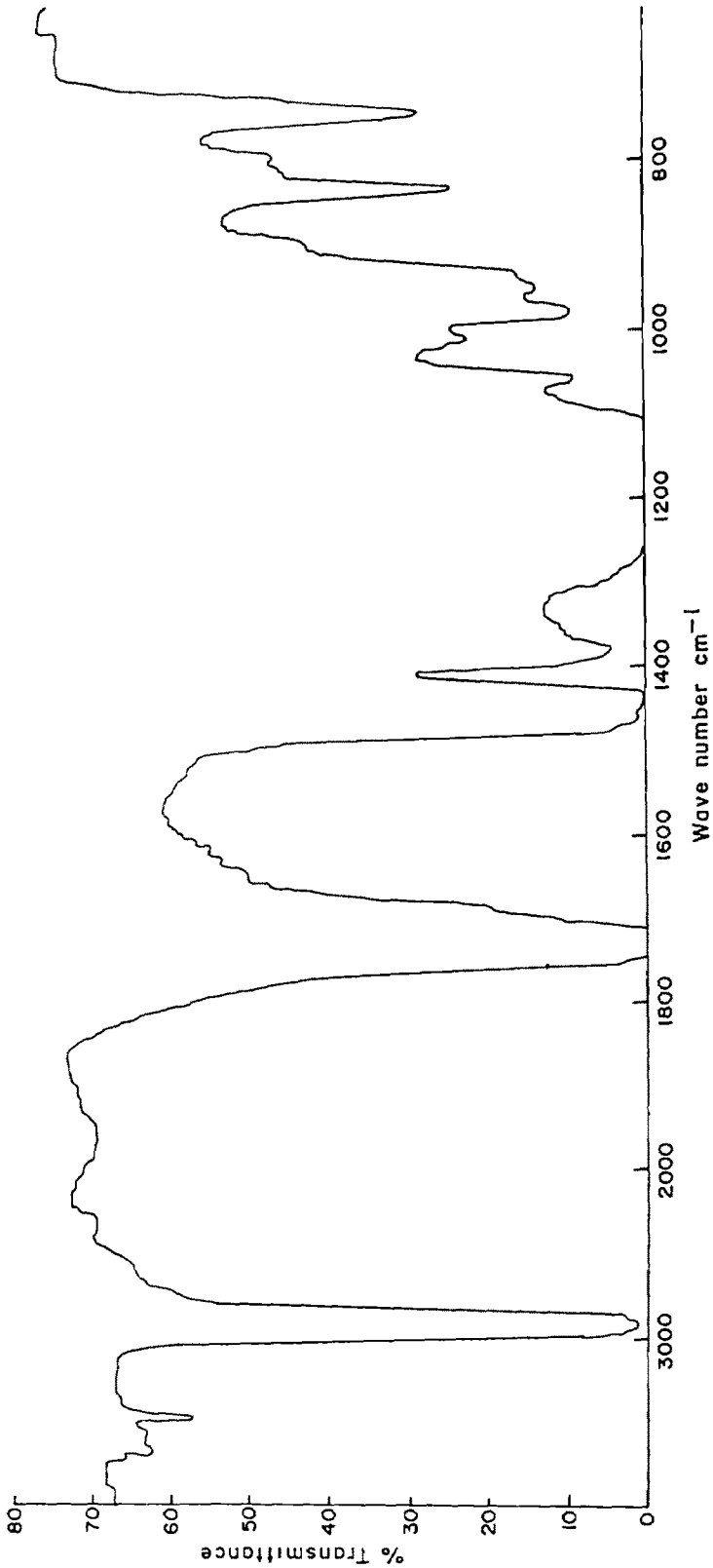

Fig. 3·18 c IR spectra of P (MMA-co-BA) synthesized from microemulsion medium

3.6.2 NMR studies

(i) Poly (methyl methacrylate)

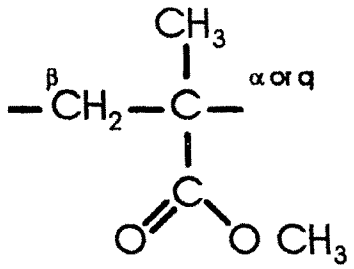

Fig 3.19

^{1}H NMR

The results obtained in high resolution ^{1}H NMR studies of PMMA synthesized in microemulsion and emulsion media are given in Table 3.6 and Figure 3.20 a and b. The NMR signal for methylene protons in predominantly syndiotactic polymer is expected to give a singlet as both the methylene protons will have similar atmosphere in the immediate vicinity. However, the singlet will show broadening due to residual isotactic resonance which complicates the spectrum with fine structure[24]. In the present study NMR signals for ester methyl protons appeared at δ3.5 ppm, β-CH_2 protons at around δ2.0 ppm and α-CH_3 protons between δ1.5 and 0.8 ppm for PMMA synthesized both in emulsion and microemulsion media. However, two signals were observed at δ1.89 and 1.80 ppm which show residual broadening due to β-CH_2 protons of PMMA synthesized in emulsion medium. From the results it can be stated that the polymers show predominance of syndiotacticity.

The PMMA synthesized from microemulsion media shows six peaks around β2.00 ppm due to β-CH_2 (methylene) protons. The methylene resonance in the isotactic polymer is expected to give AB quartet with additional syndiotactic resonance.

Table 3.6 : High resolution ^1H NMR data for homopolymers of MMA synthesized in microemulsion (PMMA-ME) and emulsion media (PMMA-E).

PMMA-ME				PMMA-E			
PEAK	FREQUENCY		INTENSITY	PEAK	FREQUENCY		INTENSITY
	[H_z]	[ppm]			[H_z]	[ppm]	
1.	1796.71	3.5925	20.0	1.	1793.79	3.5866	20.00
2.	1028.75	2.0569	0.25	2.	942.94	1.8854	2.94
3.	1014.63	2.0287	0.29	3.	900.93	1.8014	4.93
4.	969.89	1.9393	0.86	4.	713.84	1.4273	0.86
5.	947.20	1.8939	1.28	5.	599.63	1.1989	0.92
6.	934.96	1.8676	1.04	6.	503.85	1.0074	6.70
7.	902.04	1.8054	3.83	7.	417.18	0.8341	8.78
8.	715.02	1.4297	0.48				
9.	603.10	1.2059	0.56				
10.	506.59	1.0129	4.93				
11.	420.75	0.8413	5.51				
12.	414.43	0.8286	5.45				

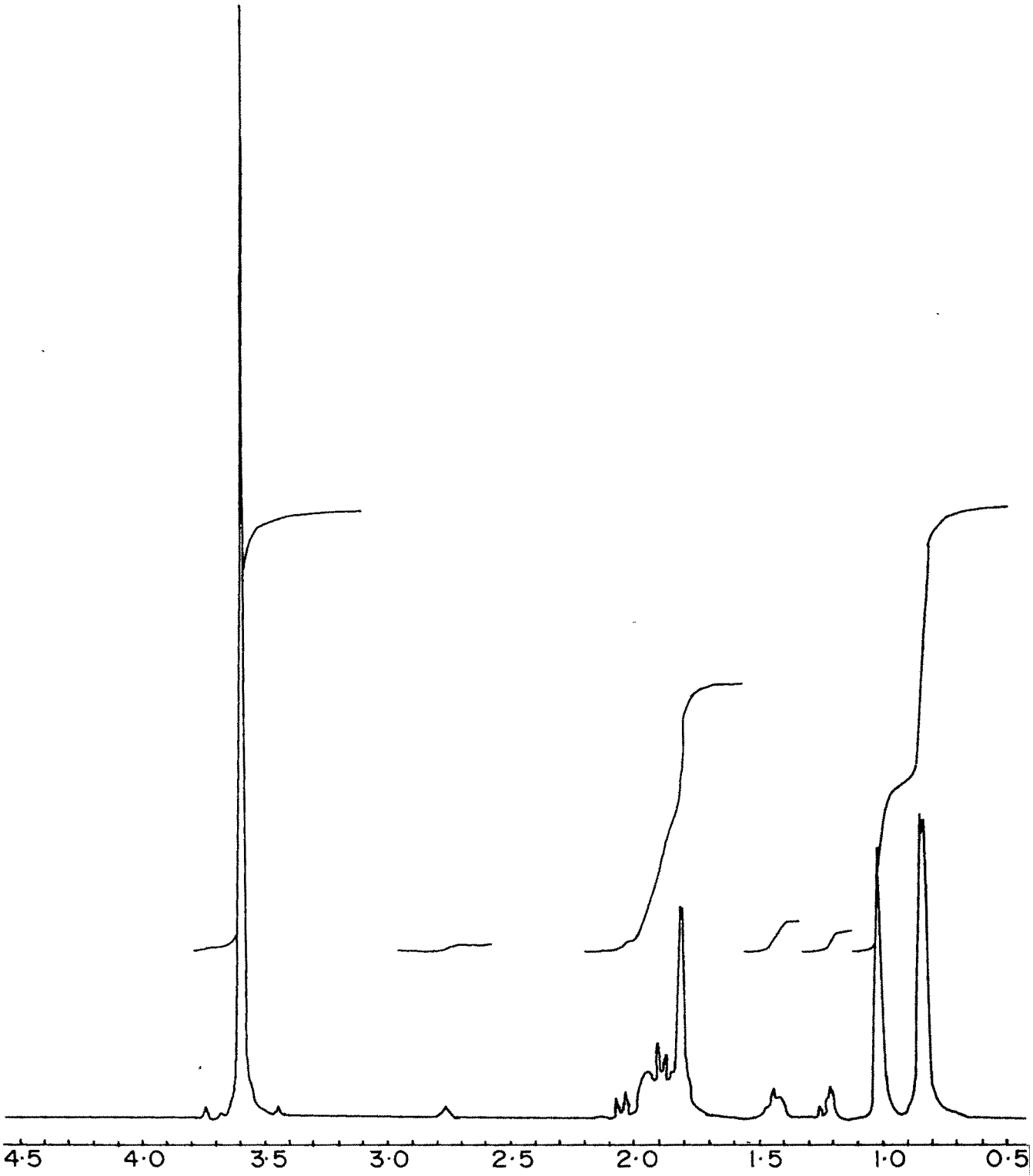

Fig. 3·20 a ^{1}H NMR spectrum of PMMA synthesized in microemulsio medium, at 80° C, 1·25 mM KPS

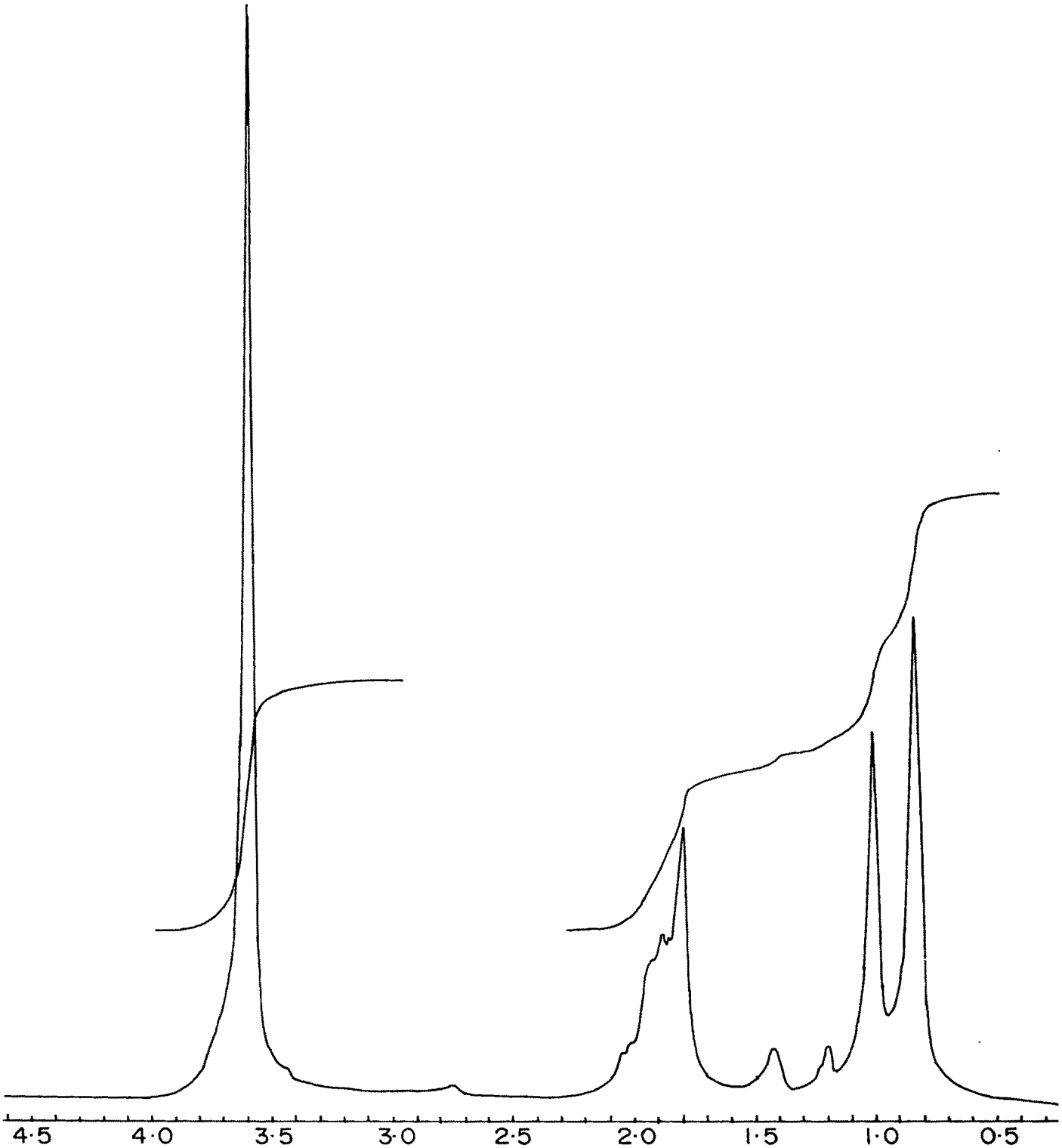

Fig. 3·20 b ^{1}H NMR spectrum of PMMA synthesized in emulsion mediu
80 C, 1·25 m M KPS

This is because each of the two β-CH_2 protons are flanked by either both α-CH_3 or ester methyl protons creating a dissimilar environment in the immediate vicinity. Thus the PMMA synthesized from microemulsion medium has higher percentage of isotacticity than the PMMA synthesized from emulsion medium.

^{13}C NMR

^{13}C NMR spectra of PMMA synthesized in microemulsion and emulsion media were recorded to throw light on the microstructure of the polymer. Figure 3.21 show the spectra of PMMA synthesized in microemulsion. The ester methyl carbon resonance appears around δ51.5 ppm where as β-CH_2 carbon absorbs around δ53.5 ppm α-CH_3 carbon gives three signals in the range of δ17-19 ppm. Quaternary carbon gives three signals in the range of δ44.8-45.7 ppm. Carbonyl carbon gives three sets of signals between δ176.0-177.5 ppm. These values agree with the reported values[25]. From these results rr, mr and mm assignments were made for α-CH_3 and quaternary carbon of PMMA synthesized in emulsion as well as in microemulsion media. From the relative intensities of rr, mr and mm of α-CH_3 and quaternary carbon fractional intensities were calculated. The fractional intensity of mm (isotacticity) for α-CH_3 carbon of PMMA synthesized in microemulsion medium is 22% higher than that for the PMMA synthesized in emulsion medium.

From the fractional intensities of mm, mr and rr, for α-CH_3 the probability of adding meso, Pm (isotactic) and racemic, Pr(syndiotactic) units were determined. The probability of adding meso, isotactic sequence, is 0.2229 for PMMA synthesized from microemulsion and 0.1980 for PMMA synthesized from emulsion.

The probability of adding racemic, syndiotactic sequence is 0.7771 for PMMA synthesized from microemulsion and 0.802 for PMMA synthesized from emulsion for α-CH_3. The values obtained for Pm and Pr indicate that the meso and racemic blocks randomly exist in the polymers synthesized in emulsion and microemulsion media. The higher values of Pr show that the polymers are atactic and are biased towards syndiotacticity. However, the probability of adding meso (isotactic) in PMMA synthesized from microemulsion medium is 12.57 % more than that of emulsion. Similar results are obtained for quaternary carbon of poly methyl methacrylate as shown in Table 3.7.

The values of Pm and Pr were used to calculate the triad sequences by using the following mathematical equations[25]

$$Pm + Pr = 1$$

$$mm = Pm^2$$

$$r\,r = (1\text{-}Pm)^2$$

$$mr/rm = 2\,(1\text{-}Pm)\,Pm$$

Various experimental values of triad sequences determined from ^{13}C NMR spectra and calculated from Bernoullian statistics[26] are given in Table 3.7. The number average sequence length (nm and nr) is defined as the ratio of number of units of specific type to the number of runs containing that units. For meso and racemic additions it is represented as n_m and n_r respectively,

$$n_m = [mm + 1/2\,(mr)] \,/\, 1/2\,(mr)$$

$$n_r = [rr + 1/2\,(mr)] \,/\, 1/2\,(mr)$$

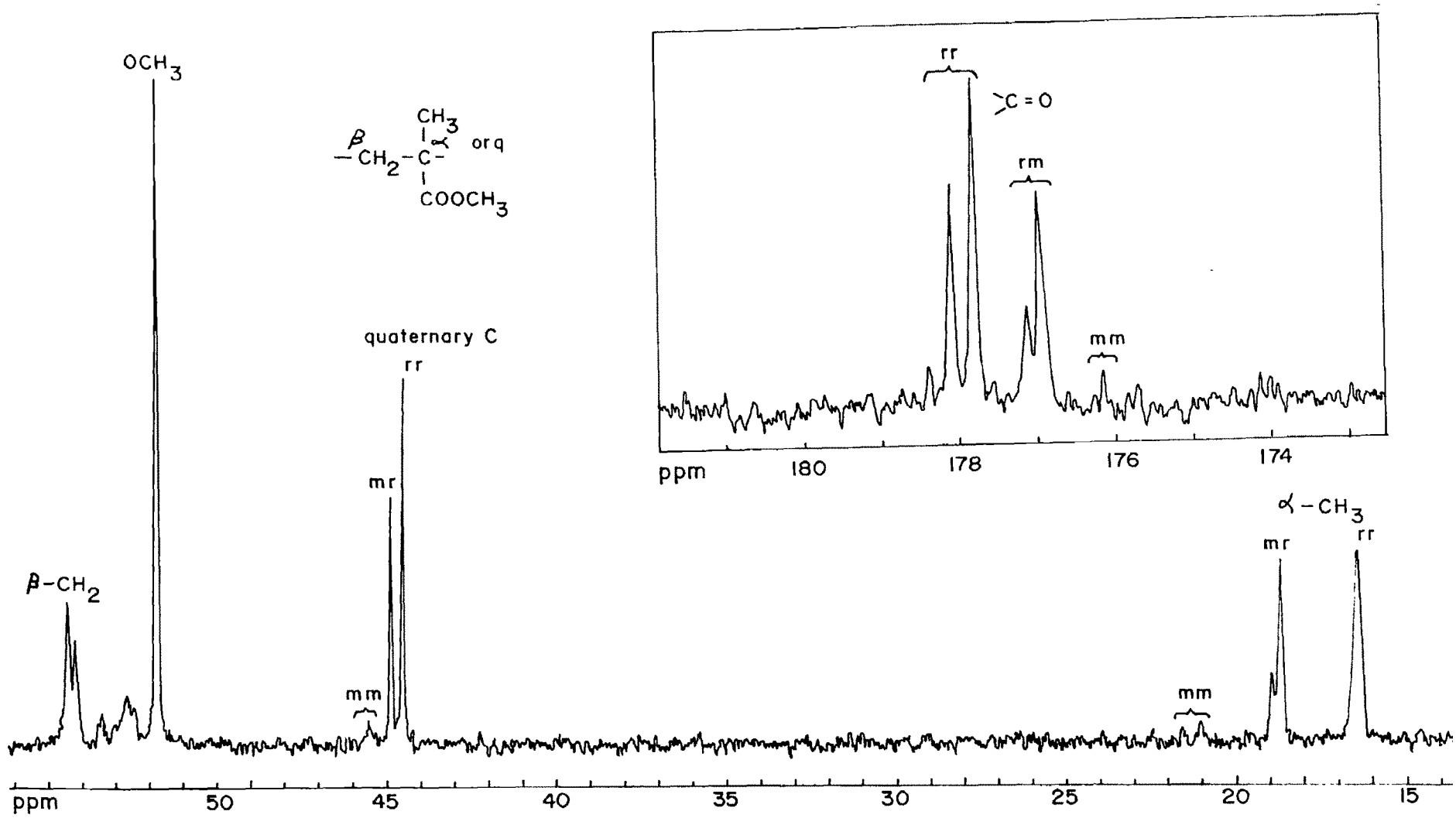

Fig. 3·21 ^{13}C NMR of poly (methyl methacrylate) synthesized in microemulsion medium

Table 3.7 : Triad comonomer distribution for Poly(methyl methacrylate) conforming to Bernoullian Behaviour.

	PMMA-ME		PMMA-E		
	α -Methyl Carbon	Quaternary Carbon	α-Methyl Carbon	Quaternary Carbon	Bernollian Triad (Pm=0.212)
mm	0.050	0.045	0.039	0.041	0.045
mr/rm	0.346	0.334	0.318	0.323	0.334
rr	0.604	0.621	0.643	0.636	0.621
n_m	1.287	1.270	1.247	1.254	1.269
n_r	4.487	4.719	5.044	4.941	4.718

ME = Synthesized in microemulsion

E = Synthesized in emulsion

From the results (Table 3.7) it can be inferred that the number average sequence length for meso configuration (n_m) is larger for the PMMA synthesized in micro emulsion medium where as the number average sequence length for racemic configuration (n_r) is larger for the PMMA synthesized in emulsion medium.

(ii) Poly (butyl acrylate)

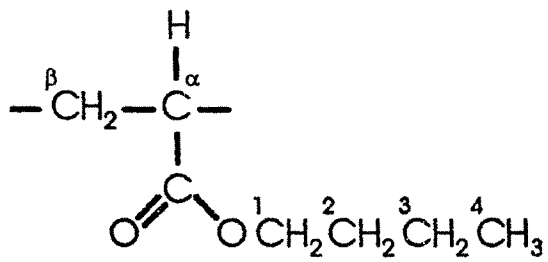

Fig. 3.22

^{1}H NMR

The high resolution ^{1}H NMR for the PBA synthesized in microemulsion medium showed triplet at around δ4.05 ppm for O^1CH_2 protons and a broad signal around δ1.6-2.5 ppm for α–CH and β–CH_2 protons. The C-2 and C-3 methyl protons gave a broad signal at δ1.1-1.6 ppm whereas $^4CH_3$ proton signal appeared at δ0.90 ppm. These values agree with the reported values[27]. The assignment of carbon is given in figure 3.22.

(iii) Poly (methyl methacrylate-co-butyl acrylate)

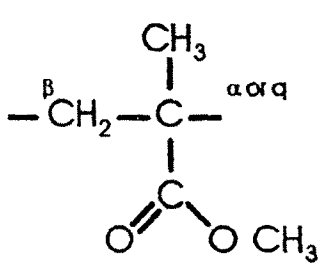

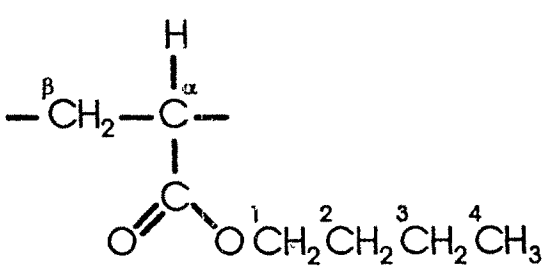

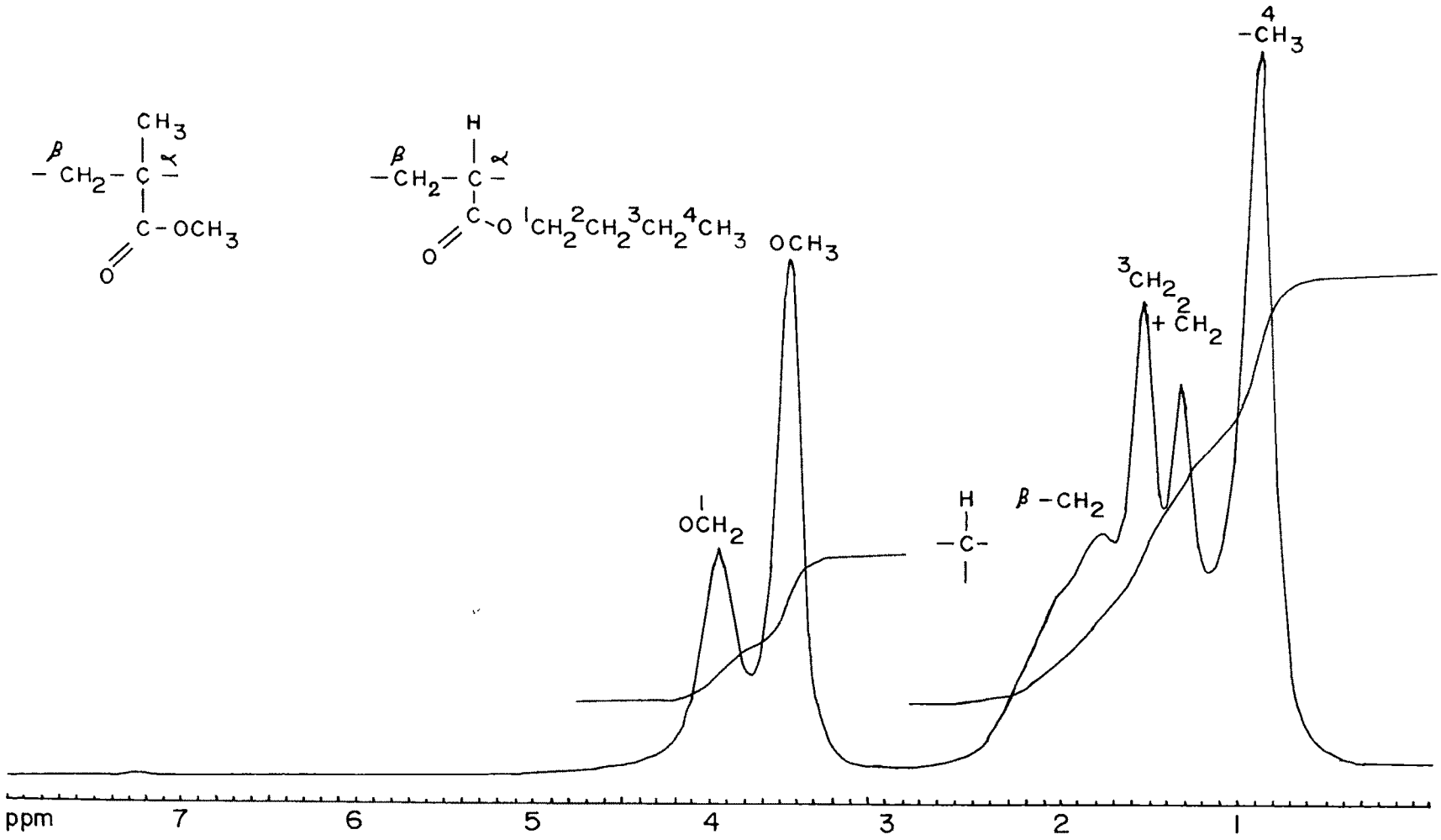

Fig. 3·23 ^{1}H NMR spectrum of poly (methylmethacrylate-co-butyl acrylate)

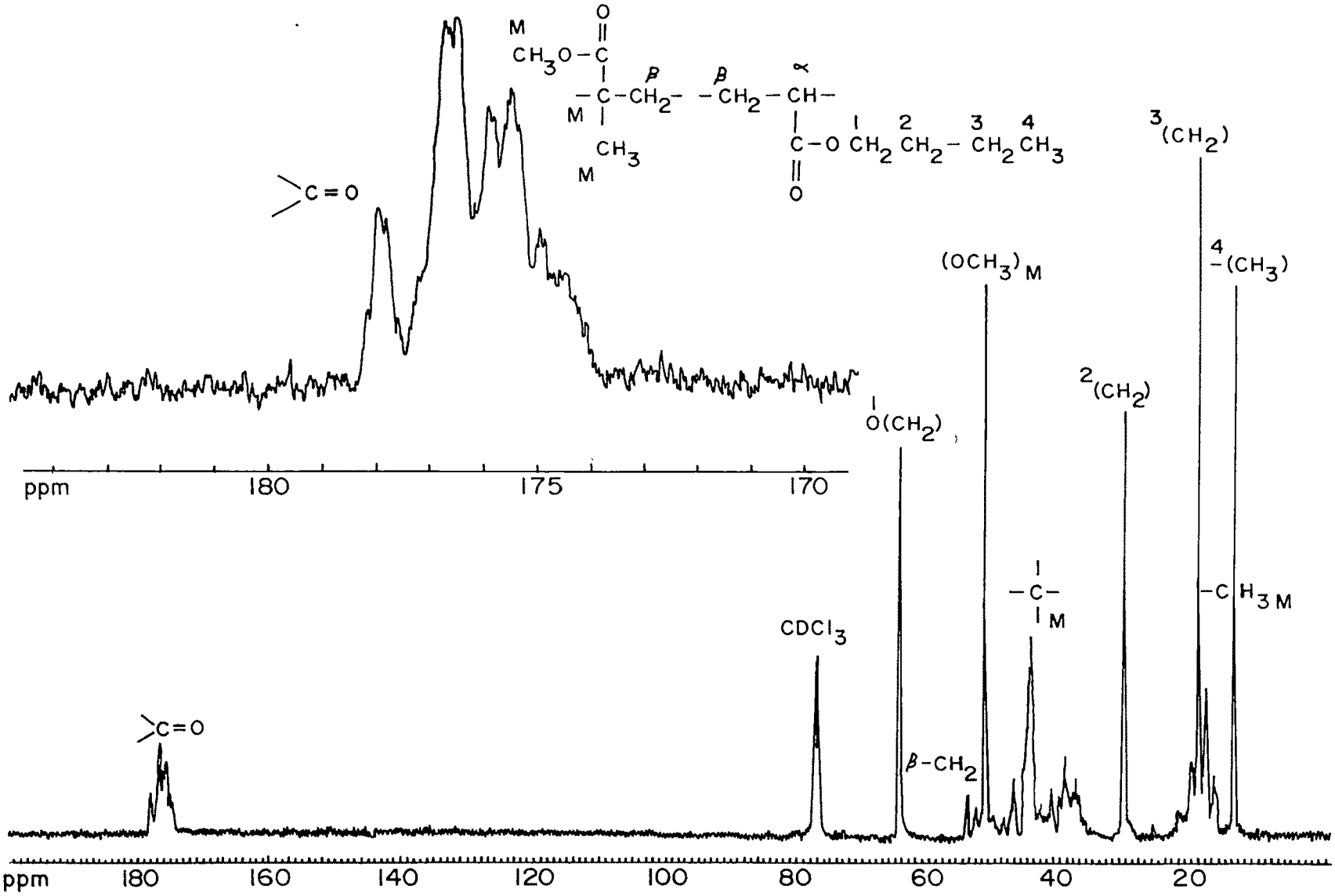

Fig. 3·24 ^{13}C NMR spectrum of poly (methyl methacrylate-co-butylacrylate)

^1H NMR

The results obtained in high resolution ^1H NMR studies of poly (methyl methacrylate-co-butyl acrylate) are given in Figure 3.23. The NMR signals for $-O^1CH_2$ protons appeared at δ3.98 ppm, for α-CH at δ2.09 ppm, for $-^2CH_2$ protons at δ1.58 ppm, for $-^3CH_2$ at δ1.36 ppm and for $-^4CH_3$ at δ0.93 ppm. The signal for ester methyl protons appeared at δ3.58 ppm and for α-CH_3 protons around δ0.8 ppm to δ1.5 ppm. The β-CH_2 protons appeared at around δ1.94 ppm. The signals and their intensities show that copolymer of methyl methacrylate and butyl acrylate has formed in equimolar proportion.

^{13}C NMR

A C^{13} NMR spectrum of P(MMA-co-BA) synthesized in microemulsion medium is shown in Figure 3.24. The carbonyl carbon appeared as multiplet at δ172.7-177.98 ppm and β-CH_2 carbon signal appeared around δ53.5 ppm. The $-O^1CH_2$ carbon signal appeared at δ64.5 ppm, $-^2CH_2$ at δ30.43 ppm and $-^4CH_3$ carbon resonance at δ13.6 ppm. The methyl ester carbon resonance appeared at δ51.6 ppm and quaternary carbon at δ44.0 ppm. The carbon resonance signals for $-^3CH_2$ of butyl acrylate and α-CH_3 of methyl methacrylate in the copolymer appeared around δ17.0-21.0 ppm.

3.6.3 Particle size and particle size distribution

Figure 3.25 illustrate the transmission electron micrographs of polymerized microemulsion latexes synthesized at optimized conditions. Average particle size was calculated by considering at least 100 particles per 25 cm^2 of TEM micrographs. Table 3.8 gives the average particle size of homo- and copolymers

studied. All the systems polymerized from microemulsion media show particles ranging between 10-30 nm except that of methyl methacrylate where particles were ~45 nm in diameter. Smaller particle size 50-100 nm obtained in the emulsion latexes was mainly due to lower concentration of monomer (11%).

In the polymerized microemulsion latexes containing pentanol (0.83%) the average particle size increased to 24.43 nm in comparison to that without pentanol where particle size was 15.63 nm.

Table 3.9 gives the results obtained in the effect of polymerization temperature on average particle size D_n (nm) and intrinsic viscosity, $|\eta|$ dl/g for the copolymers synthesized in emulsion and microemulsion media. With increase in temperature the particle size was observed to increase due to increased mobility of the particles leading to increasing probability of coalescence with other particle. A general trend of decreased intrinsic viscosity and hence molecular weight was observed for both the systems with increased temperature, as expected.

The results obtained in the study of effect of potassium persulphate concentration on average particle size of the latexes and intrinsic viscosity, of the synthesized polymers are given in Table 3.10. The average particle size increase as the initiator concentration increases in case of emulsion polymerization whereas decreases with increased concentration of initiator in case of microemulsion polymerization. This may be due to the difference in the mechanism of polymerization as discussed earlier. In case of microemulsion as initiation takes place at dispersed monomer droplets, increased flux of free radicals simultaneously initiates increased number of monomer droplets. However, in case of emulsion polymerization initiation takes place at monomer swollen micelles.

Table 3.8 : Average particle size, Dn (nm) and $|\eta|$ (dl/g) for the latex synthesized and the polymers.

Temperature 80°C, 1.25 mM KPS using SDS surfactant.

Sample	Av.Particle size, Dn (nm)	$\|\eta\|$ dl/g	% monomer conversion
1. P(MMA) ME	45.0	0.751	91
2. P(MMA) E	75.0	0.975	100
3. P(BA) ME	15.0	1.400	87
4. P(BA) E	95.0	1.725	100
5. P(MMA-co-BA) ME	15.6	1.137	89
6. P(MMA-co-BA) E	49.6	0.932	100
7. P(MMA-co-BA) ME Pentanol	24.4	1.034	

ME = synthesized in microemulsion

E = synthesized in emulsion

Table 3.9 : Effect of Temperature on Average particle size, Dn (nm) and $|\eta|$ (dl/g) for the copolymer latex synthesized and polymers with 0.5 mM KPS, using SDS as surfactant.

	Temperature			
	80°C		90°C	
	Dn (nm)	$\|\eta\|$ (dl/g)	Dn (nm)	$\|\eta\|$ dl/g)
PMMA-BA ME	16.33	1.124	25.73	0.653
PMMA-BA E	48.00	0.925	48.80	0.553

ME = synthesized in microemulsion

E = synthesized in emulsion

Table 3.10 : Effect of potassium persulphate concentration on average particle size (nm) and $|\eta|$ (dl/g) for the latex synthesized and the polymer at 80°C using SDS as surfactant.

	Potassium persulphate concentration					
	0.1 mM		0.5 mM		1.25 mM	
	Dn (nm)	$\|\eta\|$ dl/g	Dn (nm)	$\|\eta\|$ dl/g	Dn (nm)	$\|\eta\|$ dl/g
P(MMA-co-BA) ME	19.22	1.040	16.33	1.124	15.63	1.137
P(MMA-co-BA) E	43.00	0.890	48.00	0.920	49.60	0.960

ME = synthesized in microemulsion

E = synthesized in emulsion

Table 3.11 : Effect of time on average particle size, Dn (nm) and $|\eta|$ dl/g for the latex synthesized and the polymers [composition water 76.1 %, SDS 14.0 % and MMA/BA (1:1W/W) at 80°C 1.25 mM KPS concentration].

Sample	Time (min.)	% conversion	Dn (nm)	$\|\eta\|$ dl/g
PMMA-BA ME	2	4.0	7.12	1.12
	4	20.0	11.72	1.16
	15	76.5	15.40	1.13
	30	87.0	15.63	1.14
	60	88.0	15.63	1.35

ME = synthesized in microemulsion

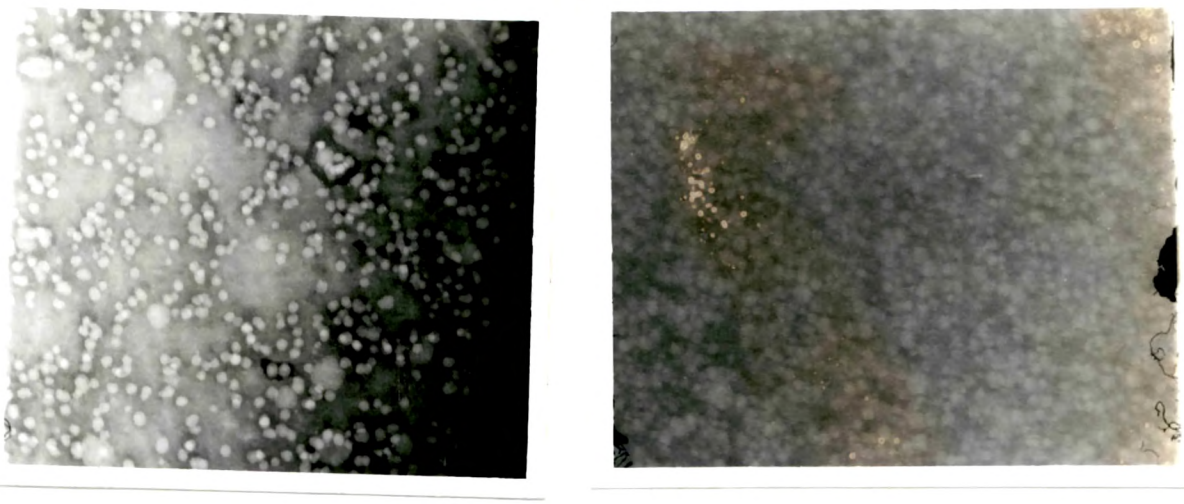

(a) (b)

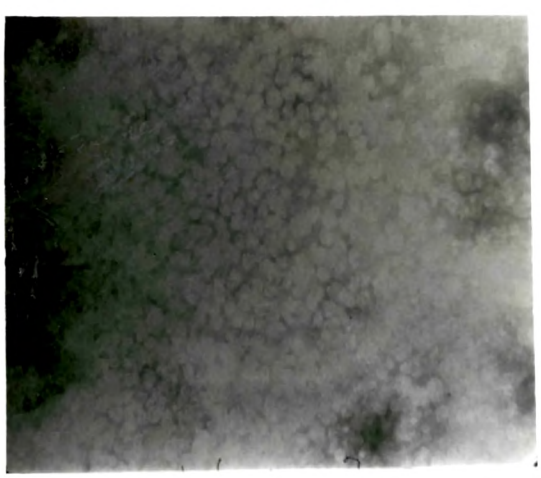

(c)

Fig. 3.25 : Transmission electron micrograph of studied samples

(a) PMMA-ME magnification X80000

(b) P(MMA-co-BA)-ME magnification X80000

(c) PBA-ME magnification X80000

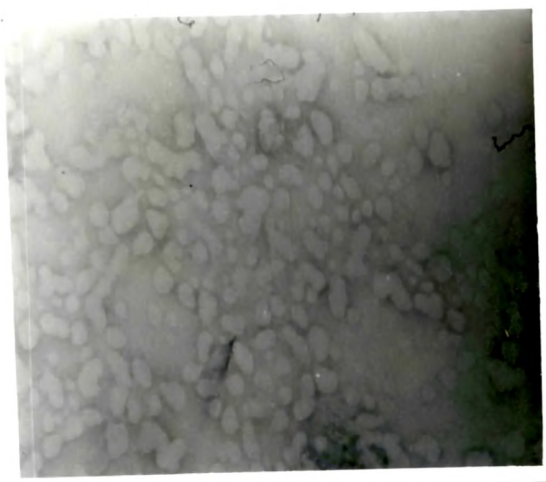

(d)

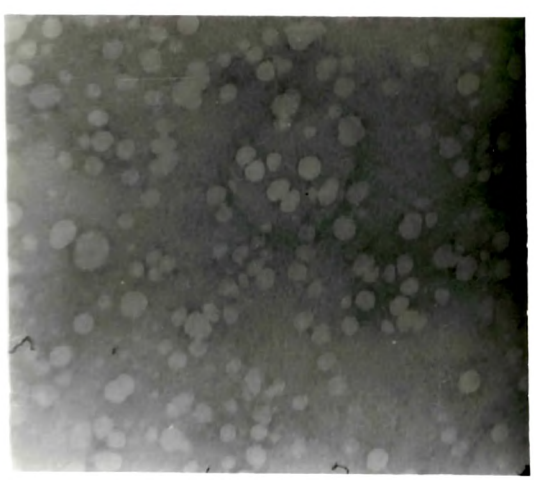

(e)

Fig 3.25 : Transmission electrom micrograph of studied samples

(d) P(MMA-co-BA) ME using Pentanol and KPS as initiator at 80°C magnification X80000

(e) P(MMA-co-BA) ME using APS at 80°C magnification X80000

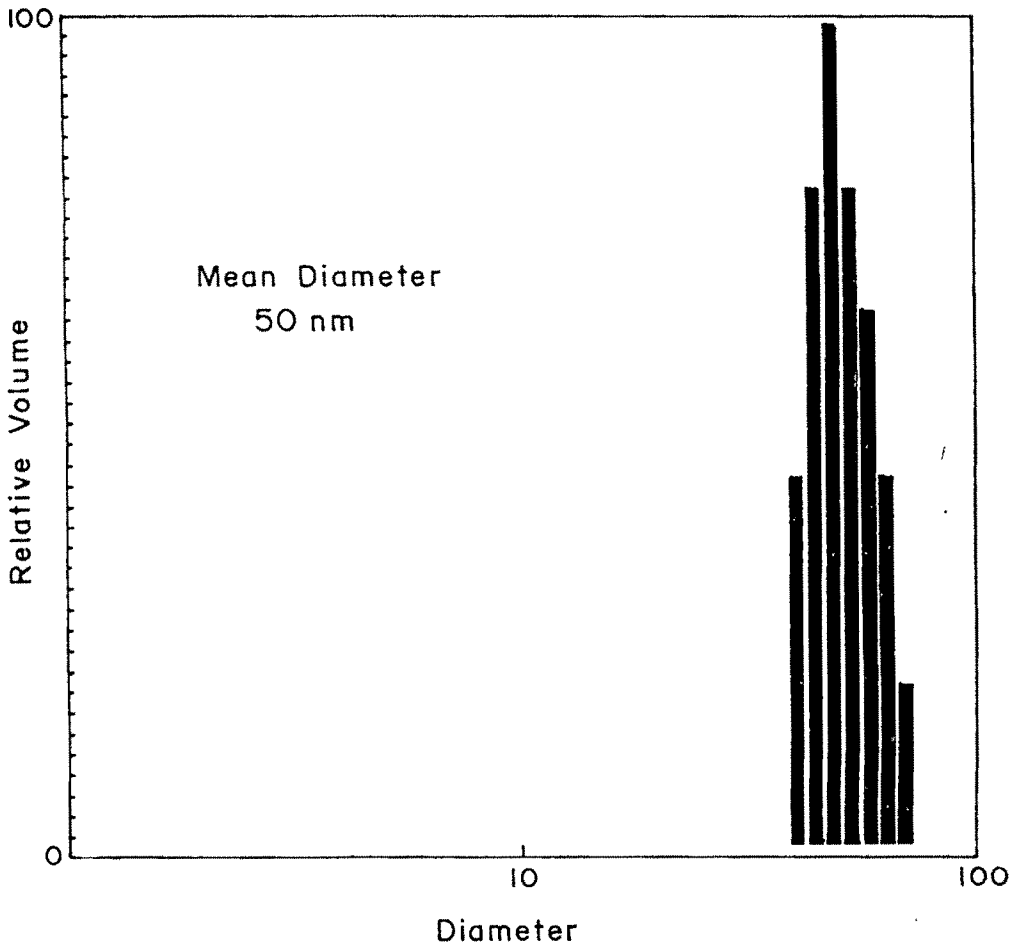

Fig. 3·26 Particle size distribution of PMMA microemulsion latex synthesized from microemulsion medium with 1·25 m M KPS at 80° C

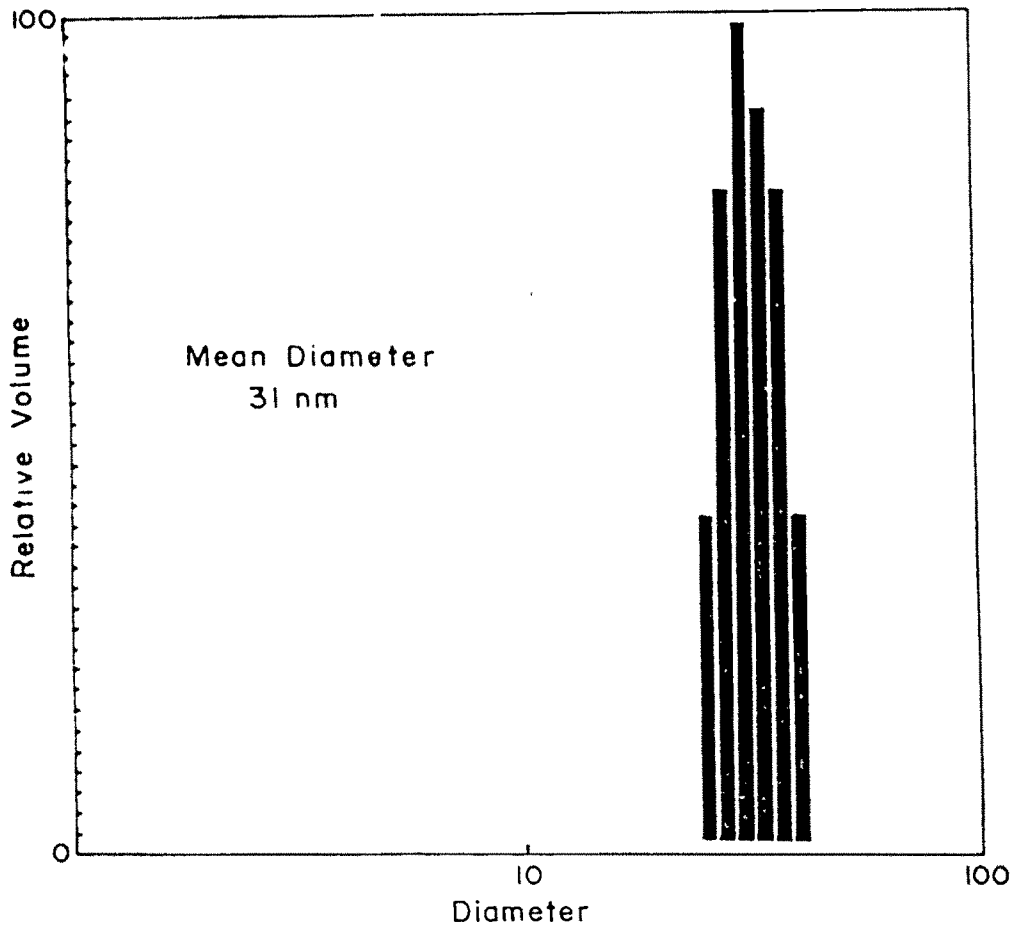

Fig. 3·27 Particle size distribution of P (MMA-co-BA) microemulsion latex synthesized from microemulsion medium with 1·25 mM KPS and at 80° C

Hence increased flux of free radicals increases the number of growing polymer chains in the same monomer swollen micelles. As the number of growing polymer chains is more in the same monomer swollen particle their growth leads to increased particle size.

Table 3.11 shows the effect of time on average particle size and intrinsic viscosity. With increasing time particle size increases and attains a constant size when maximum conversion is achieved.

Figure 3.26 and 3.27 show the particle size distribution plots from light scattering of polymerized microemulsion of methyl methacrylate and methyl methacrylate-butyl acrylate. The particle size by means of light scattering technique gave mean diameter 50 nm for polymerized microemulsion of MMA. It was found that 10% of the particles are below 37 nm, 25% below 42 nm, 50% below 47 nm, 75% below 54 nm and 90% below 61 nm. For P(MMA-co-BA) the mean diameter was 31 nm with 10% particles below 16 nm, 25% below 20 nm, 50% below 25 nm, 75% below 32 nm and 90% below 40 nm.

3.6.4 GPC Analysis

The molecular weights of the selected samples were determined by GPC as discussed earlier in section 2.10.3. Table 3.12 shows the number average, weight average molecular weights and polydispersity of these samples. PMMA synthesized from microemulsion and emulsion media shows high molecular weights. The polydispersity for both types of polymers were observed to be higher though for microemulsion based polymer it is comparatively lower. Similar results

Table 3.12 : Weight average, Number average molecular weights and polydispersity by GPC for representative samples at 80°C with 1.25 mM KPS concentration (ME in sample code denotes microemulsion medium while E denotes emulsion medium).

Sample	$\overline{M}_w$ (x 10^{-5})	$\overline{M}_n$ (x 10^{-5})	Polydispersity
P(MMA) ME	8.03	1.72	4.66
P(MMA) E	9.76	1.30	7.48
P(MMA-co-BA) ME Pentanol	8.11	4.08	1.98
P(MMA-co-BA) ME	8.68	4.78	1.81
P(MMA-co-BA) E	6.07	2.39	2.53

were observed by Gan et al[6] and Feng and Ng[8] for microemulsion polymerization of methyl methacrylate. The high polydispersity of both the polymers may be due to the possibility of two types of nucleations

(i) nucleation in monomer droplets/monomer swollen micelles and

(ii) homogenous nucleation

operating simultaneously. Comparatively lower polydispersity for microemulsion based polymer indicates predominance of nucleation in monomer droplets in microemulsion polymerization. The copolymer samples of MMA and BA (1:1 w/w) synthesized through microemulsion route show much lower polydispersity than that through emulsion. The molecular weights of the products synthesized by both the techniques were high.

When pentanol is used as a cosurfactant in the microemulsion the polymer synthesized shows lower molecular weight with higher polydispersity than the polymers synthesized from microemulsion without pentanol. This may be due to the increased probability of chain transfer reactions due to the presence of pentanol.

3.6.5 Thermal studies

(i) Thermo gravimetric analysis

Dynamic thermogravimetric analysis was carried out using nitrogen atmosphere as described in section 2.10.4. The experimental conditions are identical for all the samples. Examination of the thermograms of the homopolymers and copolymers reveal that all the polymers are stable upto 250°C (Table 3.13). T_1, T_{10}, T_{50} and T_{90} are the decomposition temperatures corresponding to 1%, 10%, 50 % and 90 %

Table 3.13 : TGA results of representative samples synthesized at 80°C using 1.25 mM KPS. (ME in sample code denotes microemulsions while E denotes emulsion medium).

Sample	T_1	T_{10}	T_{50}	T_{90}	Activation Energy
		(°C)			(KJ mol^{-1})
PMMA ME	270	328	378	400	44.81
PMMA E	280	355	390	412	65.84
PMMA-BA ME	302	362	395	422	53.17
PMMA-BA E	280	355	390	412	106.05
PMMA-BA ME Pentanol	308	358	380	414	70.73

T_1, T_{10}, T_{50} and T_{90} are the decomposition temperature corresponding to 1%, 10%, 50%, and 90% weight loss.

weight loss. It is observed that PMMA and p(MMA-co-BA) synthesized in microemulsion and emulsion decompose in a single step. Babu et al[28] has also reported one stage thermal degradation of PMMA and copolymers of MMA and vinyltriacetoxy silane.

The activation energies of thermal breakdown were calculated by integrated Broido's method[29] using equation

$$\ln [\ln 1/Y] = (-E/R)(1/T) + \text{constant}$$

The results are given in Table 3.13. The activation energy calculated for PMMA synthesized in microemulsion medium is lower than that from emulsion medium. Same is true for copolymer of methyl methacrylate and butyl acrylate. This indicates the difference in internal structure of PMMA and copolymer of MMA and BA synthesized by microemulsion and emulsion techniques. As less energy is required to degrade the PMMA synthesized in microemulsion medium, the product is expected to have higher percentage of isotacticity in comparison with PMMA synthesized in emulsion medium. This observation supports the results obtained in NMR studies.

(ii) Differential scanning calorimetry

DSC thermogram results for poly (methyl methacrylate) synthesized in microemulsion and emulsion media are given in Table 3.14. The heating rate was 10°C/minute. The glass transition temperature for PMMA synthesized from microemulsion medium is lower than that from emulsion medium. It is also

Table 3.14 DSC results of P(MMA) synthesized in microemulsion medium (PMMA ME) and in emulsion medium (PMMA E) at 80°C using 1.25 mM KPS.

	T_g(°C)	T_c(°C)	ΔH_c(J/g)	T_m(°C)	ΔH_f(J/g)
PMMA ME	90.5 (38°C)[30]	134.58	47.21	212.9 (<160°C)[30]	-
PMMA E	111.0 (105°C)[30]	157.6	9.2	242.35 (>200°C)[30]	31.43

observed in the literature[30] that glass transition temperature (Tg) for atactic and syndiotactic PMMA are higher (105°C) than for isotactic PMMA (38°C). Similarly the melting temperature for isotactic product was reported to be lower (160°C) than that for syndiotactic (200°C). The results obtained are due to the difference in internal structure of the PMMA synthesized by emulsion and microemulsion polymerization. This has been also reflected in our TGA and NMR study.

3.6.6 Viscosity Studies

The effect of temperature on the hydrodynamic behaviour of dilute polymer solutions can be studied through temperature dependence of the intrinsic viscosities (Figure 3.28 and Table 3.15). It is observed that the intrinsic viscosity shows very little change with increase in temperature. $|\eta|$ vs temperature plots are linear with the negative slope indicating that the polymer coils are not swelling to a great extent. The well known Frenkel-Eyring equation for viscous flow was used for the computation of thermodynamic parameters for viscous flow

$$\eta = (Nh/V)\exp\Delta G^{\#}_{vis}/RT$$

Where V is the molar volume and other symbols have their usual meaning. This equation can be written as,

$$\ln \eta V/Nh = \left(\Delta H^{\#}_{vis}/RT\right) - \left(\Delta S^{\#}_{vis}/R\right)$$

Where $\Delta H^{\#}_{vis}$ and $\Delta S^{\#}_{vis}$ are enthalpy and entropy for the viscous flow. Representative plots of ln ($\eta V/Nh$) vs T^{-1} are given in Figure 3.29 which show a linear relationship for P(MMA) and P(MMA-co-BA) synthesized through emulsion and microemulsion media. The calculated values of entropy $\Delta S^{\#}_{vis}$ enthalpy $\Delta H^{\#}_{vis}$ and free energy $\Delta G^{\#}_{vis}$ of activation for the viscous flow of polymers in solutions are given in Table 3.16. The small values of entropy $\Delta S^{\#}_{vis}$ and enthalpy $\Delta H^{\#}_{vis}$ indicate no cross-linking in the polymer. The free energy of activation of the viscous flow, $\Delta G^{\#}_{vis}$, is reasonably independent of temperature.

The intramolecular expansion factor for the P(MMA) and P(MMA-co-BA) in solution was calculated from the intrinsic viscosity measurements in θ solvent at 25°C using $\alpha^3 = |\eta|/|\eta|_\theta$ relationship. The spacial arrangement in the actual molecule is assumed to be expanded uniformly by the factor α as a result of intramolecular interaction. Table 3.17 shows the θ solvent composition and intramolecular expansion factor. Though $\overline{M}_V$ is smaller for P(MMA) from microemulsion system, θ solvent composition requires more solvent than that for P(MMA) from emulsion system. This may be because of the rigid structure of P(MMA) synthesized in microemulsion medium whereas in case of PMMA synthesized in emulsion medium the polymer chain is relatively of free nature. The smaller intramolecular expansion factor also indicates a more rigid meso structure for polymer synthesized in microemulsion medium. This also supports our NMR and thermal analysis results.

The relative viscosity data were used to calculate the equivalent hydrodynamic volume (voluminosity V_e), a measure of size of a solvated polymer molecule at infinite dilution (Table 3.18). It was recently used to determine the shape of

Table 3.15 : Intrinsic viscosities of sample synthesized in microemulsion and emulsion media at 80°C using 1.25 mM KPS.

Sample	$\lvert\eta\rvert$ dl/g			
	15°C	20°C	25°C	30°C
P(MMA) ME	0.753	0.752	0.751	0.750
P(MMA) E	0.995	0.985	0.975	0.965
P(MMA-co-BA) ME	1.162	1.150	1.137	1.124
P(MMA-co-BA) E	0.950	0.941	0.932	0.922

ME = synthesized in microemulsion

E = synthesized in emulsion

Table 3.16 : Entropy $\Delta S^{\#}_{vis}$, Enthalpy $\Delta H^{\#}_{vis}$ and Free Energy $\Delta G^{\#}_{vis}$ of Activation for the viscous flow of polymers, in solutions, synthesized at 80°C using 1.25 mM KPS.

Sample	$\Delta H^{\#}_{vis}$ (KJ mol^{-1})	$\Delta S^{\#}_{vis}$ (KJ mol^{-1} deg^{-1})	$\Delta G^{\#}_{vis}$ (KJ mol^{-1} deg^{-1})			
	In Acetone	In Acetone	15°C	20°C	25°C	30°C
PMMA ME	0.16	152	43.93	44.69	45.45	46.20
PMMA E	1.24	150	44.44	45.19	45.94	46.69
PMMA-BA ME	1.55	150	44.85	45.60	46.35	47.11
PMMA-BA- E	1.20	149	44.21	44.96	45.70	46.45

ME = synthesized in microemulsion

E = synthesized in emulsion

Table 3.17 : Intramolecular expansion factor and θ-solvent compositions of representative samples synthesized at 80°C using 1.25 mM KPS.

Sample	θ-solvent composition				
	Acetone %	Methanol %	$\lvert\eta\rvert$	$\lvert\eta\rvert_\theta$	α
PMMA ME	56.90	43.10	0.751	0.587	1.085
PMMA E	53.70	46.30	0.975	0.575	1.192
PMMA-BA ME	45.45	54.55	1.137	0.448	1.364
PMMA-BA E	41.67	58.33	0.932	0.281	1.491

ME = synthesized in microemulsion

E = synthesized in emulsion

Table 3.18 : Hydrodynamic volumes V_e, ml/g, of samples synthesized in Microemulsion and emulsion media at 80°C using 1.25 mM KPS.

Sample	Temperature			
	15°C	20°C	25°C	30°C
PMMA ME	28.45	28.32	28.10	27.95
PMMA E	37.70	37.50	37.27	37.05
PMMA-BA ME	44.44	43.92	43.32	42.40
PMMA-BA E	36.92	36.56	36.00	35.50

ME = synthesized in microemulsion

E = synthesized in emulsion

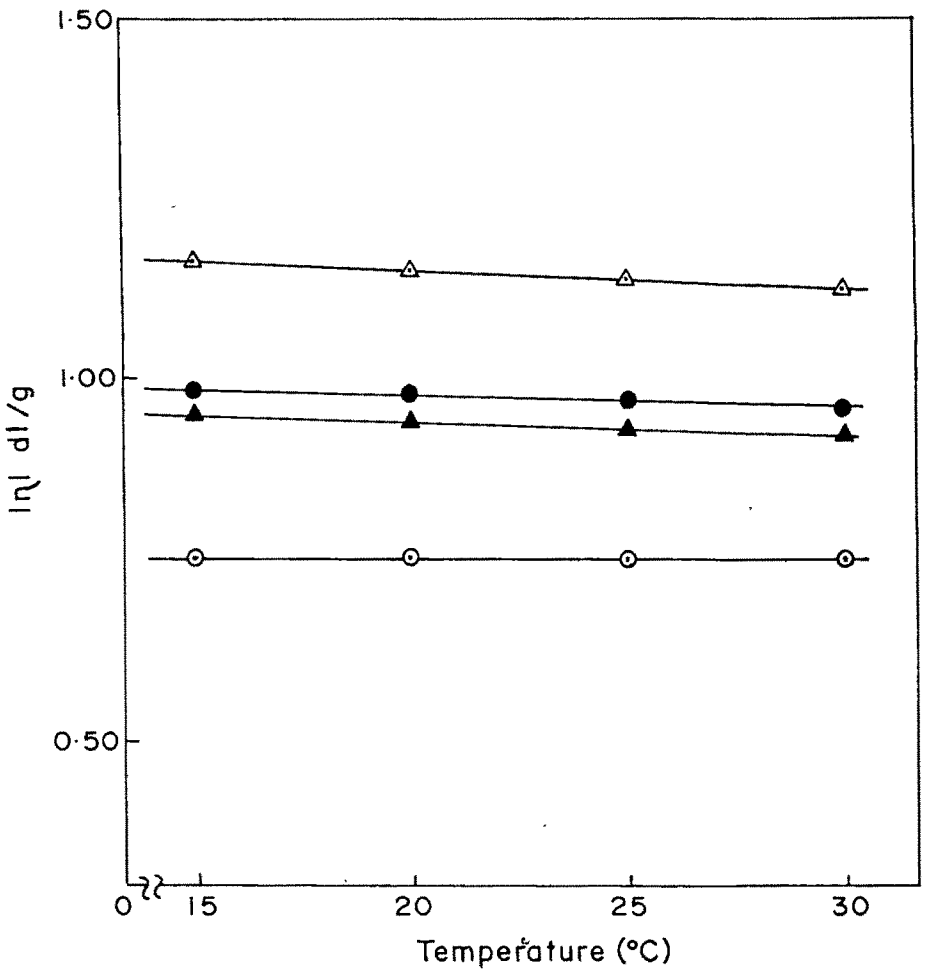

Fig. 3·28 Inη vs Temperature plots for representative samples;

⊙ PMMA synthesized in microemulsion ;

● PMMA synthesized in emulsion ;

△ P (MMA-co-BA) synthesized in microemulsion;

▲ P (MMA-co-BA) synthesized in emulsion ;

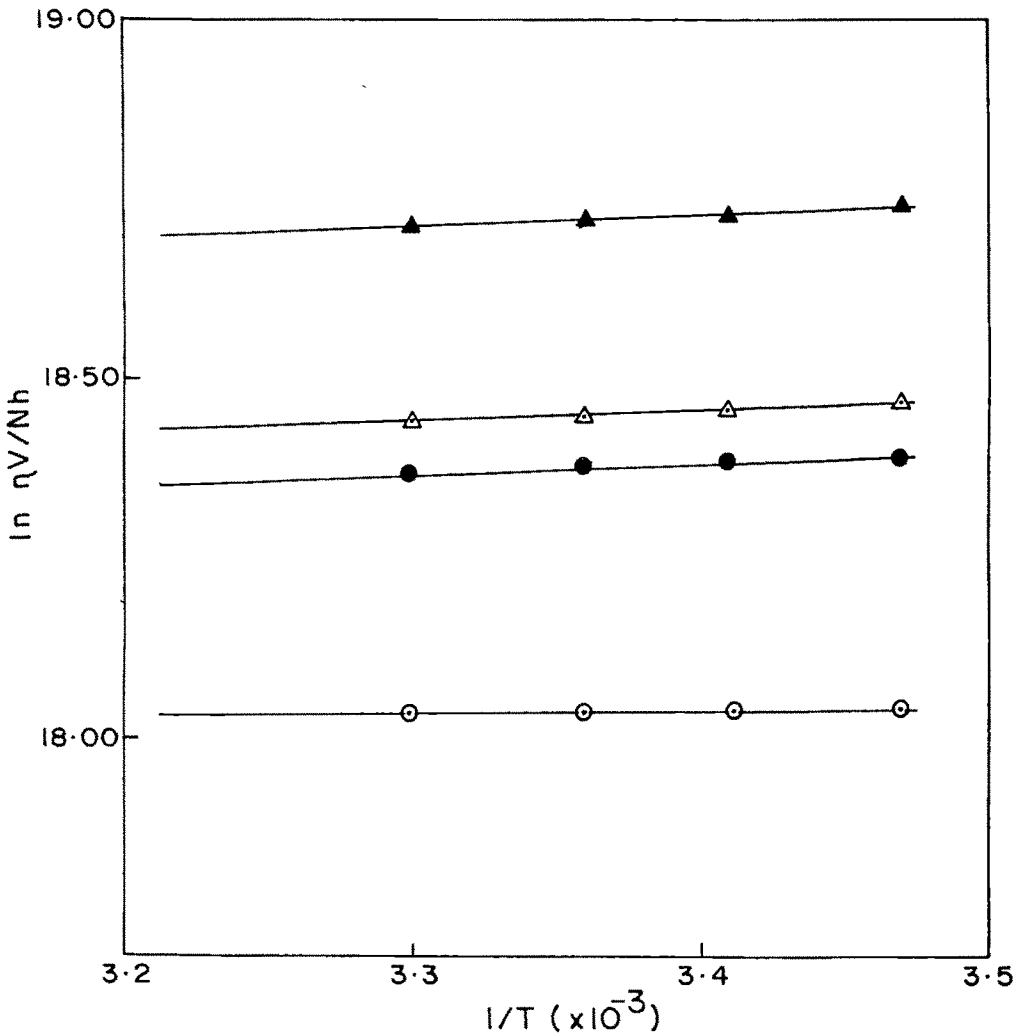

Fig. 3·29 ln ηV/Nh vs 1/T ($x 10^{-3}$) plots for representative samples

⊙ PMMA synthesized in microemulsion ;

● PMMA synthesized in emulsion ;

△ P (MMA-co-BA) synthesized in microemulsion ;

▲ P (MMA-co-BA) synthesized in emulsion ;

protein molecules (natural polymers)[32] and some acrylic polymers[31,33] in solution. In the present study the same procedure was followed for the determination of Ve by plotting

$$Y = \left[\eta_r^{0.5} - 1\right] / \left[C\left(1.35\,\eta_r^{0.5} - 0.1\right)\right] \text{ vs } C$$

and extrapolating to C=O to get V_e. The voluminosity is a function of temperature and is a measure of the volume of solvated polymer molecules. Hence in case of rigid molecules volume of solvent required to solvate the polymer molecules is less in comparison with syndiotactic polymers which are less rigid in character. Table 3.18 shows the hydrodynamic volume of polymers which decrease with increase in temperature. The Simha shape factor[34] was calculated by using the equation

$$\eta = \vartheta V_e$$

and it was observed that value for Simha shape factor for all the systems at the studied temperatures remains constant at ~2.6. This indicates that in the concentration range studied, the polymer molecules are spherical in the solution[35].

Part II

Semicontinuous Process

Semicontinuous polymerization is an important method for polymer processing in industry. The homogeneity of copolymers is a function of monomer composition in the feed and method of monomer addition[36]. By semicontinuous process, keeping the rate of monomer addition slower than the rate of polymerization, homogeneous copolymers can be obtained. The average particle size is smaller for the latexes obtained from semicontinuous process. But products show broader molecular weight distributions. Semicontinuous copolymerization of methyl methacrylate and butyl acrylate was carried out by using disodium diphenyl oxide disulponate (Dowfax 2A-1) and sodium dodecyl sulphate.

3.7 Semicontinuous microemulsion copolymerization using Dowfax 2A-1

Microemulsion composition used in the semicontinuous polymerization of methyl methacrylate and butyl acrylate in the present study are given in Table 3.19.

3.7.1 Optimization of reaction conditions

Surfactant concentration

In `S' series, reactions were carried out to optimize the surfactant concentration as discussed in section 2.9.1. Very little difference was observed in % conversion and % solid with variation in surfactant concentration upto ~3%. At low and high concentration of surfactant, coagulum formation was observed and hence 2-3% surfactant for ~30% monomer was observed to be optimum. This results into [monomer] / [surfactant] + [cosurfactant] ratio 10-12. The latex particle size was observed to be of ~40 nm (Table 3.20). At low concentration of anionic surfactant, Dowfax 2A-1, coagulum formation takes place due to increased

electrostatic instability of the latex particles. Decrease in the repulsive double layer forces with decrease in surfactant concentration results in decreased stability of the latex particles. At higher surfactant concentration also the stability of the latex decreases due to increase in ionic concentration of the continuous phase. Similar results were reported by Masa et al[37].

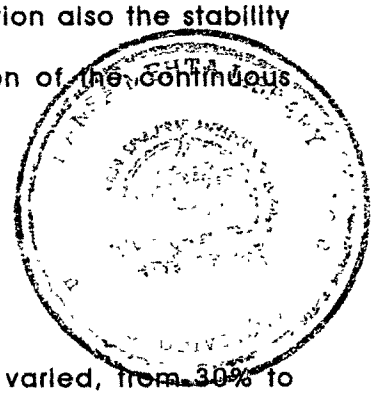

Monomer concentration

To improve % solid in the latex, monomer concentration was varied, from 30% to 50% w/w keeping MMA-BA ratio 1:1 and [monomer] / [surfactant] + [cosurfactant] ratio ~10. The initiator concentration with respect to monomer was kept constant. At higher concentration of monomer (above 45%), coagulum formation was observed due to reduced stability of the latex with increase in ionic concentration of the continuous phase. As the % solid increased viscosity went on increasing. At 37% solid the viscosity was 0.15 poise while at 45.2% it was 4.04 poise. At 52% solid, the viscosity increased considerably.

Homopolymers synthesized under identical conditions showed 22 nm and 60 nm particle size for PMMA and PBA latexes (Table 3.20). On copolymerization of 1:1 mixture of MMA-BA under identical conditions, copolymeric latex had the particles with almost the average size of PMMA and PBA particles (Table 3.20) i.e. 40.5, 22 and 60 nm for copolymer of MMA and BA, PMMA and PBA respectively.

Effect of cosurfactant concentration

In the D set of reactions, effect of cosurfactant on polymerization was studied. The compositions were prepared by using pentanol and acrylamide, as

cosurfactants and without cosurfactants (Table 3.19 and 3.20). The average particle size of the polymerized latex was observed to be smaller for the composition with acrylamide (DA) than for the composition without cosurfactant (D). However, when pentanol was used as a cosurfactant, % solid decreased and latex particles showed ~25% increase in size. TEM micrographs of the system without acrylamide show bimodal distribution of average particle size - one around average particle size 28 nm and the other 50.8 nm. This is shown in Figure 3.30 (a) and (b). The bimodal distribution to particles was also observed in particle size distribution analysis and is discussed in section 3.7.2.

Type and Effect of Initiator Concentration

In series `I', various water and oil soluble initiators such as potassium persulphate (KPS), ammonium persulphate (APS), azobisisobutyronitrile (AIBN) and benzoyl peroxide (BPO) were used. Among them, ammonium persulphate gave the latexes with highest % solid, without coagulum formation, with smallest latex particles and higher intrinsic viscosity. With ammonium persulphate latexes with average particle size 35.4 nm and $|\eta| = 1.413$ dl/g were obtained where as with KPS average particle size was 45.31 nm and $|\eta| = 1.152$ dl/g. With AIBN system at 40.2% solid average particle size was observed to be small (37.50 nm) but latex was viscous whereas with BPO latexes resulted into emulsions with large amount of coagulum formation.

Hence the effect of ammonium persulphate concentration was studied at 80°C for systems with and without acrylamide, A-APS 1-4 and APS 1-4, respectively. The results obtained are given in Table 3.20 and show dcrease in intrinsic viscosity and hence decrease in viscosity average molecular weight with increased initiator

concentration. This is due to increased free radical flux resulting early termination of growing chains.

Temperature

In the study of effect of temperature (at 70°C to 90°C) on copolymerization using ~40% of monomer (MMA-BA 1:1) concentration, it was observed that at high temperature % solid and % conversion is lower and coagulum formation takes place. Average particle size increases too. At 80°C, latexes with highest % conversion and lowest particle size were obtained.

Most of the surfactants reported for microemulsion polymerization have only one ionic charge per molecule whereas Dowfax 2A-1 has two. The structural formula shows that each molecule of Dowfax 2A-1 surfactant consists of a pair of sulphonate groups on a diphenyl oxide backbone. Two charged groups in close proximity yield an overlapping zone of enhanced negative charge. This higher local charge density results in greater intermolecular attraction and therefore increasing the probability for solvating and coupling action. The ether linkage between two benzene rings of each molecule of Dowfax 2A-1 surfactant is flexible. In particlular, this flexibility allows the benzene rings to rotate round the oxygen. Thus the distance between the sulphonates is variable, allowing the molecule to interact readily with structures as compact as individual ions or as bulky as long chain hydrocarbon.

Table 3.19 : Recipes used in the series of experiments using Dowfax 2A-1 surfactant

	Monomer %	Water %	Dowfax 2A-1	Cosurfactant %	Initiator %	% conversion	% solid	% coagulum
				Acrylamide	APS			
MMA	31.08	65.60	2.85	0.32	0.15	98.52	32.48	-
BA	31.08	65.60	2.85	0.32	0.15	98.93	32.62	-
MMA-BA	31.08	65.60	2.85	0.32	0.15	99.10	32.67	-
	Variation of Surfactant concentration :							
S-1	31.44	66.37	1.71	0.33	0.15	99.78	32.70	4.5
S-2	31.40	65.88	2.25	0.32	0.15	100.00	33.00	-
S-3	31.08	65.60	2.85	0.32	0.15	99..10	32.67	-
S-4	31.00	64.84	3.69	0.32	0.15	90.62	30.19	3.0
S-5	30.39	63.31	5.85	0.31	0.14	90.25	30.47	5.0
	Variation in monomer concentration, keeping monomer : (surfactant + cosurfactant) ratio constant :							
M-1	31.08	65.60	2.85	0.32	0.15	99.10	32.67	-
M-2	35.53	60.75	3.2	0.38	0.14	98.15	36.95	-
M-3	40.39	55.37	3.72	0.40	0.12	98.61	42.18	-
M-4	42.56	52.64	4.24	0.45	0.11	99.91	45.20	-
M-5	48.86	45.55	4.99	0.50	0.10	100.00	51.96	8.0

	Variation in initiator type :							
I-1	40.39	55.36	3.72	0.40	KPS 0.13	91.30	39.05	2
I-2	40.39	55.37	3.72	0.40	APS 0.12	98.61	42.18	-
I-3	40.39	55.40	3.72	0.40	AIBN 0.08	96.52	40.25	3
I-4	40.39	55.38	3.72	0.40	BPO 0.11	-	33.48	14
	Effect of cosurfactant :							
DP	40.39	55.37	3.72	Pentanol 0.40	APS 0.12	90.03	37.61	3
DA	40.39	55.37	3.72	Acrylamide 0.40	0.12	98.61	42.18	-
D	40.45	55.70	3.73	-	0.12	96.15	40.8	-
	Variation in temperature :							
MBA-70	40.39	55.37	3.72	Acrylamide 0.40	0.12	97.87	41.86	-
MBA-80	40.39	55.37	3.72	0.40	0.12	98.61	42.18	-
MBA-90	40.39	55.37	3.72	0.40	0.12	83.26	35.61	6.3
MB-70	40.45	55.70	3.73	-	0.12	89.64	38.04	-
MB-80	40.45	55.70	3.73	-	0.12	96.15	40.8	-
MB-90	40.45	55.70	3.73	-	0.12	93.92	39.86	8.2

Variation of ammonium persulphate concentration (based on water) :

A-APS	1.	40.39	55.37	3.72	0.40	0.01 M(0.12%)	98.61	42.18	-
	2.					0.02 M	100.00	42.84	-
	3.					0.03 M	100.00	42.84	-
	4.					0.05 M	100.00	42.84	-
APS	1.	40.45	55.70	3.73	-	0.01 M(0.12%)	96.15	40.8	-
	2.					0.02 M	100.00	41.48	-
	3.					0.03 M	100.00	41.48	-
	4.					0.05 M	100.00	41.48	-

Table 3.20 Average particle size D_n (nm) and $|\eta|$ (dl/g) for the latexes synthesized and the polymers.

	Solid %	Av.Particle size (nm)	$\|\eta\|$ dl/g
MMA	32.48	22.0	1.22
BA	32.62	60.0	
MMA-BA	32.67	40.5	1.39
S-2	33.00	42.5	1.37
S-3	32.67	40.5	1.39
M-1	32.67	40.5	
M-3	42.18	35.4	1.41
M-4	45.20		1.68
D	40.80	39.4	1.73
DP	37.60	49.7	1.06
DA	42.18	35.4	1.41
I-1	39.05	45.3	1.15
I-2	42.18	35.4	1.41
I-3	40.25	37.5	1.50
MBA 70	41.86		1.55
MBA 80	42.18	35.4	1.41
MB 70	38.04		1.33
MB 80	40.80	39.3	1.73
A-APS-1	42.18	35.4	1.41
A-APS-2	42.84		1.45
A-APS-3	42.84		1.38
APS-1	40.80	39.3	1.73
APS-2	41.50		1.53
APS-3	41.50		1.30
APS-4	41.50		1.06

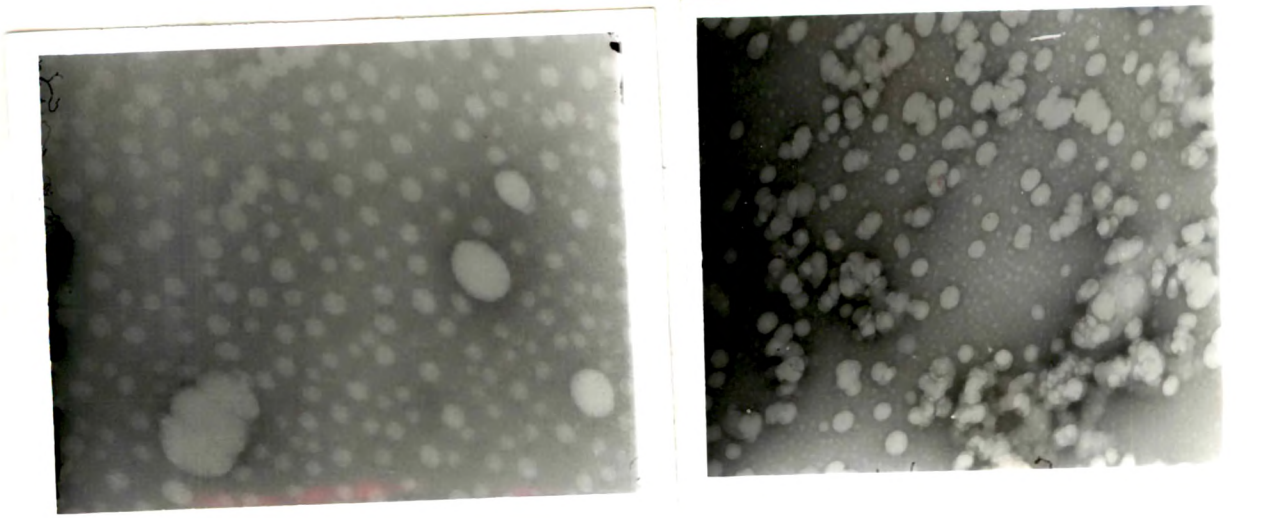

(a) (b)

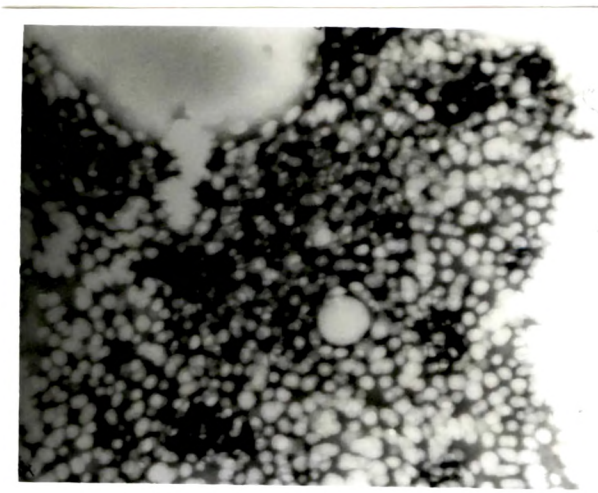

(c)

Fig 3.30 : Transmission electron micrograph of studied samples

(a) D magnification X100000

(b) D magnification X50000

(c) DA magnification X50000

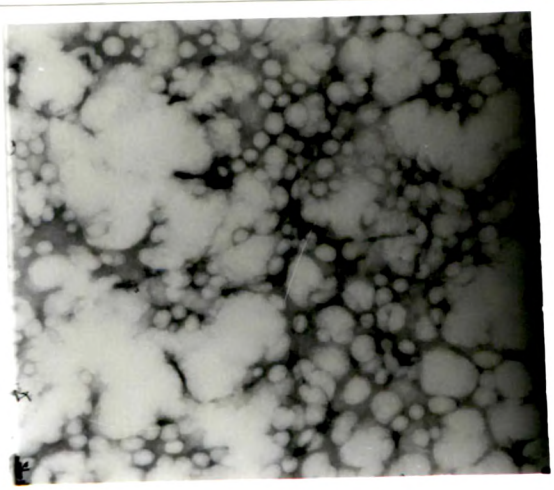

(d)

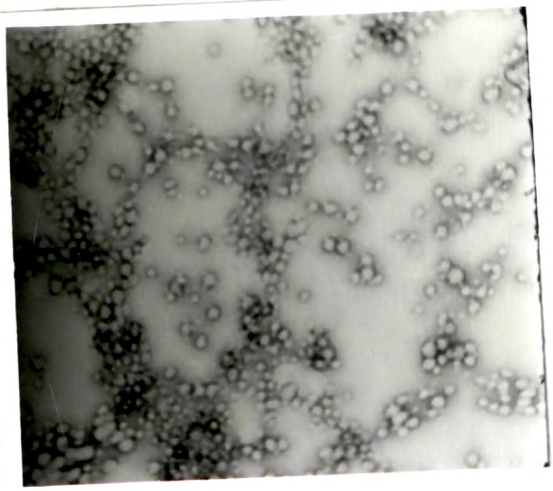

(e)

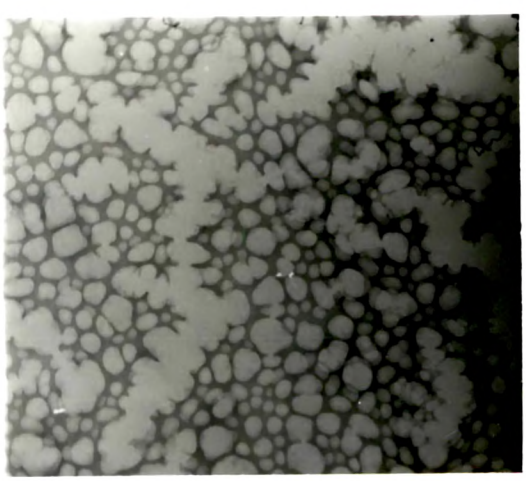

(f)

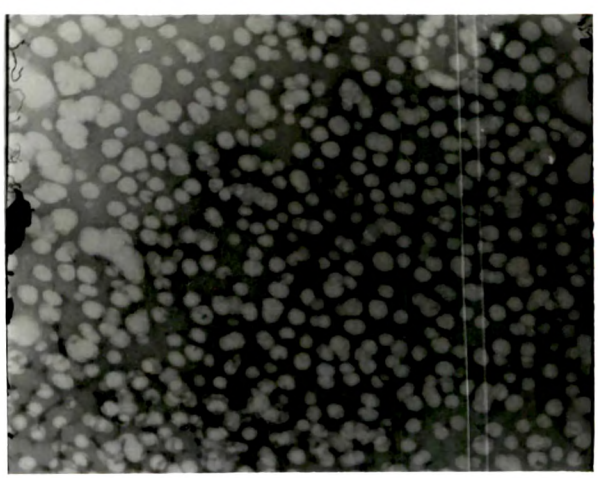

(g)

Fig 3.30 : Transmission electron micrograph of studied samples

(d) BA magnification X80000

(e) MMA magnification X50000

(f) DP magnification X50000

(g) M-1 magnification X50000

3.7.2 Characterization

NMR study

Figure 3.31 shows the signals obtained in high resolution ^1H NMR for methyl methacrylate and butyl acrylate copolymers. In the figure the triplet around δ4.00 ppm may be assigned to $-O^1CH_2$ protons and at δ2.09 ppm due to α-CH proton of butyl acrylate. The signal at δ1.6 ppm may be assigned to $-^2CH_2$ and at δ0.9 ppm to $-^4CH_3$ protons of butyl acrylate.

The signals obtained at δ3.6 ppm can be assigned to $-OCH_3$ and at δ1.10 ppm and δ1.25 ppm to α-CH_3 of methyl methacrylate. The β-CH_2 signal appears at δ2.0 ppm and δ1.81 ppm. These values agree with the values reported for PBA[27] and PMMA[25]. The intensities, of signals at $-^1OCH_2$ and $-OCH_3$ of butyl acrylate and methyl methacrylate respectively, per proton indicate that the monomer units are in equimolar proportion in the polymer unit. This may be because of the reactivity ratios calculated by us in microemulsion medium (section 3.4) for MMA and BA are identical, 0.854 and 0.878 respectively, which results in their incorporation in the copolymer in almost 1:1 ratio.

GPC Analysis

The products synthesized were characterized for their molecular weight and molecular weight distribution by GPC as discussed in section 2.10.3. Table 3.21 shows the weight average, number average molecular weights and polydispersity of representative samples. M-2 and M-4 are the systems with ~37% and 45% solid content and `D' is a system without acrylamide with ~41% solid content. The

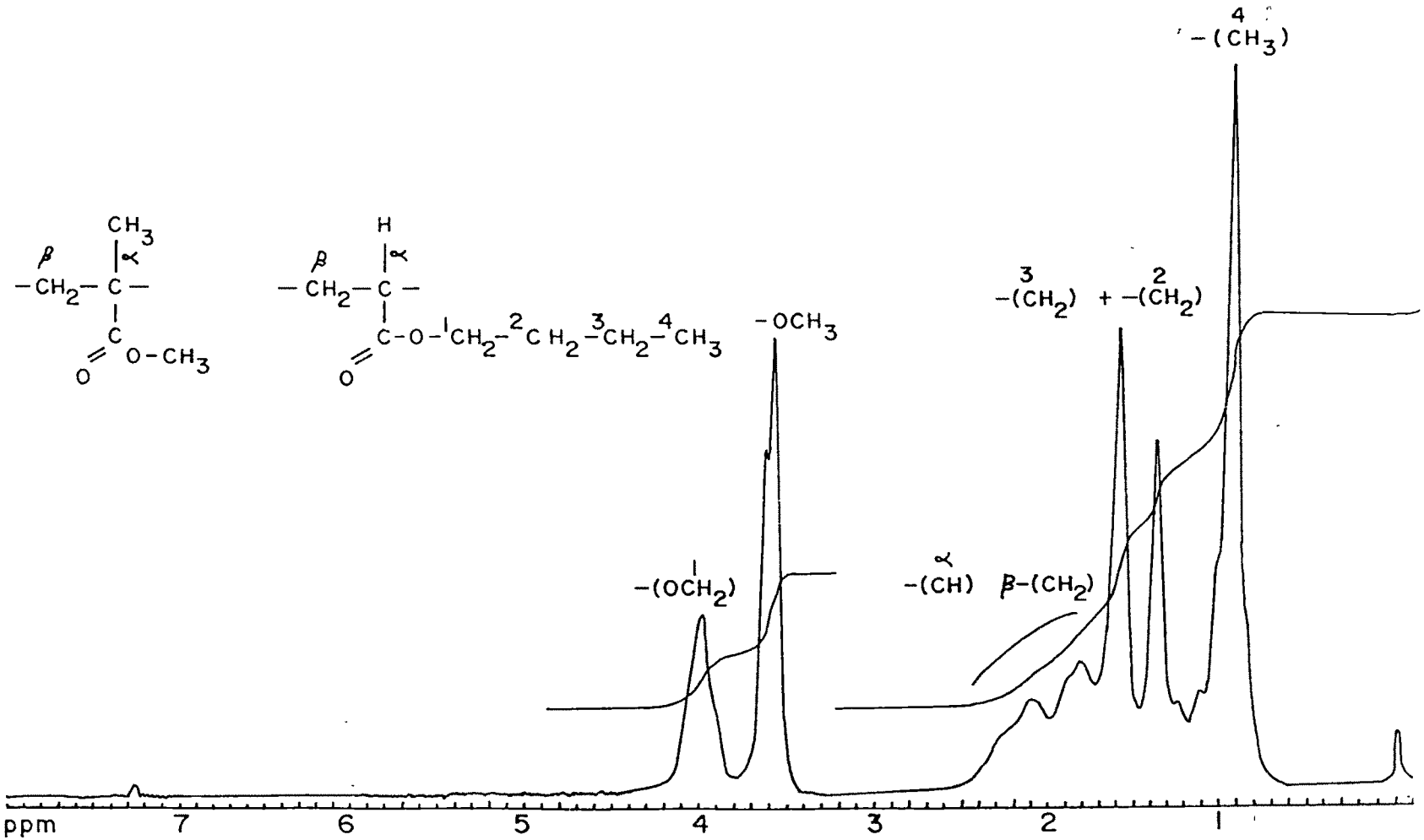

Fig. 3·31 ^{1}H NMR spectra of P(MMA-co-BA) using Dowfax 2A-1 surfactant

system D shows bimodal distribution with overall molecular data : $\overline{Mn}$ = 4.18 x 10^5, $\overline{Mw}$ = 11.96 x 10^5 and polydispersity 2.86. When the data quantitation is carried out for both the peaks, the values obtained were for peak (1) : $\overline{Mn}$ = 24.28 x 10^5, $\overline{Mw}$ = 26.89 x 10^5 and polydispersity 1.11 while for peak (2) : $\overline{Mn}$ = 3.08 x 10^6, $\overline{Mw}$ = 5.59 x 10^5 with polydispersity 1.79. Bimodal molecular weight distribution has been reported by other research workers[8,38,39] also. Johnson and Gulari[38] reported two populations with average polymer molecular weights of 3 x 10^5 and 3 x 10^6 by GPC and Quasi elastic light scattering. They attributed this bimodal distribution to the presence of two competing mechanisms for initiation : one in monomer droplets and other in monomer swollen micelles. The polydispersity of samples M-2 and M-4 are 5.56 and 5.14 (Table 3.21). The high polydispersity is also indicative of more than one competing mechanism for initiation i.e. in monomer droplets and in monomer swollen micelles or homogeneous nucleation or all three operating simultaneously.

Particle size distribution

Synthesis of nanoparticle is an important aspect of the present study. It results in increased surface area and enhances the performance of latex as binder. Another important dimension is that it results in one or two polymer chains of high molecular weights with low polydispersity. Hence particle size was extensively studied using TEM techniques as discussed earlier. Figure 3.32 and 3.33 show the particle size distribution of the latex from recipe D and DA (Table 3.19). The average particle size was calculated from Transmission electron micrographs as shown in figure 3.30.

Table 3.21 Weight average, number average molecular weights and polydispersity results of the studied samples synthesized using Dowfax 2A-1 at 80°C using ammonium persulphate (0.3 % with respect to monomer).

Sample	$\overline{M}_w$(x 10^{-5})	$\overline{M}_n$(x 10^{5})	Polydispersity
M-2	7.12	1.28	5.56
M-4	11.7	2.27	5.14
D	11.96	4.18	2.86
	(I) 26.89	(I) 24.28	(I) 1.11
	(ii) 5.59	(ii) 3.08	(ii) 1.78

* D shows bimodal distribution.

M-2, M-4, D compositions as given in Table 3.19.

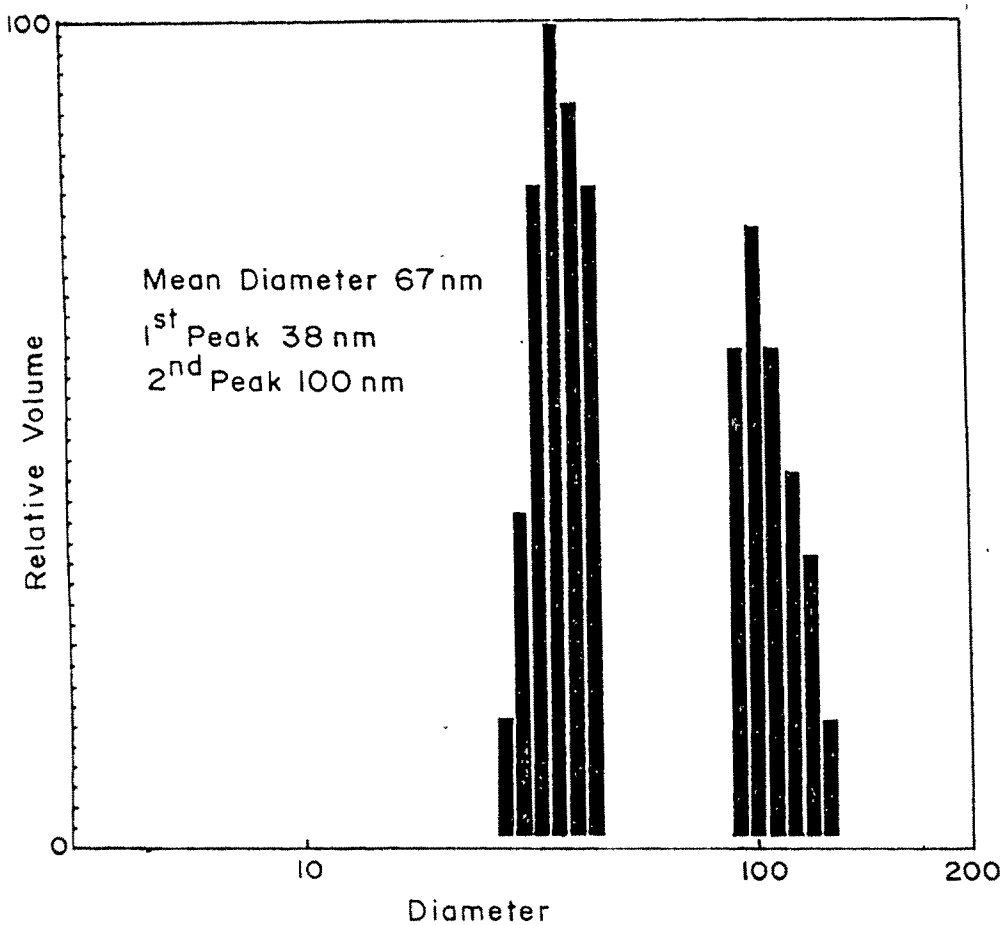

Fig. 3·32 Particle size distribution of sample D, at 80° C with ammonium persulphate (0·3% of monomer conc.), using Dowfax 2A-1 surfactant, no acrylamide (composition of D in Table 3·19)

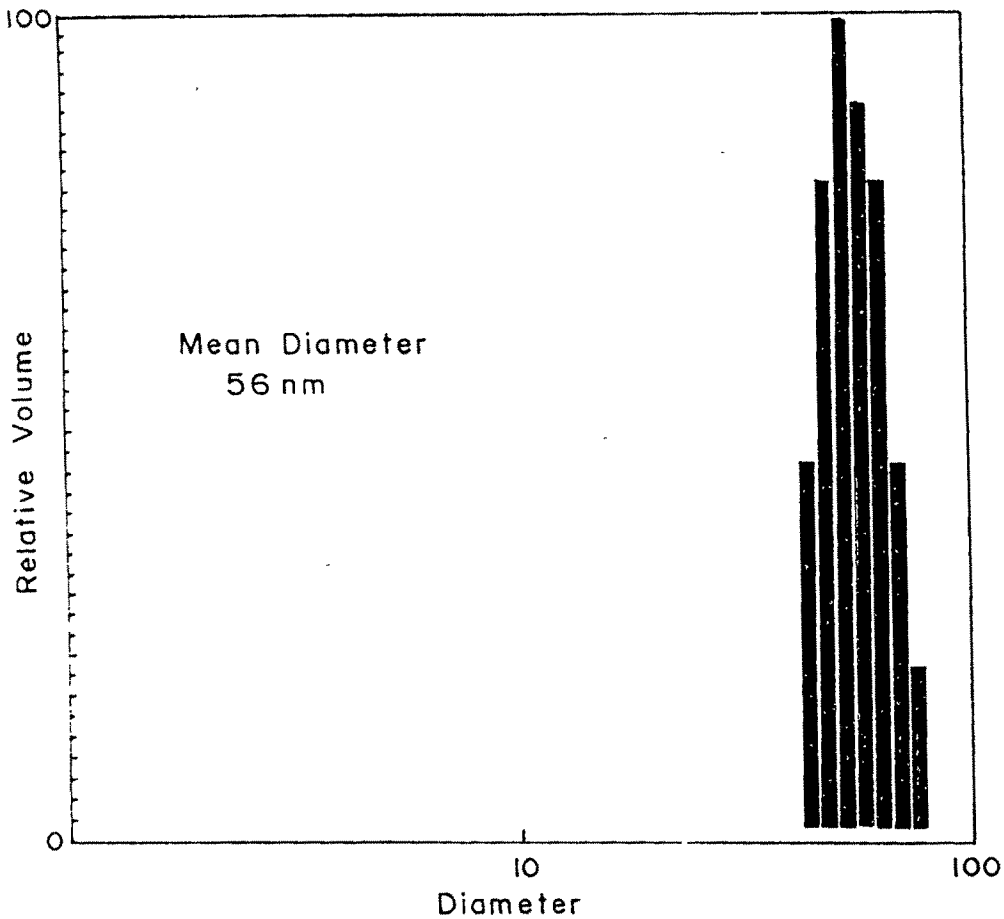

Fig. 3·33 Particle size distribution of sample DA, at 80° C with ammonium persulphate (0·3% of monomer concentration), using Dowfax 2A-1 surfactant, with acrylamide (composition of DA in Table 3·19)

Bimodal distributions have been reported in styrene emulsion systems where water soluble initiators were used. The emulsion produced by Ugelstad et al[40] contained small amount of hexadecanol and yielded a bimodal distribution of latex particles. These authors claimed that this was the evidence of a initiation mechanism that involved both monomer droplets and monomer swollen micelles. Piirma and Chang[41] reported the appearance of bimodal distribution around 40% conversion of styrene, water and Emulphogene BC 840 system and proposed that the emulsifier released by the polystyrene and the uninitiated micelles caused a secondary nucleation that greatly increased the reaction rate. Tang et al[42] also reported a bimodal distribution in an o/w styrene microemulsion system and proposed that it resulted from the initiation of monomer droplets and monomer swollen micelles.

Thermal studies

Thermogravimetric analysis

Dynamic thermogravimetric analysis of representative sample was carried out using nitrogen atmosphere as described in section 2.10.4. The experimental conditions were identical for all the samples. Examination of the thermograms of all the polymers (Table 3.22) reveal that they are stable upto around 200°C and 90% degradation takes place around 420°C. Samples DA (Figure 3.34) and M-2 are showing two step thermal degradations whereas sample D (Figure 3.35a) and DP show single step degradation pattern. This may be due to the incorporation of acrylamide in the polymeric chain. Figure 3.35b shows a straight line plot of negative slope when ln [ln 1/Y] was plotted against 1/T for the sample D.

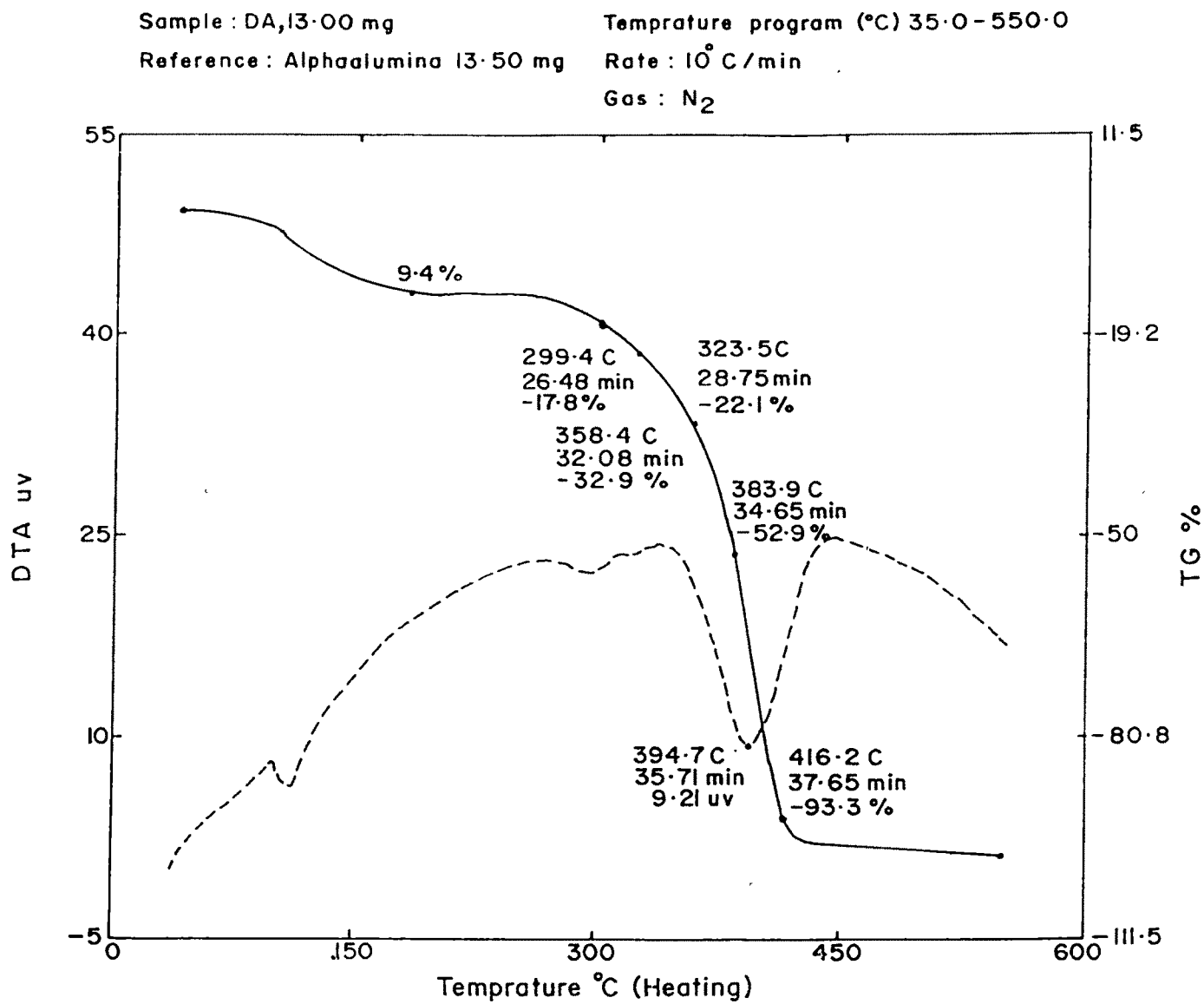

Fig. 3·34 TGA and DTA curve for sample DA synthesized at 80° C, with ammonium persulphate initiator

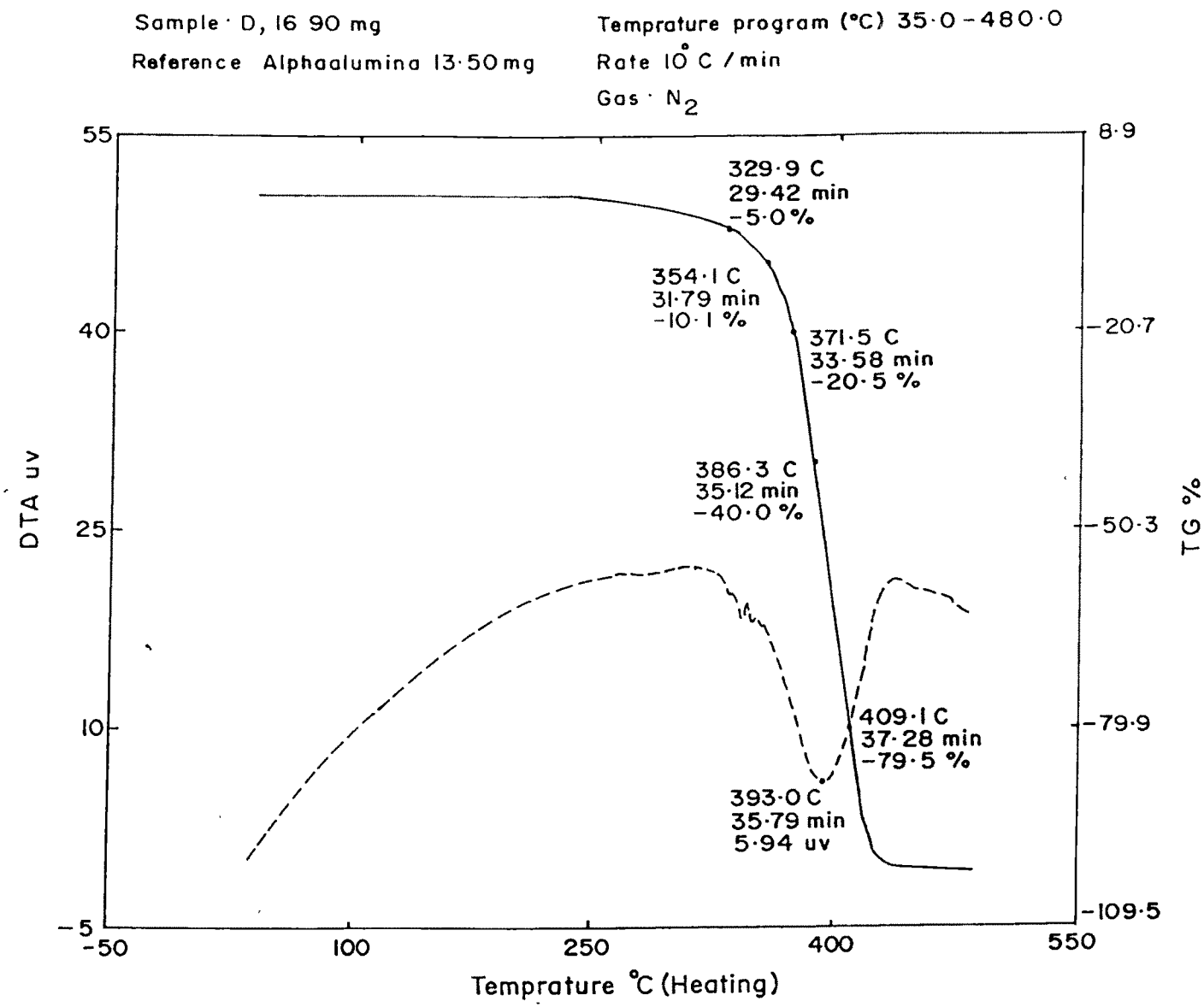

Fig. 3·35a TGA and DTA curve for sample D at 80° C with ammonium per sulphate initiator

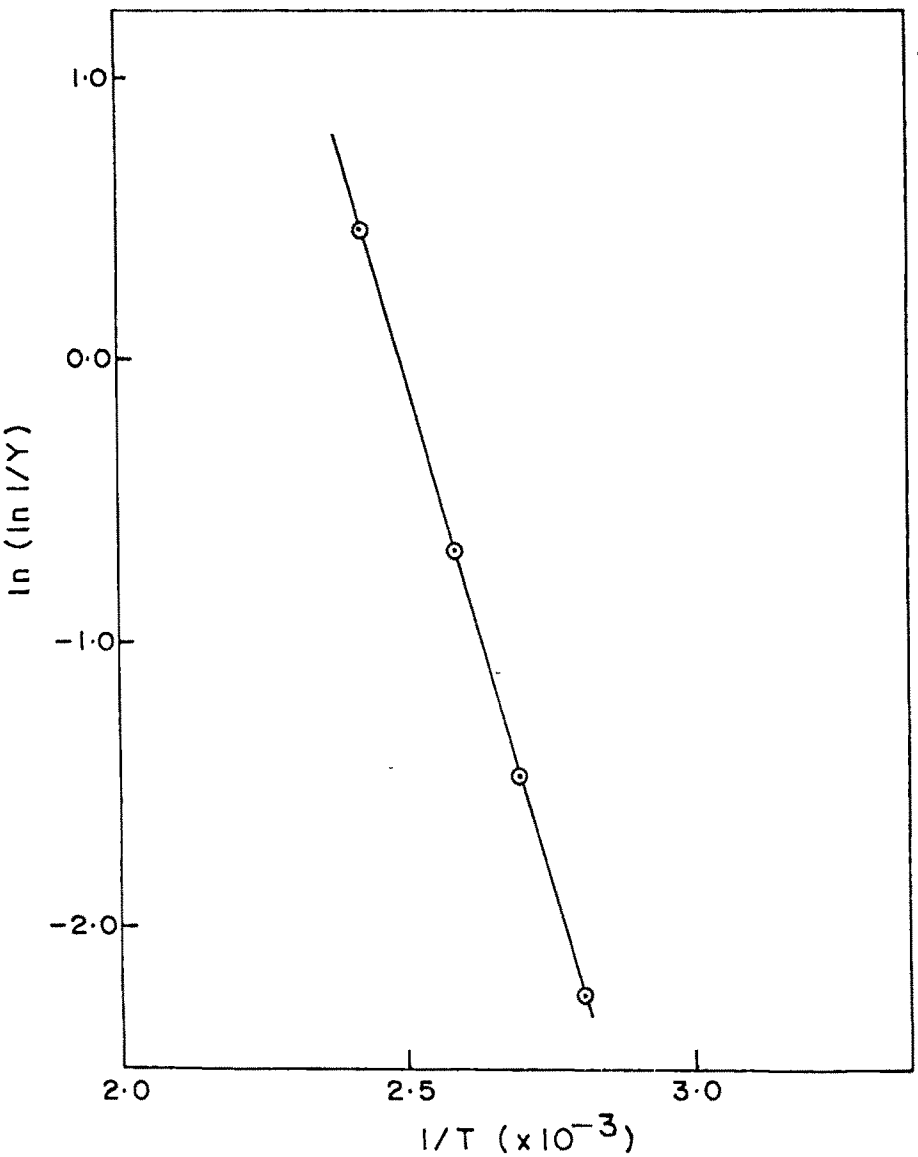

Fig.3·35b ln (ln 1/Y) vs 1/T ($x10^{-3}$) plot for sample D

Table 3.22 : Thermogravimetric analysis of representative samples synthesized at 80°C.

Sample		T_1	T_{10} (°C)	T_{50}	T_{90}	Activation Energy KJ mol^{-1})
DA ME	Dowfax Acrylamide	207.5	250.9	380.3	414.5	37.18
DP	Dowfax Pentanol	223.9	318.5	370.8	396.2	45.56
D ME	Dowfax	261.0	354.0	388.8	415.0	61.99
M-2 ME	Dowfax	220.0	330.0	386.0	405.0	55.42
PMMA-BA ME	SDS	220.0	285.0	347.0	371.0	32.19

T_1, T_{10}, T_{50} and T_{90} are the degradation temperature corresponding to 1 %, 10 %, 50 % and 90 % weight loss.

ME = synthesized in microemulsion

E = synthesized in emulsion

Activation energy was calculated by using Broido's equation as discussed earlier. Babu et al[28] observed one step thermal degradation of acrylates as discussed earlier in section 3.6.5.

Differential thermal analysis

DTA curve for sample DA shows the melting temperature 296.25°C and decomposition temperature 394.7°C (Figure 3.34) and for D it was 330°C and 393°C (Figure 3.35) respectively. Lower melting temperature for DA may be due to the lower viscosity average molecular weight (i.e. lower $[\eta]$ dl/g as given in Table 3.20).

Table 3.23 : Differential Thermal Analysis of representative samples synthesized using Dowfax 2A-1, at 80°C with APS initiator.

	T_m	T_d
DA	296.2°C	394.7°C
D	330.0°C	393.0°C

DA and D compositions as given in Table 3.19.

Viscosity studies

The effect of temperature on the hydrodynamic behaviour of dilute polymer solutions can be studied through temperature dependence of the intrinsic viscosities (Table 3.24 and Figure 3.36). It is observed that the intrinsic viscosity

$|\eta|$ decreases in general with increase in temperature. $|\eta|$ vs temperature plots are always linear with the negative slope indicating that the polymer coils are not swelling to a great extent.

The well known Frenkel-Eyring equation for viscous flow,

$$\eta = (Nh/V) \exp(\Delta G^{\#}_{vis}/RT)$$

can be rewritten as,

$$\ln (\eta V/Nh) = (\Delta H^{\#}_{vis}/R\,T) - (\Delta S^{\#}_{vis}/R)$$

Representative plots of $\ln \eta V/Nh$ vs T^{-1} are given in figure 3.37 which shows linear relationship for all the samples studied. The calculated values of entropy $\Delta S^{\#}_{vis}$, enthalpy H_{vis} and free energy $\Delta G^{\#}_{vis}$ for the viscous flow of polymers in solutions are given in Table 3.25. The small values indicate no cross-linking in the samples. The free energy of activation of the viscous flow, $\Delta G^{\#}_{vis}$, is reasonably independent of temperature.

The intramolecular expansion factor for P(MMA-co-BA) synthesized by semicontinuous method was calculated from the intrinsic viscosity measurements in 0 solvent at 25°C and using,

$$\alpha^3 = |\eta|/|\eta|_\theta$$

relationship. The spacial arrangement in the actual molecule is assumed to be expanded uniformly by the factor α as a result of intramolecular interaction. Table

3.26 shows the θ solvent compositions and intramolecular expansion factor values. The intramolecular expansion factor for the samples synthesized by semicontinuous process are much higher than those for products synthesized by batch process (Table 3.17). It indicates less rigid structure for the samples synthesized by semicontinuous method.

The relative viscosity data was used to calculate the equivalent hydrodynamic volume (voluminosity, Ve), a measure of size of a solvated polymer molecule at infinite dilution (Table 3.27). It was recently used to determine the shape of protein molecules (natural polymers)[32] and some acrylic polymers[31,33] in solution. In the present study the same procedure was followed for the determination of Ve by plotting

$$Y = \left[\eta_r^{0.5} - 1\right] / \left[C\left(1.35\,\eta_r^{0.5} - 0.1\right)\right] \text{ vs } C$$

and extrapolating to C=O to get Ve. The voluminosity is a function of temperature and is a measure of the volume of solvated polymer molecules. As the temperature increases the Ve decreases. From $|\eta| = \vartheta Ve$, the Simha shape factor ϑ[34] was calculated. For sample DP it was 2.25, for DA it was 2.48 and for D it was 2.75. Einstein computed a value of ν as 2.5 for spherical particles where as for oblate or prolate shape the values in solution differ widely from 2.5[35]. This indicates that DA particles have spherical shape whereas others show some deviation from the spherical nature.

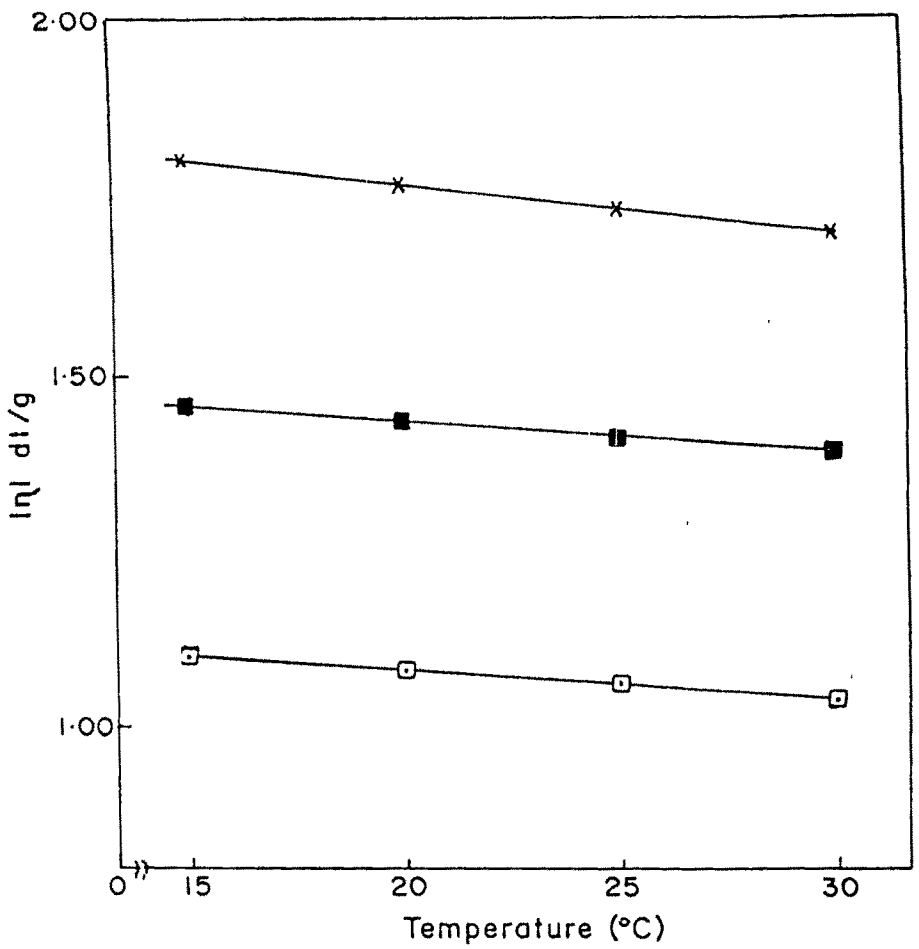

Fig. 3·36 [η] vs T plots for representative samples synthesized using Dowfax 2A-1, at 80°C with APS initiator ×: D, ■: DA, ⊡: DP, (composition of D, DA and DP in Table 3·19)

Table 3.24 : Intrinsic viscosities of representative samples at different temperature.

Sample	$\lvert\eta\rvert$ dl/g			
	15°C	20°C	25°C	30°C
DP	1.10	1.08	1.06	1.04
DA	1.46	1.44	1.41	1.39
D	1.80	1.7	1.73	1.70

Composition of D, DP and DA in Table 3.19.

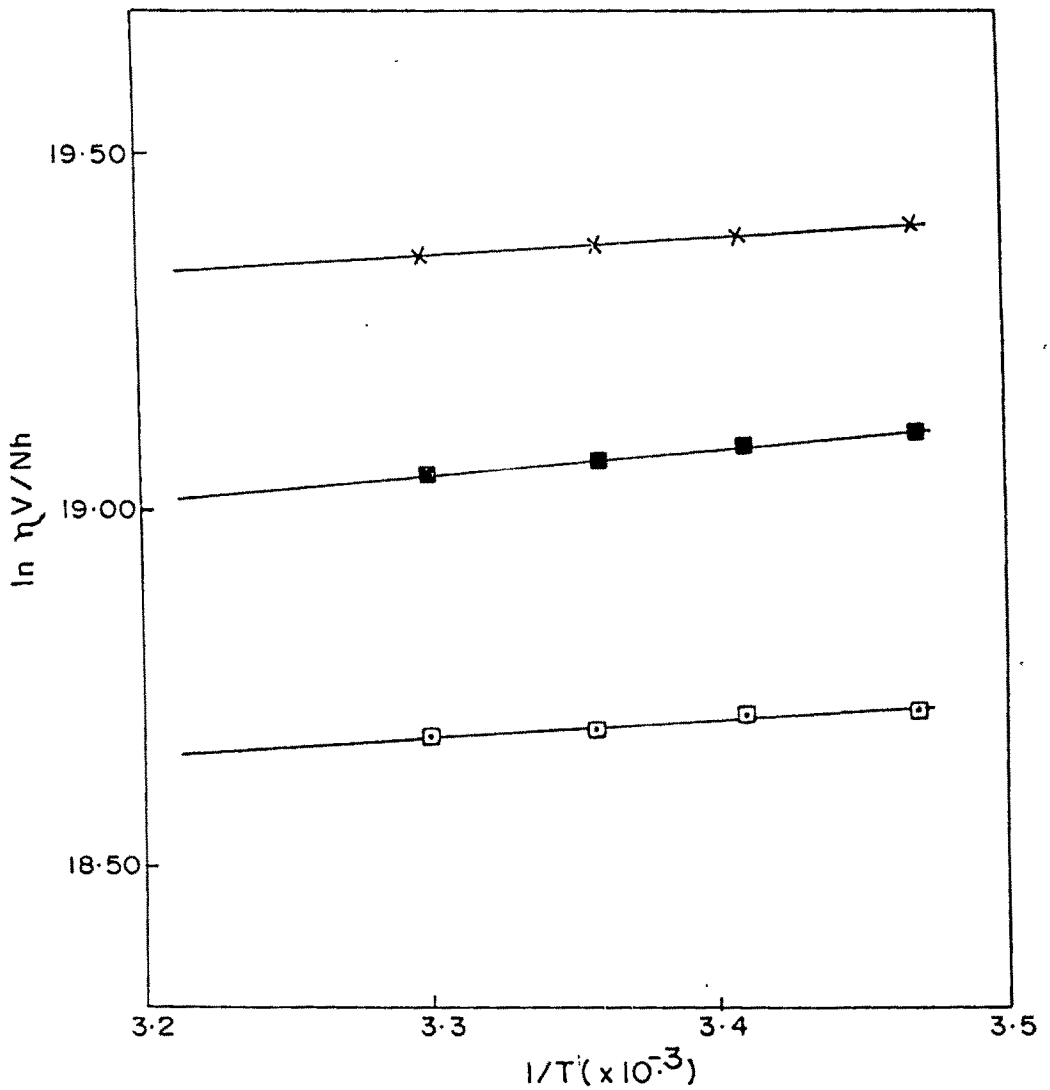

Fig. 3·37 ln $\eta V/Nh$ vs $1/T$ ($\times 10^{-3}$) plots for representative samples using Dowfax 2A-1, at 80° C with APS initiator ; x:D, ■:DA, ⊡:DP

Table 3.25 : Entropy $\Delta S^{\#}_{vis}$, Enthalpy $\Delta H^{\#}_{vis}$ and free energy $\Delta G^{\#}_{vis}$ of Activation for the viscous flow of representative polymers in solutions.

Sample	$\Delta H^{\#}_{vis}$ (KJ mol^{-1})	$\Delta S^{\#}_{vis}$ (J mol^{-1} deg^{-1})	$\Delta G^{\#}_{vis}$ KJ/mol			
	In Acetone	In Acetone	15°C	20°C	25°C	30°C
D	2.08	154	46.47	47.24	48.00	48.78
DP	2.08	148	44.84	45.59	46.33	47.07
DA	2.88	149	45.79	46.53	47.28	48.02

Table 3.26 : Intramolecular expansion factor and θ solvent composition of representative samples.

Sample	θ-solvent composition		$\|\eta\|$	$\|\eta\|_\theta$	α
	Acetone %	Methanol %			
D	36.4	63.6	1.733	0.411	1.616
DP	33.3	66.7	1.060	0.185	1.789
DA	30.0	70.0	1.413	0.154	2.090

Composition of D, DP and DA in Table 3.19.

Table 3.27 : Hydrodynamic volumes of representative samples at different temperature.

	Hydrodynamic volume, Ve ml/g			
Sample	15°C	20°C	25°C	30°C
DP	48.08	47.60	47.00	46.20
DA	58.10	57.60	57.00	56.60
D	64.00	63.60	63.32	62.84

Composition of D, DP and DA in Table 3.19.

3.8 Semicontinuous microemulsion copolymerization using sodium dodecyl sulphate

Semicontinuous copolymerization of MMA-BA was carried out using SDS as surfactant. A series of experiments was carried out to optimize the surfactant : monomer ratio for microemulsion polymerization of MMA and BA. From the results given in Table 3.28 it is observed that translucent microemulsion latexes were obtained when surfactant : monomer ratio varied from 0.9 to 0.5. However, below 0.5 ratio latexes were somewhat turbid. The maximum % solid obtained was 24%. An experiment was also performed by taking the optimized conditions for the batch polymerization where 22% solid content was observed.

Table 3.28: Semicontinuous reactions using SDS as surfactant and MMA-BA as monomer.

Code No.	Composition %	Solid %	Conversion %	Comments
IA	Water 76.03 SDS 14.05 Monomer 9.92	21.87	91.24	Viscosity 8 cps 70 % UV-Vis Light transmission at 600 nm. Particle size 14 nm
	(composition as per the batch process)			
IB	Water 80.80 SDS 8.73 Monomer 10.47	17.39	90.57	Viscosity 5 cps Microemulsion
IC	Water 81.51 SDS 7.92 Monomer 10.57	16.09	87.02	Viscosity 4 cps Microemulsion
ID	Water 82.24 SDS 7.10 Monomer 10.66	15.38	86.59	Viscosity 4 cps Microemulsion

IE	Water	77.32	20.00	88.18	Viscosity 6 cps
	SDS	7.56			Microemulsion
	Monomer	15.12			
IF	Water	73.6	23.91	90.57	Viscosity 15.5 cps
	SDS	7.2			Particle size ~80 nm
	Monomer	19.2			

Part III

Applications

3.9 Applications

The use of polymer latexes (polymerized emulsions or microemulsions) in applications such as adhesives, foams, paints, paper, coatings and textile sizings requires the latex to be of quality with respect to electrolytic stability, mechanical stability, freeze thaw stability with optimum % solid, particle size, viscosity and pH. It requires the latex to form a continuous film upon drying. The morphology and mechanical properties of films, however depend upon the composition and structure of the polymer and also upon the drying conditions and environment[43,44]. During film formation, the latex particles are known to move around with random Brownian motion until a critical solid concentration (74% solids of monodisperse latexes packed in a rhombohedral array) is reached. Later, a continuous film results from the coalescence of the particles provided the forces[45,46] produced during the further evaporation of water are of sufficient magnitude to overcome the resisting forces caused by coulombic repulsion forces of the charged particles and the particle rigidity. Film properties are further improved by the interdiffusion of the polymer molecules across the area of contact of the particles - a process known as further gradual coalescence[47].

Three microlatexes with compositions shown in Table 3.29 were selected and their microemulsion and film properties were evaluated. Films were casted on glass panels using 150 μm applicator and were tested to evaluate their suitability for use in paints.

Table 3.29 : Composition of representative samples polymerized at 80°C with initiators ammonium persulphate for M-2 and M-4 and KPS for SDS-20.

	SDS-20	M-2	M-4
Surfactant %	14.1	3.20	4.24
MMA/BA(1:1 w/w) %	9.9	35.53	42.56
Water %	76.0	60.75	52.64
Acrylamide %	-	0.38	0.45
Initiator	KPS	APS %	APS %
	1.25×10^{-3} M	0.14	0.11

SDS 20 : Table 3.28 Code 1A; M-2, M-4 : Table 3.19.

3.10 Microemulsion properties

Mechanical Stability

The microemulsion latexes from composition SDS-20, M-2 and M-4 (Table 3.29) were tested for mechanical stability at 14000 r.p.m. for 10 minutes. All the latexes showed good mechanical stability with no coagulum formation. No increase in particle size was observed.

Electrolytic stability

The microemulsion latexes from composition SDS-20, M-2 and M-4 were also tested for electrolytic stability using 5 % aluminium sulphate as discussed in

Table 3.30 : Microemulsion properties of the representative samples.

	SDS-20	M-2	M-4
1. Appearance	Translucent	Translucent	Translucent
2. Solid %	21.87	36.95	45.20
3. Particle size (nm)	< 30	< 30	< 30
4. Molecular weight $\overline{M}_w$	-	7.12×10^5	11.70×10^5
5. Viscosity (poise)	0.08	0.15	4.04
6. Electrolyte stability $Al_2(SO_4)_3$ 5 % (ml)	300.00	20.0	18.0
7. Mechanical stability 14000 rpm for 10 min. coagulum (gms)	Nil	Nil	Nil
8. Freeze-Thaw stability 25°C 24 hrs. -10°C 24 hrs.			
1st Cycle	+	+	+
2nd Cycle	+	+	+
3rd Cycle	+	+	+
9. pH	2.17	2.12	2.21

section 2.11.5. 100 gm of SDS-20 microemulsion latex required 300 ml, M-2 required 18 ml and M-4 required 20 ml of $Al_2(SO_4)_3$ for complete coagulation. SDS and Dowfax 2A-1 are anionic emulsifiers which promote electrostatic stability of the microemulsion. Addition of $Al_2(SO_4)_3$ electrolyte decreases the double layer thickness (primarily responsible for stability of latex) resulting in coalescence. The volume of $Al_2(SO_4)_3$ required for complete coalescence is the measure of the stability of the latex.

Freeze-thaw stability

Latex can freeze during storage or transportation and therefore resistance to freeze-thaw cycles is very important for commercialization of the product. The microlatexes from SDS-20, M-2 and M-4 compositions were tested for freeze-thaw stability. It was done as discussed in section 2.11.6. All the microlatexes, SDS-20, M-2 and M-4 showed excellent stability to three cycles. When freezing occurs, ice crystals separate from the unfrozen latex, reducing the volume of the continuous phase and increasing the ionic concentration of this phase. As a result, the stability of the latex is reduced and the latex which is subjected to high pressure may coagulate[37].

Particle size and Molecular weight

Particle sizes for the three microlatexes were observed to be below 30 nm on Shimadzu Said 2001 particle size analyzer. Lower particle size is desired for paint formulation as it would improve the dispersion of the pigments and enhances the performance of the microlatex as binder. Average molecular weight was observed (Table 3.30) to be high with broad polydispersity.

3.11 Film properties

Films of thickness 150 μm were casted on glass panels. Preliminary tests regarding water resistance and alkali resistance were carried out. The films were examined for their clarity, bits and tackiness. The results are in Table 3.31.

3.12 Paints

Emulsion paints have gained wide acceptance by both the consumers and industry.

The advantages of emulsion paints are listed below :

(i) Easy to apply.

(ii) Quick drying (within an hour or two).

(iii) Equipment used in applying latex paint can be conveniently washed with water.

(iv) Little or no odour.

(v) Excellent resistance to alkalies in fresh plaster, stucco or masonry.

(vi) Long-term outside durability.

(vii) Excellent resistance to blistering on wood surfaces.

However they also have certain disadvantages such as :

(i) Spread easily.

(ii) Require protection against freezing.

(iii) Greater permeability to moisture than oil based paints.

(iv) Leads to poor adhesion on improperly prepared surfaces.

Table 3.31 : Preliminary film properties of the film (150 μm)casted on glass panels of the representative samples.

	SDS 20	M-2	M-4
Clarity	Hazy	Clear Glossy	Clear
Bits	None	None	None
Tack	No	No	No
Water Resistance			
1st hour	7	8	8
2nd hour	6	7	7
4th hour	6	6	6
24th hour	5	5	5
Alkali Resistance			
a) Resistance	Blistering	No whitening or blistering	No whitening or blistering
b) Weight loss	50 %	-	-

3.12.1 What is paint?

Paint is used to protect, decorate and obscure a surface. The two basic ingredients in paints are the pigment and the vehicle. Pigments are particles of opaque nature which impart colour and hiding power or ability to obscure a surface to paint.

The vehicle (carrier for the pigments) is the liquid part of the paint and consists essentially of two components :

(i) the thinner and

(ii) the binder

The former is the volatile part of the paint that evaporates, leaving behind a solid paint film.

The binder remains in the paint film to bind the pigment particles into an uniform film after the volatile liquid evaporates. Binder type and amount largely determines most of the paint properties such as durability, washability, toughness and adhesion.

As work with acrylic emulsions were carried out, brief account is given here.

3.12.2 Acrylic Emulsions

Acrylic emulsions were introduced in 1953 as they are noted for their toughness, outdoor durability and good adhesion to a wide variety of surfaces. Acrylic latex paints are defined as those with predominant concentration of polymers and copolymers of the esters of acrylic or methacrylic acid. Chemically the acrylics

are long chain polymers of methacrylate and acrylate esters.

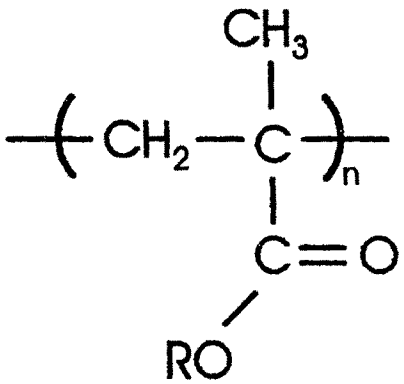

Poly methacrylate

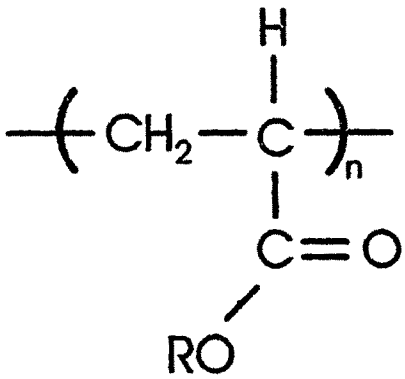

Poly acrylate

Where R is an alkyl group such as ethyl, butyl or 2-ethyl hexyl. Smaller groups (e.g. methyl or ethyl) result in hard, tack-free and tough polymers. The substitution of larger chains in ester groups results in soft, tacky polymers. The methyl group in the α-carbon of the methacrylate polymers also have an important influence on polymer properties.

3.12.3 Paint Manufacturing process

Proper paint-formulation techniques are just as important as the choice of emulsion type in getting desirable paint properties. The process involves pigment dispersion (called grinding), followed by the addition of emulsifier and other additives, adjustment of pH, viscosity and tinting.

Much of the equipment used in paint making is for mixing and dispersing pigments. The most critical part of paint making is dispersing of the pigment with the binder. Frequently used for these operations are high speed impeller mills and sand mills. Other equipments, such as ball and roller mills are also used as per requirement.

With the impeller mill, the production of latex paint is divided into two operations : pigment dispersing at about 5400 ft/min (disk peripheral speed) and mixing at about 1500 disk peripheral speed (the let down). Usually the dispersing and wetting agents, coalescents, antifoamer, water and thickener are charged to a tank and mixed. The pigments and extenders are then slowly added as the mixer speed is increased. The pigment paste is then mixed at a high impeller speed until all aggregates are broken down and pigments are homogeneously dispersed. This is known as mill base.

After this, the dispersed pigment paste is diluted by adding the bulk of the emulsion vehicle, defoamer and additional water or thickeners as necessary to adjust viscosity. Mixing continues at a low impellar speed until the paint batch is thoroughly blended. Finally the pH of the finished latex paint is adjusted. The product is then ready for packaging[48].

Paint preparation

The formulation of the paint prepared in the present study is given in Table 3.32. It was prepared as discussed in section 2.13.

3.13 Characterization of Paints

Paints are characterized for their following properties :

3.13.1 Viscosity

The viscosity was measured for formulation II paints. M 2 II and M 4 II were stiff

Table 3.32 : Paint formulated with microemulsion M-2, M-4, SDS-20 and standard (emulsion).

		Formulation I	Formulation II
Water		47.0	17.22
Surfactant	Hyoxyd AAO	0.5	-
	Nolgen NP 15	-	0.10
	Avipol GM	-	0.30
Pigment	TiO_2	6.0	12.00
Extender	China clay	14.0	12.00
	Steatite 700 M	1.0	28.00
	Calcite	2.9	-
	Whiting	-	10.00
Thickener	Natrosol MR	1.0	0.40
Wetting Agent	Pine oil	1.0	0.50
Preservative	SHMP	-	0.10
	Santobrite	-	0.15
Defoamer	NOPCO NXZ	0.2	0.02
	NH_3 (liquor)	0.1	0.13
		73.70	80.92

contd.

	SDS-20		M-2		M-4		Standard	
Formulation	I	II	I	II	I	II	I	II
Mill base	65.72	80.92	73.70	80.92	73.70	80.92	73.70	80.92
Emulsion	34.28	18.91	24.20	12.32	20.00	9.68	17.95	8.84
Water	-	0.17	2.10	6.76	6.30	9.40	8.35	10.24

paints with high viscosity and penetrometer was used to measure, where higher divisions of penetrometer indicate lower viscosity i.e. M 4 II has higher viscosity than M 2 II. SDS 20 II and Standard II was measured in stormer viscometer, KU being kreb unit.

3.13.2 Colour intensity

The microemulsion based paints were tested for colour intensity as given in section 2.14.2. Results are illustrated in Table 3.33. Figures 3.38.I A, B and C and Figures 3.38.II A, B and C show the reflectance vs wavelength plots for the formulated paints with respect to standard. M-4 I gives the highest color intensity among formulation I paints while SDS-20 II gives the highest intensity among formulation II paints.

3.13.3 Stain resistance

Microemulsion based paint was tested for stain resistance with gilsonite solution as given in section 2.14.3. M-4 I has highest stain resistance compared to others of the same formulation i.e. formulation I. Standard II gives highest stain resistance compared to others of the same formulation.

3.13.3 Scrub resistance

The microemulsion based paint was applied on black scrub panel and tested for scrub resistance as given in section 2.14.4. For M-2 I and M-4 I (composition in Table 3.32) scrub resistance was over 25000 scrubs for formulation II. For SDS-20, it was too low for both the formulations (Table 3.33). SDS-20 I and II has high

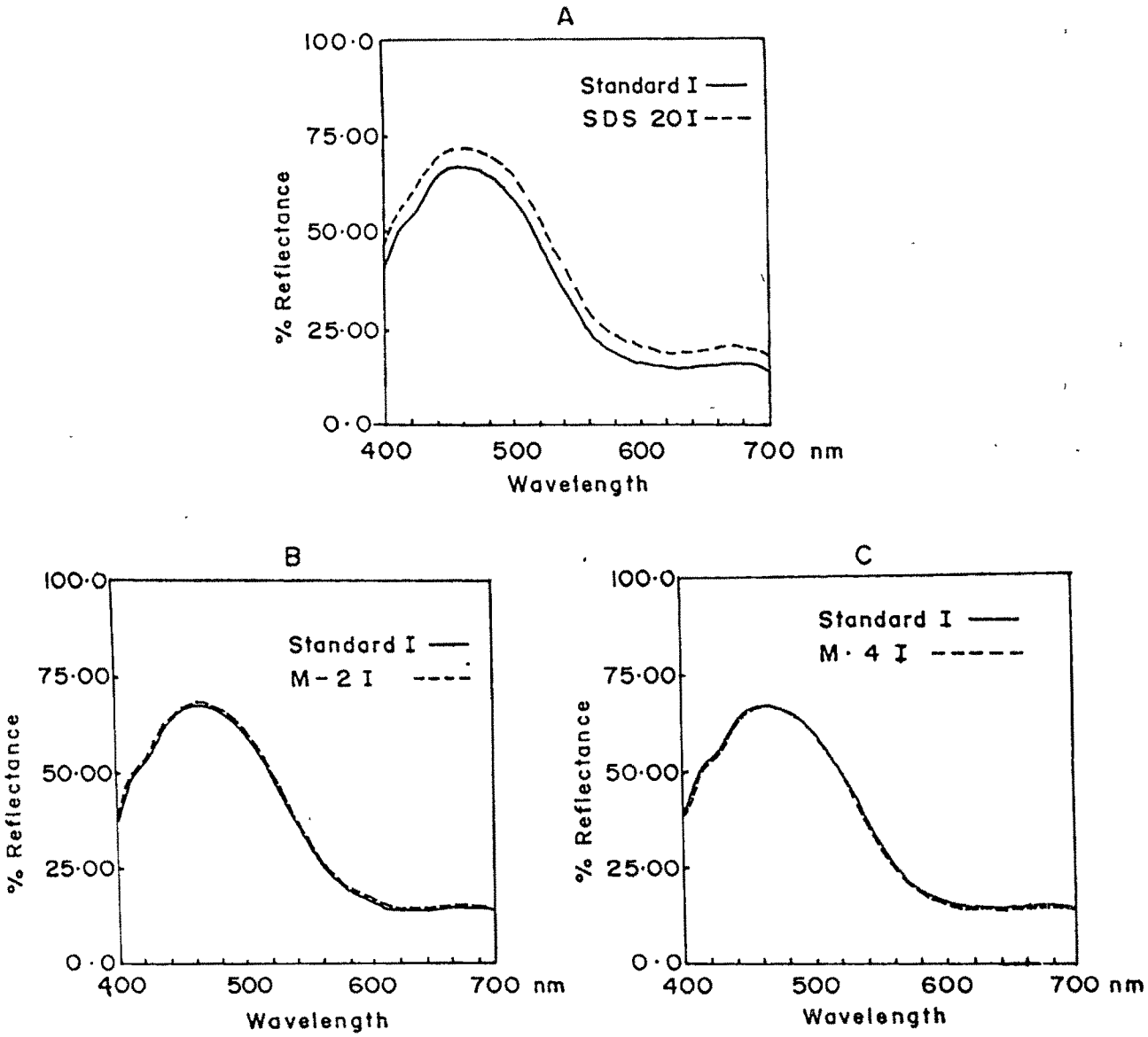

Fig.3·38 IA,B and C shows % Reflectance vs Wavelength plots for microemulsion based paints with respect to standard

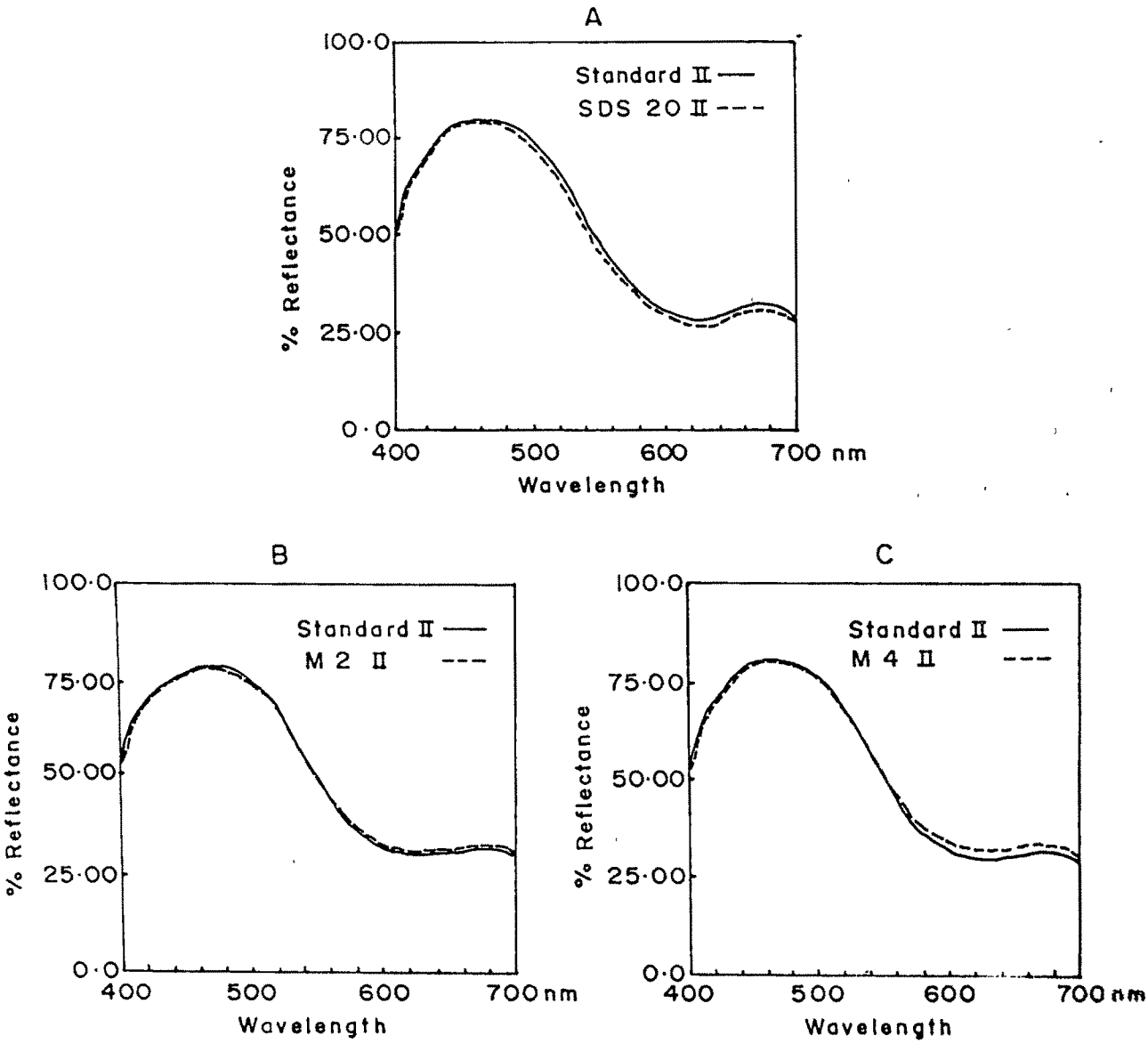

Fig.3·38 II A,B,and C shows % Reflectance vs Wavelength plots for microemulsion based paints with respect to standard

Table 3.33 : Characterization of the formulated paints using microemulsion M-4, M-2, SDS-20 and standard (emulsion).

	M-4		M-2		SDS-20		Standard	
Formulation	I	II	I	II	I	II	I	II
Scrub Resistance	>27203	>10000	>25806	>10000	6	20	-	-
Stain Resistance	10	8	9	9	8	7	7	10
Colour Intensity	111.05	83.12	97.41	94.41	62.94	116.76	100.00	100.00
Viscosity	-	295 DOP	-	327 DOP	-	76 KU	-	90 KU

DOP = Division of penetrometer

KU = Krebs unit

percentage of surfactant and hence acts as poor binder. The very high scrub resistance for M-2, I and II and M-4, I and II indicates that with decrease in particle size (microemulsion), keeping surfactant concentration at optimum level, results in enhanced performance as binder.

Reference

1. F. Bleger, A. K. Murthy, P. Fernand and E. W. Kaler Macromolecules, 27, 2559 (1994).
2. V. H. Perez-Luna, J. E. Puig, V. M. Castano, B. E. Rodriguez, A. K. Murthy and E. Kaler, Langmuir, 6, 1040 (1990).
3. A. Jaykrishnan and D. O. Shah, J. Polym. Sci., Polym. lett. Ed., 22, 31(1984).
4. P. Potisk and Capek I. Eur. Polym. J., 31, 1269 (1995).
5. J. S. Guo, M. S. El Aasser and J. W. Vanderhoff J. Polym. Sci. Polym. Chem. Ed. 27, 691 (1989).
6. L. M. Gan, C. H. Chew, S. C. Ng and S. E. Loh., Langmuir, 9, 2799 (1993).
7. S. Roy and S. Devi. J. Appl. Polym. Sci. (in press).
8. L. Feng and K. Y. S. Ng, Macromolecules, 23, 1048 (1990).
9. F. R. Mayo and C. Walling, Chem. Revs., 46, 191 (1950).
10. T. Kelen and F. Tudos, J. Macromol. Sci, Chem. A-9 1 (1975).
11. M. Fineman and S. R. Ross, J. Polym. Sci., Polym. Lett., 5, 259 (1950).
12. J. C. Bevington and D.O. Harris. J. Polym. Sci., B 5 799, 1967.
13. N. Grassie, B. J. D. Torrance, J. D. Fortune and J. D. Gemmel, Polymer, 6, 653 (1965).
14. J. M. Corpart, J. Selb and F. Candau, Makromol. Chem. macromol. Symp. (Huthig Wefp Verlag, Basel, Heidelberg, New York 1992) 53, 253.
15. J. J. Kozakiewicz and D. W. Lipp U. S. Patent n° 285938 (1988)[CA 113 212851e (1990)].
16. S. Ponratnam and S. L Kapur Makromol. Chem., 178, 1029 (1977).
17. C. Pichot, C. Graillat, V. Glukikh and M. L. Llauro, Polymer Latex II (Plastic Rubber Institute, London, 1985) P II/1.
18. F. Candau, Z. Zekhnini and F. Heatley Macromolecules, 19, 1895 (1986).

19. D. Hunkeker, A. E. Hamielec and W. Baade, Polymers in Aqueous Media, J. E. Glass, Ed. (ACS Symposium series n° 223 1989) Chap. 10 pp. 175-190.

20. W. V. Smith and R. W. Ewart., J. Chem. Phys., 16, 592 (1948).

21. R. M. Fitch and C. H. Tsai in Polymer Collids, R. M. Fitch Ed., Plenum, New York 1971 p. 73.

22. J. Ugelstad, M. S. ElAsser and J. W. Vanderhaff, J. Polym. Sci. Polym. lett. Ed., 11, 503 (1973).

23. B. J. Chamberlain, D. H. Napper and R. G. Gilbert, J. Chem. Soc. Faraday Trans. 1, 78, 591 (1982).

24. J. L. Koenig, `Chemical Microstructure of polymer chains', John Wiley and Sons 1980 Chap.8, p.225.

25. A. S. Brar, H. Sunita and G. S. Kapur, J. Polym. Mater., 8, 225 (1991).

26. J. C. Randall, `Polymer sequence determination Carbon-13 NMR method' (Academic press, New york), 1977, chapter 2, pg.112.

27. A. S. Brar, H. Sunita and C. V. V. Satyanarayana, Polymer J. 24, 9, 879 (1992).

28. G. N. Babu, A. R. Atodaria and A. Deshpande, J. Inorg. Nucl. Chem., 25, 1067 (1963).

29. A. Broido, J. Polym. Sci., Part A-2, 7 1761 (1969).

30. J. Brandrup and E. H. Immergunt Ed., `Polymer Handbook' , John Wiley and Sons, New York, 1975.

31. A. K. M. Asaduzzaman, A. K. Rakshit and S. Devi, J. Appl. Polymer Sci., 47, 1813 (1993).

32. A. S. Narang and V. C. Garg. J. Ind. Chem. Soc., 66, 214 (1989).

33. R. Joseph, S. Devi ad A. K. Rakshit Polym. Int., 26, 89 (1991).

34. R. Simha, J. Phys. Chem., 44, 25 (1940).

35. A. Einstein, Ann. Phys., 19, 289 (1906).

36. M. S. El Aasser, J. Makgawinata and J. W. Vanderhoff, J. Polym Chem. Ed., 21, 2363 (1983).

37. J. A. Masa, J. Forcada and J. M. Asua, Polymer, 34, 2853 (1993).

38. J. L. Johnson and E. Gulari J. Polym. Sci., Polym. Chem. Ed., 22, 3967 (1984).

39. H. I. Tang, P. L. Johnson and E. Gulari, Polymer, 25, 1357 (1984).

40. J. Ugelstad, M. S. El Aasser and J. W. Vanderhoff, J. Polym. Sci., Polym. Lett. Ed., 11, 503 (1973).

41. I. Piirma and M. Chang, J. Polym. Sci., Polym. Chem. Ed., 20, 489 (1982).

42. H. I. Tang, P. L. Johnson and E. Gulari, Measurement of suspended particles by Quasi elastic light scattering, B. Dahneke Ed., Wiley, New York, 1983, pp. 461-482.

43. R. E. Dillon, L. A. Matheson and E. B. Bardford, J. Colloid Sci., 6, 108 (1951).

44. G. L. Brown, j. Polym. Sci., 22, 423 (1956).

45. D. P. Sheetz, J. Appl. Polym. Sci., 9, 3559 (1965).

46. J. W. Vanderhoff, H. T. Tarkowski, M. C. Jenkins and E. B. Bardford, J. Makromol. Chem., 1, 361 (1966).

47. S. S. Voyuyskii, J. Polym. Sci., 32, 528 (1958).

48. G. Allyn in `Emulsions and Emulsion Technology' Ch.7, Editor K. J. Lissant, Marcel Dekker Inc., New York, 1974.